SPACE SCIENCES LABORATORY

AEROPHYSICS SECTION

(6) RADIANCE OF SPECIES IN HIGH TEMPERATURE AIR

(7) NA
(8) NA
(9) NA (10) by

Maria Nardone, R. G. Breene,*
Saydean Zeldin, T. R. Riethof

and

(11) Jun 63,

(15) Work performed under United States Air Force
Contract AF 04(694)-222

(12) 28p.

(13) NA

*Consultant, "Physical Studies, Inc."

(14) Rept. no.
R63SD3
June, 1963

(16-19) NA

(20) U

(21) NA

MISSILE AND SPACE DIVISION

GENERAL ELECTRIC

ABSTRACT

The spectral and total radiance of the radiating systems in high temperature air have been computed for temperatures between 3000°K and 25000°K, and for relative densities ~~(ρ/ρ₀)~~ between ~~10⁻³~~ and 10. The total and spectral radiance of equilibrium air over the same temperature and density range has been computed from the composition of equilibrium air and the absorption coefficients of the individual systems. The results are compared with those obtained by pervious investigators.

The results are presented in graphical form and equations approximating the results in regions of low emissivity are derived.

* degrees
+ 1/1000

CONTENTS

LIST OF FIGURES

INTRODUCTION

This report considers the theories utilized in the calculations of the equilibrium spectral radiance of the chemical species in high temperature air. The knowledge of the radiance of each of the radiating systems combined with a knowledge of the composition of air as a function of temperature and density permits the calculation of the total equilibrium radiation of high temperature air. These calculations apply equally well to air which is at equilibrium, or to air which is in chemical non-equilibrium, provided only that all other degrees of freedom are assumed in equilibrium, and provided that the state (temperature, species concentrations) of the non-equilibrium air is defined.

The input parameters involved in using the theory in the calculation of spectral absorption coefficients are discussed in some detail. The best present values are cited, giving the methods by which they were obtained when pertinent. The influence of one particular parameter, the oscillator strength, is shown by comparison of the results obtained by other workers (Kivel and Bailey[30], Treanor, Wurster, et al[42,43,47,49,50,51,52], Meyerott, Sokoloff and Nicholls[22]) with results from air computations using the currently accepted oscillator strength values. It is particularly significant to note that the curves for the radiance of a given system as obtained by Kivel and Bailey[30] and as obtained by the later computations[7] differ mostly by a constant factor, showing that the main change is due to the better experimental oscillator strengths values now available.

This report includes a series of figures which give:

1. The total Radiance of Equilibrium Air as a function of relative density for temperatures between 3000°K and 25,000°K. A cross-plot, giving the radiance as a function of temperature at different relative densities is also presented.
2. The spectral Radiance of Equilibrium Air.
3. The total Radiance of Equilibrium Air as a function of temperature, indicating the relative contributions of the various radiating systems.
4. The Radiance of each radiating system as a function of optical depth for a range of temperatures. A second set of figures crossplots the data, giving the radiance of each system as a function of temperature at several different concentrations. For each system, the spectral radiance is indicated at several temperatures.

Figures are included to show the comparison of the present results with earlier data, some of which used incorrect oscillator strengths and approximate calculation methods.

THEORETICAL BASIS

In any quantitative description of the radiation from a gas one may choose to deal with the linear gaseous absorption coefficient, the gaseous emissivity, or the actual intensity in units of energy per unit of surface area emitted by some boundary of the gas. All three will be discussed, so that the table user may choose the one most suited to his needs.

Lambert's law for the absorption of radiant energy is given as:

$$I = I_o e^{-KL} = I_o e^{-N\sigma L} \tag{1}$$

where I_o is the intensity in the incident beam, I is the intensity in the beam after it traverses L units of the gas, "K" is the linear absorption coefficient of the gas, "σ" is the cross section for this absorption, and "N" is the number density of absorbing particles. Insofar as this equation is concerned, one may consider it as applying (1) at a particular radiant frequency, (2) as a mean over a band of frequencies, or (3) as a mean over the entire spectrum. K and σ must be individually considered for each of the types of radiation absorbing processes, and, if there are several for the frequency or frequency region of interest, they must be summed.

In the present treatment it will be assumed that local thermodynamic equilibrium is maintained, or, equivalently, that Kirchhoff's law[20, 38] holds. Under these conditions the gaseous emissivity may be written as:

$$\epsilon = 1 - e^{-KL} \tag{2}$$

Here again the emissivity may be taken at a particular frequency or as averaged over some band.

Finally, the emissivity expressions of the last two equations may be used to obtain the actual radiant intensity;

$$I_\lambda \, d\lambda = \epsilon_\lambda B_\lambda \, d\lambda = B_\lambda \, (1-e^{-\sigma NL}) \, d\lambda \text{ watts/ster-micron} \tag{3}$$

$$B_\lambda \, d\lambda = \frac{2hc^2}{\lambda^5} \left[\exp\left(\frac{hc}{\lambda kT}\right) - 1 \right]^{-1} \tag{4}$$

where $B_\lambda \, d\lambda$ is the Planck blackbody function. Here one refers to a particular frequency, but if the result over the entire spectrum is desired one may write:

$$I = \frac{\bar{\epsilon}\bar{\sigma}T^4}{\pi} \text{ watts/cm}^2\text{-steradian} \tag{5}$$

Here $\bar{\sigma}$ is the usual Boltzmann constant and $\bar{\epsilon}$ is the average emissivity. Now the problem is one of obtaining the cross section or absorption coefficient for whatever processes contribute to the radiation from high temperature air. First one lists those processes which are considered important for such radiation in the temperature range of interest:

1. Ultraviolet-visible band spectra
   a. The beta system of NO
   b. The gamma system of NO
   c. The Schumann-Runge system of oxygen
   d. The first positive system of nitrogen
   e. The second positive system of nitrogen
   f. The first negative system of positive nitrogen
2. Infrared band spectra
   a. The infrared spectrum of NO

3. Bound free continua

   a. The bound free continuum of oxygen

   b. The deionization continuum of oxygen ions

   c. The deionization continuum of nitrogen ions

4. Free-free continua

   a. The free free continuum of oxygen

   b. The free free continuum of nitrogen

   c. The free free continuum of N^+, N^{++}, O^+, and O^{++}

At higher temperatures other radiation processes become important, but these will suffice here. In the following subparagraphs each of these processes and the methods of treating them will be discussed.

1. Ultraviolet-visible band spectra

The Mayer[32] - Goody[24] model for an electronic-vibrational band was used in developing the programs for ultraviolet-visible emissivity or absorption coefficient calculations. In developing their band model these authors suppose a statistical distribution of spectral lines in a particular region of the spectrum. Analytical expressions for the form of the absorption coefficient are then developed from this supposition. We have added the assumption that the half widths of the spectral lines are very large. This assumption simply leads to an effectively continuous distribution of radiation within the confines of the electronic-vibrational band. The bands possess the degraded shape typical of these bands. The frequency dependent emissivity expression is now:

$$\epsilon_{\nu} = 1 - \exp\left[-D\Sigma\mu\right] \tag{6}$$

$$\mu = \left(\frac{f_{nm}}{2\left|B_{v'} - B_{v}\right|}\right)(g/Q)\exp(-hc\,G_{el,v}/kT)\exp - \left[\frac{hcB_{v}}{kT}\left(\frac{\tilde{\nu} - \tilde{\nu}_{vv'}}{B_{v'} - B_{v}}\right)\right] \tag{7}$$

$$D = L\frac{\pi e^{2}}{mc^{2}} N \left(1 - e^{-h\nu/kT}\right) \tag{8}$$

Considering first the summation in equation 6, one may suppose that the band system under consideration is degraded toward shorter wavelengths; then, at any particular wavelength, there will be a contribution to the radiation from all band systems whose heads are toward longer wavelengths from that in question. "Q" is the partition function which is taken as a product of electronic, vibration and rotation functions. The B_v are the rotational constants; the $G_{el,\,v}$ are the energies of the electronic-vibrational term values; "g" is the degeneracy of the lower state, a factor which is cancelled by the electronic partition function when the lower state is the ground state; the $\tilde{\nu}_{vv'}$ are the frequencies of the band heads; "L" is the thickness of the emitting layer; N is the number density in particles per cm^3 as given by Browne[23], and "f_{nm}" is the oscillator strength for the band in question. The oscillator strengths are determined from experimental measurements (cf. Penner[37]). The uncertainties in the knowledge of the oscillator strengths are directly reflected in corresponding uncertainties in the values of the emissivities.

2. Infrared Band Systems

Although the physical processes involved are quite distinct, the

rotational constants really give rise to the obvious differences between an electronic-vibrational band and a rotation-vibrational band. In the latter case the rotational constants are practically the same in the upper and lower states. When one makes this assumption[8] one obtains a form of Eqs. 6 - 8 leading to the symmetric distribution of intensity in the band typical of infrared spectra. The emissivity expressions are:

$$\epsilon_\nu = 1 - \exp\left[-D\Sigma\mu\right] \tag{9}$$

$$\mu = \frac{f_{vv'}\left|\tilde{\nu} - \tilde{\nu}_{vv'}\right|}{4B_v^2 Q} \exp(-G_v/kT) \exp\left[-(\nu-\nu_{vv'})^2 \frac{hc}{4B_v kT}\right] \exp\left[-(\nu-\nu_{vv'}) \frac{hc}{2kT}\right] \tag{10}$$

$$D = L \frac{\pi e^2}{mc^2} N\left[1-e^{-h\nu/kT}\right] \tag{11}$$

The symbols are effectively the same although no electronic transition takes place here as was the case with the considerations of the last subsection. Thus, for example, the oscillator strength will simply be that of the vibrational transition. It should be noted that only one infrared spectrum was considered, that of NO, where the oscillator strengths used were those computed by Breene and Todd[8], based on the integrated intensity measurements of Weber and Penner[48]. (See also Benitez and Penner[2])

3. Bound Free Continua

a. Oxygen free bound continuum. In the medium temperature region (6000° - 9000°K) the important Bound-Free continuum is that of oxygen. This continuum arises from the attachment of an electron

to an oxygen atom, with the consequent emission of a photon. The cross section utilized is the one for the inverse process, namely the absorption of a photon by an 0^- ion. The cross section for this process can be calculated, but for the present computations the cross sections obtained by Branscomb et al[6] in scattering experiments, were used.

It should be noted that the cross section is both temperature and density independent. It is true that the absorption coefficient will depend on both these factors, but this will only be through the dependence of the particle concentration on these quantities.

b. N^+ and O^+ deionization continua. The deionization cross-sections for N^+ and O^+ have been computed by Breene[17] and compared with the hydrogenic cross sections for the recombination process given by Bates et al[1]. In view of the fact that good agreement was obtained, the more complete table of cross sections of Bates et al[1] was applied to the present problem.

The relationship between the cross section for ionization (σ_A) required in the present calculations, and the recombination cross section (σ_E) given by Bates[1] is:

$$\sigma_A = \frac{mE_k c^2}{h^2 \nu^2} \sigma_e \qquad (12)$$

$$E_k = [\, hc\omega + \frac{k^2}{2} \; (4.35 \times 10^{-11})] \qquad (13)$$

ω = the frequency (wavenumbers) of the absorption edge. The absorption coefficient K is given by

$$K = \sigma NQ \qquad (14)$$

where Q is the usual partition function, including the appropriate degeneracy factors. Details of the procedure are given by Breene[19].

4. The Free-Free Continua

A. Neutral Atom-Continua. Classically, these continua may be considered as arising due to the deflection of the incident electron by the atom with the resultant acceleration radiation from the deflected electron. From the quantum point of view such radiation results from transitions on the part of the free electron between different states in the presence of the particular atom.

The cross section for these continua were calculated, obtaining first the wave functions[12, 14, 16] for the free electron in the field of the neutral atom in question. Originally[10, 11] these calculations were carried out under the assumption of no electron exchange of core polarization. The calculations for the wave functions have been repeated[17, 18], without these limiting assumptions and the new results are used in the present tabulations. It should be noted that the new wave functions[17] yield cross section about one-tenth those computed earlier[12] where free electron wave functions without polarization were used. The cross section values obtained for oxygen are 5.8×10^{-39} at 1.5 microns, 17×10^{-39} at 3 microns and 50×10^{-37} at 4.5 microns. The results are in excellent agreement with the data of Taylor[41].

B. Ion Continua. The continua for the ion-electron deflection (Bremsstrahlung) are computed directly from the formula originally developed by Kramers, and given by Unsole[45] as

$$\sigma = \frac{3.7 \times 10^{8} Z^{2}}{\nu^{3} \sqrt{T}} \tag{15}$$

where Z is the charge on the ion. (1 for the case of N^{+} and O^{+}, 2 for N^{++} and O^{++} etc.).

INPUT PARAMETERS

The input parameters which were used in the calculations are specified in the following in order that the table user may be aware of the extent, if any, to which more accurate values for these parameters will affect the tables.

1. The Beta Bands of NO

This system arises from the transition between the two doublets $X^2\Pi_{3/2,\,1/2} \rightarrow B^2\Pi_{3/2,\,1/2}$ leading effectively to a double system. The values of the constants were obtained from p. 558 of Herzberg.[26]

One can designate the oscillator strength for an electronic vibrational band as

$$f_{nm} = f_{el}\, f_{vv'}\, R_e^2\,(v) \qquad (16)$$

$f_{vv'}$ is proportional to the square of the appropriate overlap integral, this being the integral over the product of the upper and lower vibrational state wave functions. These integrals have been computed using vibrational wave functions of various degrees of sophistication, i.e., harmonic oscillator functions, Morse potential functions, and various solutions to the Schroedinger equation with specific potentials from experiment or theory. For this beta system, as well as for systems to be subsequently described, we have appealed to the best available calculation of the overlap integrals.

The electronic oscillator strength is not, of course, a constant over an electronic vibrational band system. This is perfectly obvious from the most elementary considerations. Nevertheless, it is convenient to define a constant quantity for a band system which we call the electronic oscillator strength and which we refer to above as f_{el}. This constant is

then corrected for the various pairs of vibrational states leading to the system bands. A convenient way of doing this is with the so-called r-centroid function, R_e^2, of Nicholls. In this system, as well as in the ones to be considered subsequently, we have applied the most accurate r-centroid available. In certain cases the r-centroid function has not been evaluated from experiment for as many vibrational bands as we desire to treat. In these cases we simply extrapolate the r-centroid function as the best available representation for these bands.

Bethke[4] measured the absorption of nitric oxide gas at room temperature and calculated the oscillator strength to be 0.0015, a value in general agreement with the results of Daiber and Williams[21]. The values of $f_{v v'}$ were computed by Kivel, Mayer and Bethe[31], and the function $R_e(\bar{r})$ was derived from the experimental work and tabulated as a function of frequency by Nicholls[35].

The $f_{vv'}$ values for $2\Pi_{3/2}$ were multiplied by the factor $\exp[-hc\nu/kT]$ $\nu = 120$, in order to account for the distribution over the lower members of the doublet.

Any degeneracy in the lower state is cancelled here by the electronic partition function.

2. The Gamma Bands of NO

This system arises from the transition between the $A^2\Sigma^+$ level and the $X^2\Pi_{3/2,\,1/2}$ ground doublet. The constants required were obtained from page 558 of Herzberg.[26]

The value of the electronic oscillator strength was obtained by Bethke[4] as .0024. A slightly higher value is quoted by Daiber and Williams.[21] The vibrational overlap integrals were taken from Jarmain, Fraser, and Nicholls.[27] The function of $R_e^2(\bar{r})$ was derived by Robinson and Nicholls[39].

The factor $\exp[-hc\tilde{\nu}/kT]$, $\tilde{\nu} = 120$, was again included. No lower state degeneracy was considered.

3. The Schumann-Runge system of O_2

This system arises from the transition $X^3\Sigma_g \rightarrow B^3\Sigma_g^-$. The constants required were obtained from Herzberg,[26] pages 559, 560.

The electronic oscillator strength was obtained by Bethke[5] as 0.17. (Note: There is no discrepancy with the value of 0.048 quoted by Treanor and Wurster[43], since these authors evaluated their oscillator strength at a different wave length). The vibrational overlap integrals were obtained from Fraser, Jarmain, and Nicholls[22], while $R_e^2(\bar{r})$ was obtained from Nicholls[34].

4. The First Negative System of N_2^+

This system arises from the transition $X^2\Sigma_g \rightarrow B^2\Sigma_\mu^+$. The constants were taken from page 554 of Herzberg.[26]

The electronic oscillator strength was obtained from radiative life-time measurements by Bennett and Dalby[3] as 0.04. The vibrational overlap integrals were obtained from Jarmain, Fraser, and Nicholls.[27] Nicholls[34] provided the function of the r-centroid.

5. The First Positive System of N_2

This system arises from the transition between the two upper states $B^3\pi_g$ and $A^3\Sigma_\mu^+$. The constants were taken from Herzberg.[26]

The electronic oscillator strength of 0.0095 was obtained from the measurements on high temperature nitrogen of Wurster.[49] (The oscillator strength quoted by Wurster[49] is .0028. However, a comparison of the experimentally measured absorption coefficient with our calculated absorption coefficient gives an electronic oscillator strength of .0095. Through correspondence with Treanor their present electronic oscillator strength is .0038. The difference in these values is due to the difference in the theoretical consideration in obtaining the absorption coefficient.)

The electronic partition function involves the degeneracy of the ground electronic state, which in this case is unity. The lower state involved in the transition, however, is not the ground state but an upper state of degeneracy three. Therefore, the degeneracy is not cancelled by the partition function as in previous cases, and the factor three must be included. Here $(g/Q_e) = 3$.

The vibrational overlap integrals were obtained from Nicholls, Jarmain, and Fraser[36] and the r-centroid function by Turner and Nicholls.[44]

Heath[25] has noted that the radiation due to the nitrogen first positive system in air may be less than the values predicted from measurements in pure nitrogen since there appears to be a radiationless depopulation of the "B" state in the presence of O_2 or NO.

6. The Second Positive System of N_2

This system arises from the transition between the two upper states $C^3\Pi_\mu$ and $B^3\Pi_g$. The parameters were obtained from page 552 of Herzberg.[26]

The electronic oscillator strength was obtained from Bennett and Dalby[3] as 0.038. Since the lower state is not the ground state, the factor (g/Q_e) was taken as six.

The vibrational overlap integrals were taken from Turner and Nicholls[44] while the r-centroid function is obtained from Wallace and Nicholls.[46]

7. Comparison of Electronic Oscillator Strengths

In summary, it is illustrative to list the oscillator strengths used in the present calculations compared with the values used by other authors.[28,33]

	THIS REPORT	KECK, ET AL[28]	MEYEROTT[33]
NO Beta	.0015	.006	.008
NO Gamma	.0024	.001	.0025
N_2 First Positive	.0095	.025*	.02
N_2 Second Positive	.04	.09	.07
N_2^+ First Negative	.04	.18	.2
O_2 Schumann-Runge	.163	.028	.259

*A revised value of 0.013 is given in a later report (Avco Everett Research Labs., Semi-Annual Report, June, 1961).

DISCUSSION OF RESULTS

The results of the computations are presented in figure form, giving the radiance, either spectral or total, as a function of temperature and density, for equilibrium air and for the individual radiating species. The data is given in abbreviated form in Table I, which includes the radiating system, the process involved, together with the pertinent critical parameter, and a reference to the techniques used. The total radiance for each radiating system is given by an equation of the form

$$J = A\,(N)\,\exp(-B/T)$$

where (N) is the number concentration of the pertinent species, T is the temperature in ^{o}K, and A and B are constants. The equations are only valid over the straight line portion of the curves in the cited figures, since they ignore self-absorption. In addition, the equations for the ion continua are applicable only to temperatures above $8000^{o}K$.

The total radiance of equilibrium air is shown in Figures 1 through 10. The first three of these figures show the variation of the radiance as a function of temperature and relative density, while the next five indicate the variation of total radiation and fraction contributed by each radiating system as a function of temperature, at five specific relative densities.

Figure 9 compares the total radiance of equilibrium air computed by our techniques with the earlier results of Kivel and Bailey[30]. The spectral region which was considered by Kivel and Bailey is between .2 and 10μ. Our results are shown for the region .2 to 10μ and also for the extended region .05 to 10μ. It is obvious that this additional spectral region contributes significantly to the radiation from air and cannot be neglected. The

TABLE 1

Radiance of Species in High Temperature Air

System	Process	Critical Parameter	Source	Results (ω/cm^3-ster.)*	Figures
O_2 Schumann-Runge	$B^3\Sigma_u \rightarrow X^3\Sigma_g^-$	f = 0.16	5	$3.6 \times 10^{-13}[O_2]e^{-57,000/T}$	15-19
N_2 First Positive	$B^3\pi_g \rightarrow A^3\Sigma_u^+$	(see text) f = 0.014	47,49	$1.8 \times 10^{-14}[N_2]e^{-83,000/T}$	20-24
N_2 Second Positive	$C^3\pi_u \rightarrow B^3\pi_g$	f = 0.04	3	$1.3 \times 10^{-12}[N_2]e^{-120,000/T}$	25-29
N_2^+ First Negative	$B^2\Sigma_u^+ \rightarrow X^2\Sigma_g^+$	f = 0.04	3	$1.3 \times 10^{-13}[N_2^+]e^{-31,000/T}$	30-34
NO Beta	$B^2\pi_{3/2,1/2} \rightarrow X^2\pi_{3/2,1/2}$	f = 0.0015	4	$1.6 \times 10^{-13}[NO]e^{-67,000/T}$	35-38
NO Gamma	$A^2\Sigma^+ \rightarrow X^2\pi_{3/2,1/2}$	f = 0.0024	4	$1.4 \times 10^{-13}[NO]e^{-67,000/T}$	39-43
NO Infrared	Rotation-Vibration	Oscillator Strength	2,8	$2.1 \times 10^{-19}[NO]e^{-7600/T}$	44-46
O Free-Bound	$O + e \rightarrow O^- + h\nu$	Cross-Sections	6	$2.5 \times 10^{-12}[O^-]e^{-33,000/T}$	47-50
N Free-Free	$N^* + e \rightarrow N + e + h\nu$	Cross-Sections	18	$2 \times 10^{-34}[N][e]e^{-52,000/T}$	51-54
O Free-Free	$O^* + e \rightarrow O + e + h\nu$	Cross-Sections	18	$3 \times 10^{-34}[O][e]e^{-42,000/T}$	55-59
N^+ Deionization (.2-5.μ)	$N^+ + e \rightarrow N + h\nu$	Cross-Sections	1	$1 \times 10^{-10}[N]e^{-180,000/T}$	60-62
N^+ Deionization (.05-.2μ)	$N^+ + e \rightarrow N + h\nu$	Cross-Sections	1	$8 \times 10^{-13}[O]e^{-59,000/T}$	69-71
O^+ Deionization (.2-5.μ)	$O^+ + e \rightarrow O + h\nu$	Cross-Sections	1	$9 \times 10^{-11}[O]e^{-170,000/T}$	63-75
O^+ Deionization (.05-.2μ)	$O^+ + e \rightarrow O + h\nu$	Cross-Sections	1	$8 \times 10^{-13}[O]e^{-59,000/T}$	72-74
($N^+ + O^+$) Free-Free	$N^+* + e \rightarrow N^+ + e + h\nu$ $O^+* + e \rightarrow O^+ + e + h\nu$	Z = 1	20	$9 \times 10^{-33}([N^+] + [O^+])[e]e^{-14,000/T}$	66-68

*Equations are valid only over linear region of curves in the cited figures

comparison of the data between .2 and 10μ shows AVCO's data to be higher by about a factor of 2. At high temperatures the difference is due to an approximate technique used by Kivel[30] to calculate the Kramers radiation. (Kivel in a later paper[29] indicates that the effective charge assumed was high and that hence the results are high) The differences at lower temperatures are due to different theoretical techniques used to calculate radiation from molecular bands and to the difference in the electronic oscillator strengths used.

Figure 75 predicts the radiant intensity of equilibrium air using normal shock temperatures and densities as given by Wittliff[53]. These predictions can be described by the equation

$$\log J = .12\,V - 3.5 \times 10^{-2} H + 1.6$$

where V - ambient velocity (kFT./sec); H is the altitude in kFT. and J is the radiant intensity in watts/cm^3-ster. This equation is accurate for velocities between 18 and 26 Kft/sec and altitudes between 40 and 160 Kft. At higher altitudes it overestimates the radiation by a factor of 2.

The spectral radiance of equilibrium air at three different temperatures, and at a relative density of 10^{-1} is given in Figures 11 and 12, which differ only in the wavelength range covered.

Figure 13 compares the spectral radiance of air obtained in our computations at 8000°K and a relative density of 1 with the results given by Keck et al[28] and Meyerott et al[33]. (Meyerott gave his data as absorption coefficients, which were multiplied by the blackbody function to obtain the curve shown in Figure 13).

Figure 14 compares our spectral absorption coefficients with those of Meyerott[33] at 12,000°K, the highest temperature given in that reference. The agreement is generally good, the smoother shape of Meyerott's curve being due to the fact that this author considered fewer absorption edges in his computation of the deionization continua, and these are the dominant radiators under these conditions. Quite probably, particularly at the higher temperatures, the chief uncertainty in the radiation due to equilibrium air is the uncertainty in the concentration of some of the radiating species.

The radiance of the oxygen Schumann-Runge bands is given in Figures 15 through 19, and these figures also show the comparison with the results of Kivel and Bailey, again high because of the early oscillator strengths values they used. The data of Bethke[5] used in these computations has since been corroborated by the work of Treanor and Wurster[43].

The results for the nitrogen first positive system are given in Figures 20 through 24. Since this is a transition between two excited states, the oscillator strength cannot be obtained from absorption measurements carried out at low temperature. We have utilized the data of Wurster[49] to compute an "effective oscillator strength" for this system which, matched with out computation scheme, reproduces the measured absorption coefficients.

Similar graphs are given for the other radiating systems, both band systems and continua.

Recent experimental measurement by Wurster, Treanor & Thompson[52] have indicated an additional group of nitric oxide electronic bands located between 0.9 and 1.4 microns. They have tentatively been identified as

transitions between various excited state of NO, and Wurster et al[52] have indicated that they can be roughly approximated as having an equivalent excitation energy of 7 e.v. and an effective oscillator strength of about 0.07. Measurements in air at 6300°K and $\rho/\rho_o = 1$ indicate an average radiance of 5 w/cm^3 - steradian - micron over the wavelength interval from 1 to 1.3 microns. The absorption coefficient for a unit density of nitric oxide $(\rho/\rho_o)_{NO} = 1$ is about 0.12 at 6300°K for the previously indicated wavelength interval (1 - 1.3μ).

The radiation from this system is <u>not</u> included in the present tabulation.

APPLICATION OF RESULTS

The results of the computational programs are presented in graphical form to permit application to various problems involving radiation from air or its component gases.

The data is presented in such a form that it can be conveniently used to determine radiation from equilibrium air, from the individual radiating species in equilibrium air, or from individual radiating species in non-equilibrium air. In each case, one need only find the pertinent figure (see Table I) and read off the radiation for the appropriate temperature and concentration (or relative density - as the case may be). It should be noted that for non-equilibrium compositions the pertinent concentrations are those of the reactants, and caution must be exercised in using some of the figures (particularly Fig. 60 through 68) which for computational convenience are given in terms of the concentration of reaction products. Under conditions of chemical equilibrium the two concentrations of reactants and reaction products are related by the equilibrium constant, and hence either one can be used.

The quantity tahulated is

$$J_T = \frac{(1-e^{-KL})\sigma T^4}{\pi} \text{ watts/ster.-cm}^2 \tag{17}$$

where L = 1 cm

For $J_t \ll \frac{\sigma T^4}{\pi}$; $(1-e^{-KL}) < .1$

$$\frac{J_T}{L} = \frac{K\sigma T^4}{\pi} \text{ watts/ster.-cm}^3 \tag{18}$$

The application of the results to two specific problems is considered in some detail in the next two sections:

1. Irradiance from a Distant, Optically Thin Source

To determine the radiation emitted by a known volume of gas, as viewed at a distance, one simply takes the appropriate value of J from the tables, multiplies it by the volume (in cubic centimeters) and divides by the slant range (also in centimeters) squared to directly obtain irradiance in watts/centimeter^2.

This computation applies equally well to spectral radiation or to total radiation, and to either radiation from equilibrium air, or to that from any particular radiating system of air.

The only assumption made is that the radiating layer is "optically thin". This is generally true when considering gas caps associated with re-entry vehicles. The definition for an optically thin radiator here is that the total spectral emissivity $K_\lambda L$ is less than about 0.2 or, as applied to air radiation, that the total emissivity $K_T L$ is less than 0.1. (This takes into account that in high temperature air the radiation is not distributed spectrally in the same manner as blackbody radiation). In general, if one deals with radiating layers more than a few centimeters thick, it is wise to check if the gas is actually optically thin by evaluating $K_T L$ (where L is the path length in the line of sight direction), or by performing the equivalent calculation; i.e., taking the product of (J_T) (L) and dividing by J_T for a blackbody radiator at the same temperature. For convenience, curves of the total blackbody

radiation ($\bar{\sigma} T^4/\pi$) or a convenient fraction thereof are included in Figures 3 through 8. A typical spectral blackbody distribution curve for 8000°K is included in Figure 13.

In general, the plotted data is designed to be applied only to regions of constant temperature and - at least approximately - constant density. The hazards of using an "average" temperature are best indicated by noting the dependence of the total air radiation on temperature in Figure 3.

One important special case of varying temperature and density distribution is the equilibrium flow field around a hemispherical body in supersonic flow. Computations were performed to obtain the radiation from the bow shock region of hemispherical bodies (at zero angle of attack) at several different altitudes and velocities. It was found possible to relate the total radiation to the radiation from the stagnation region and the cube of the radius of the hemisphere such that

$$J_{i_{total}} = \text{constant } J_{i_{stagn}} R^3 \text{ watts/steradian} \qquad (19)$$

J stagnation (watts/cm^3 - steradian) is a function of T stagnation and $\rho_{stagnation}$, which in turn are a function only of velocity and altitude. "i" refers to a species of equilibrium air, or to the total equilibrium air. The following constants have been evaluated for hemispherical bodies:

System	Constants
Equilibrium Air	0.25
Oxygen Schumann-Runge Bands	0.36
Nitrogen First Positive System	0.28
Nitrogen Second Positive	0.21
Nitrogen Ion First Negative System	0.17
Nitric Oxide Gamma Bands	0.31
Nitric Oxide Betta Bands	0.28
Nitric Oxide Infrared Bands	0.61
Oxygen Atom Free - Bound Continuum	0.23
Nitrogen Atom Free - Free Continuum	0.19
Oxygen Atom Free - Free Continuum	0.23

The constants are applicable in general to equilibrium air radiation from bow shock regions of vehicles with hemispherical noses, travelling at velocities between 15,000 and 25,000 ft/sec. and at altitudes between 250,000 and 70,000 ft. The data is also applicable to "blunt" vehicles, of the sphere-cone type, for cone half angles of less than 15^{o}.

2. Radiation Heat Transfer

The radiation incident or one square centimeter of surface from an infinitesimal thickness of an optically thin layer is given by

$$Q_R = 2\pi L \left[\epsilon \frac{\sigma T^4}{\pi} \right] \text{ watts/cm}^2 \qquad (20)$$

where the quantity in brackets is the radiance of equilibrium air, as given in figures 1 through 8, and L is the thickness of the radiating layer.

The factor two is exactly applicable only for the case of an infinite plane, and for the case where KL (more exactly $K_\lambda L$ is much less than 1. As KL approaches 1, the factor 2 also approaches 1, and the limiting case, for an opaque gas is simply the blackbody equation:

$$Q_R = \pi \left(\frac{\bar{\sigma} T^4}{\pi} \right) = \sigma T^4 \text{ watts/cm}^2 \tag{21}$$

Mayer [32] has considered the radiative heat transfer for typical blunt re-entry vehicles travelling at velocities of the order of 20,000 ft./sec. and has evaluated that

$$Q_R = 1.8 \pi L \left[\epsilon \frac{\sigma T^4}{\pi} \right] \text{ watts/cm}^2 \tag{22}$$

REFERENCES

1. Bates, Buckingham, Massey & Unwin, Proc. Roy. Soc. A170, 322 (1939)

2. Benitez, L. E. and Penner, S. S., J. Appl. Phys. 21, 907 (1950)

3. Bennett, R. G. and Dalby, F. W., J. Chem. Phys. 31, 434, (1959)

4. Bethke, G., J. Chem. Phys. 31, 662, (1959)

5. Bethke, G., J. Chem. Phys. 31, 669, (1959)

6. Branscomb, L. M., Burch, D. S., Smith, S. J., and Geltman, S., Phys. Rev. 111, 504, (1958)

7. Breene, R. G. and Nardone, Maria, "Radiant Emission from High Temperature Equilibrium Air", General Electric Co. TIS R62SD20 May 1961, see also J.Q.S.R.T. 2, 272, (1962)

8. Breene, R. G. and Todd, M., J. Chem. Phys. 28, 11, (1958)

9. Breene, R. G., J. Chem. Phys. 29, 512, (1958)

10. Breene, R. G. and Nardone, Maria, J. Opt. Soc. 50, 1111, (1960)

11. Breene, R. G. and Nardone, Maria, J. Opt. Soc. 51, 692, (1961)

12. Breene, R. G. and Nardone, Maria, Phys. Rev. 115, 93, (1959)

13. Breene, R. G., General Electric TIS R60SD478, (Dec. 1960) - "Wave Functions of the Free Electron II. The Inclusion of Polarization and Exchange"

14. Breene, R. G. Phys. Rev. 111, 1111, (1958)

15. Breene, R. G. Phys. Rev. 113, 809, (1959)

16. Breene, R. G. Phys. Rev. 119, 1615, (1960)

17. Breene, R. G., J. Chem. Phys. 35, 625, (1961)

18. Breene, R. G., "Effect of Polarization and Exchange on the Free-Free Continuum" (to be published)

19. Breene, R. G., "Deionization Continuum for Oxygen" (to be published)

20. Chrandrasekhar, S., "Radiative Transfer", Dover Publications, New York (1960)

21. Daiber, J. N. & Williams, M. J., "Transition Probabilities for NO in the Far Ultraviolet" J.Q.S.R.T. (in press)

22. Fraser, P. A., Jarmain, W. R. and Nicholls, R. W., Astrophys. J. 119, 286, (1954)

23. Browne, W. G., "Thermodyanic Properties of the Earth's Atmosphere" Radiation and Space Physics TM #2 1962

24. Goody, R. M., Quart. J. Roy. Met. Soc. 78, 165, (1952)

25. Heath, D. F., Los Alamos Scientific Laboratory LA-2335, (Jan. 1960)

26. Herzberg, G., "Molecular Spectra and Molecular Structure, Diatomic Molecules" Van Nostrand, New York, (1950)

27. Jarmain, W. R., Fraser, P. A. and Nicholls, R. W., Astrophys. J. 118, 228, (1953)

28. Keck, J., Camm, Kivel, B. and Wentink, T., Ann. Phys. 7, 1, (1959)

29. Kivel, B. "Radiation From Hot Air and Stagnation Heating" AVCO Res. Rpt. 79, (October 1959)

30. Kivel, B. and Bailey, K., "Tables of Radiation From High Temperature Air" AVCO Res. Rpt. 21, (December 1957)

31. Kivel, B., Mayer, H. and Bethe, H., Ann. Phys. 2, 57, (1957)

32. Mayer, H., LA-647 Los Alamos Scientific Laboratory, (1947)

33. Meyerott, R. E., Sokoloff, J. & Nicholls, R. W., "Absorption Coefficients of Air" Geophysical Research Paper No. 58, GRD-TN-60-277 (July 1960)

34. Nicholls, R. W., Proc. Phys. Soc. 69, 741, (1956)

35. Nicholls, R. W., Proc. Phys. Soc. 129, 957, (1958)

36. Nicholls, R. W., Jarmain, W. R., and Fraser, P. A., Can. J. Phys. 31 1019, (1953)

37. Penner, S. S., "Quantitative Molecular Spectroscopy and Gas Emissivities" Addison Wesley, Mass. (1959)

38. Planck, M., "The Theory of Heat Radiation" Dover Publications, New York (1959)

39. Robinson, D. and Nicholls, R. W., Proc. Phys. Soc. 71, 957, (1958)

40. Rose, P. H. & Teare, J. D. "On Chemical Effects and Radiation in Hypersonic Aerodynamics" AVCO AMP 72, (March 1962)

41. Taylor, R. L., "Continuum Infrared Spectrum of High Temperature Air" AVCO Research Report 88, (June 1960)

42. Treanor, C. E., "Radiation at Hypersonic Speeds", C.A.L. Rept. CAL-109, (July 1961)

43. Treanor, C. E. and Wurster, W. H., J. Chem. Phys. 32, 758 (1960)

44. Turner, R. G. and Nicholls, R. W., Can. J. Phys. 32, 475, (1954)

45. Unsold, A. "Physik Der Sternatmospharen", Berlin Springer, 1938, pp. 117-118

46. Wallace, L. V. and Nicholls, R. W., J. Terr. Atmos. Phys. 7, 101. (1955)

47. Williams, M. J. and Treanor, C. E., "A Method for Calculating Diatomic Spectra Using a Computer Program", C.A.L. Rept. QM-16261A15, May 1962

48. Weber, D. and Penner, S. S., J. Chem. Phys. 21, 649 (1953)

49. Wurster, W. H., "Measured Transition Probability for the First Positive Band System of Nitrogen", C.A.L. Rept. QM-1626-A-3 (January 1962)

50. Wurster, W. H., Glick, H. S. and Treanor, C. E., "Radiative Properties of High Temperature Air - Final Report" AFSWC-TR-58-35 (September 1958) C.A.L.

51. Wurster, W. H. & Marrone, P.V., "Study of Infrared Emission in Heated Air", Annual Report - QM-1373-A-4, July 1961 C.A.L.

52. Wurster, W. H., Treanor, C. E. and Thompson, H. M., "Nitric Oxide Bands Near 1 Micron in Shock Heated Air", C.A.L. Rept. QM 1626-A-6 (June 1962)

53. Wittliff, C. E., Curtis, J. T., "Normal Shock Wave Parameter in Equilibrium Air," C.A.L. Rept. CAL-111 (November 1961)

Figure 1. Total Radiance of Equilibrium Air (3000°K - 9000°K)

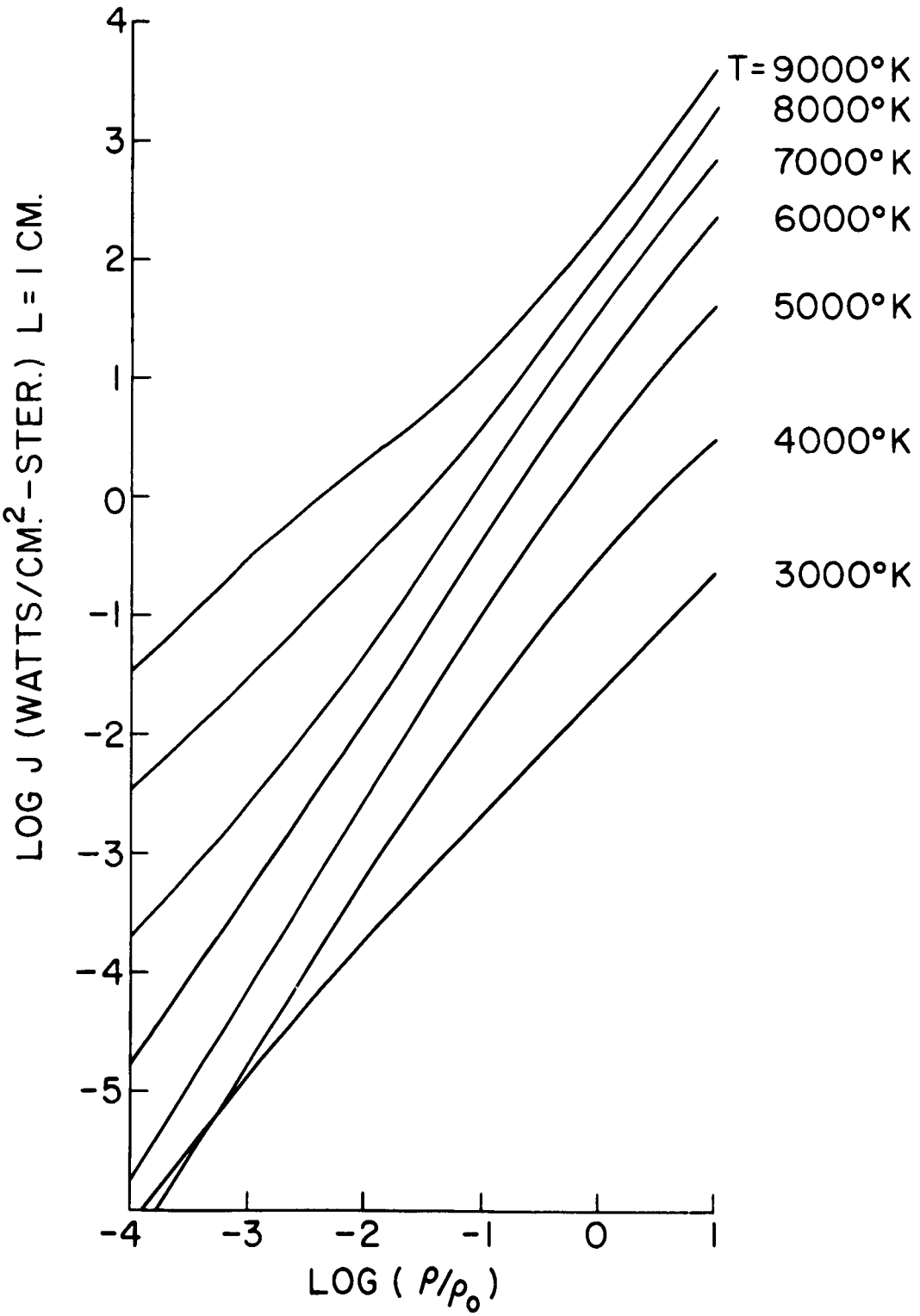

A203 A515

Figure 2. Total Radiance of Equilibrium Air (10,000°K - 25,000°K)

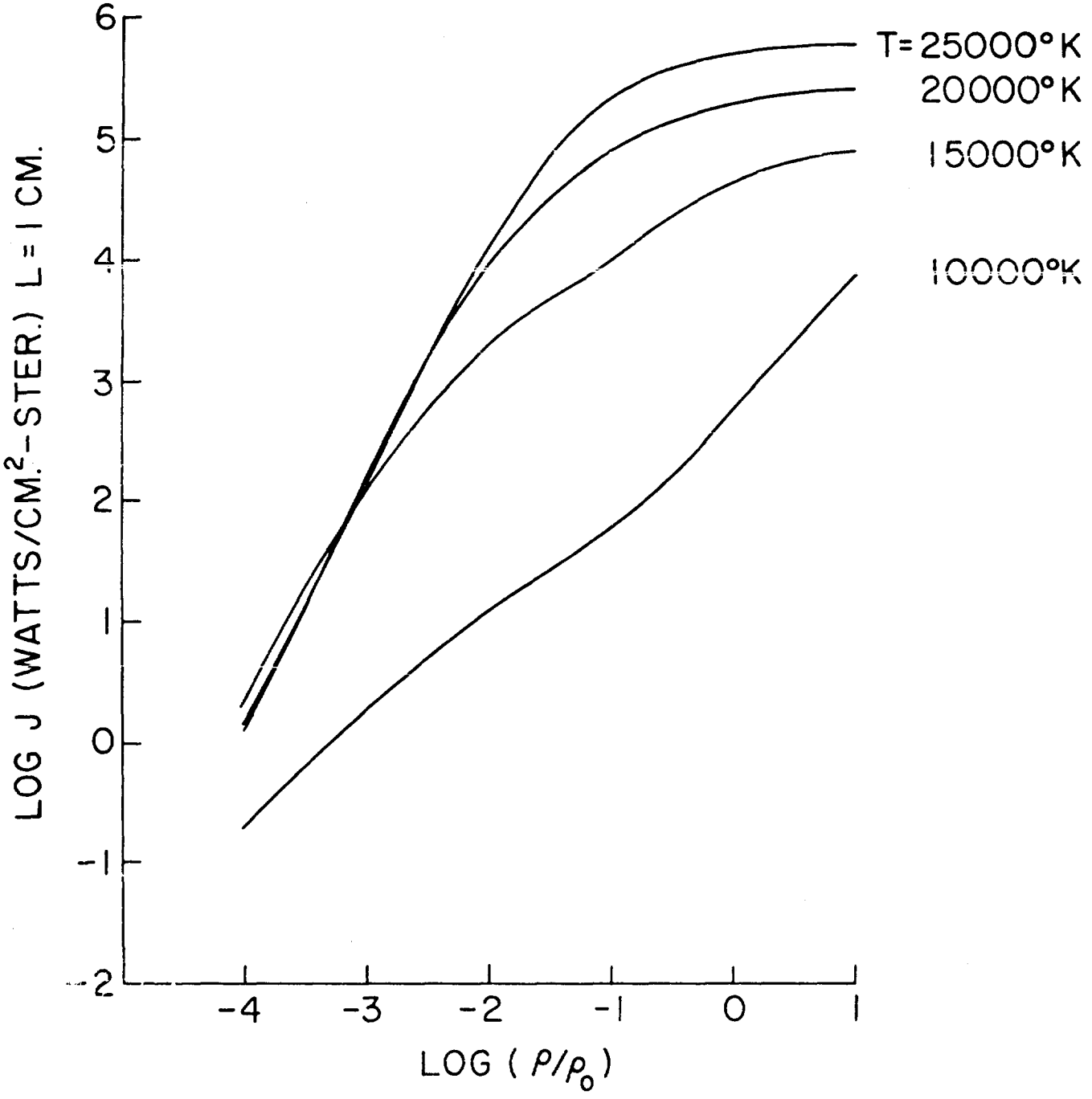

Figure 3. Total Radiance of Equilibrium Air (10^{-3} to 10^{1} ρ/ρ_o)

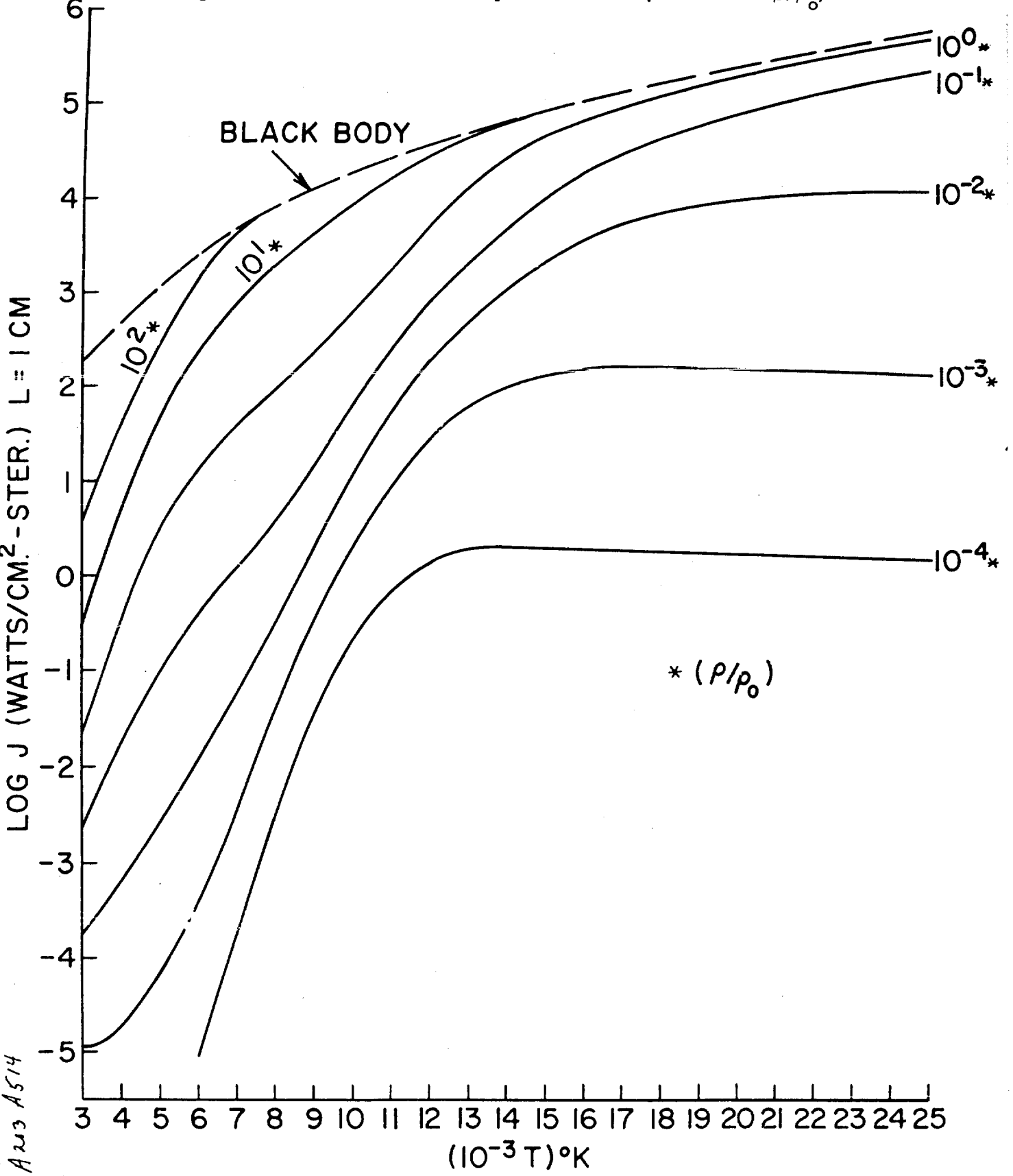

A23 A514

Figure 4. Radiance of Equilibrium Air vs. Temperature ($\rho/\rho_o = 10^{-3}$)

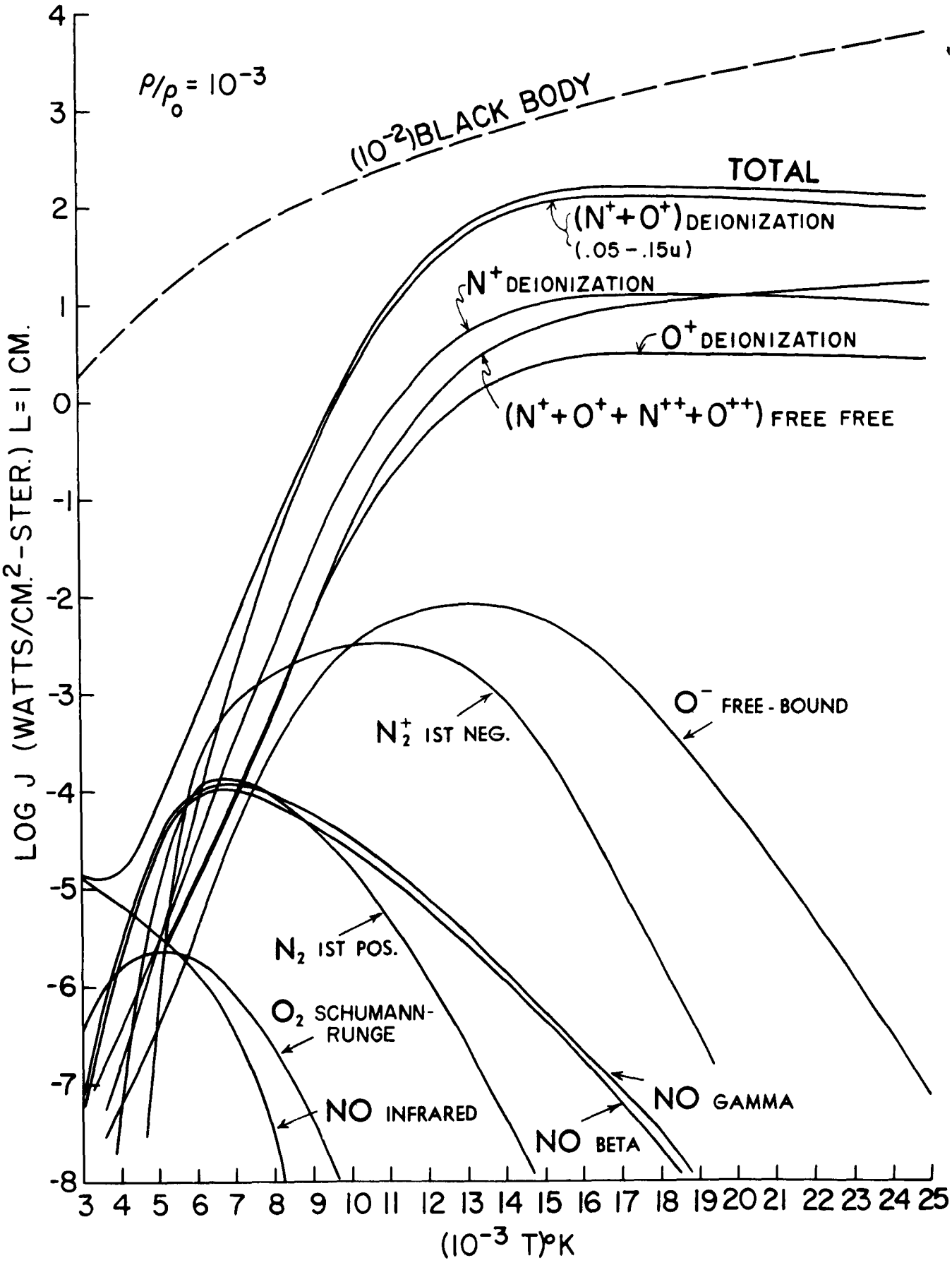

Figure 5. Radiance of Equilibrium Air vs. Temperature ($\rho/\rho_o = 10^{-2}$)

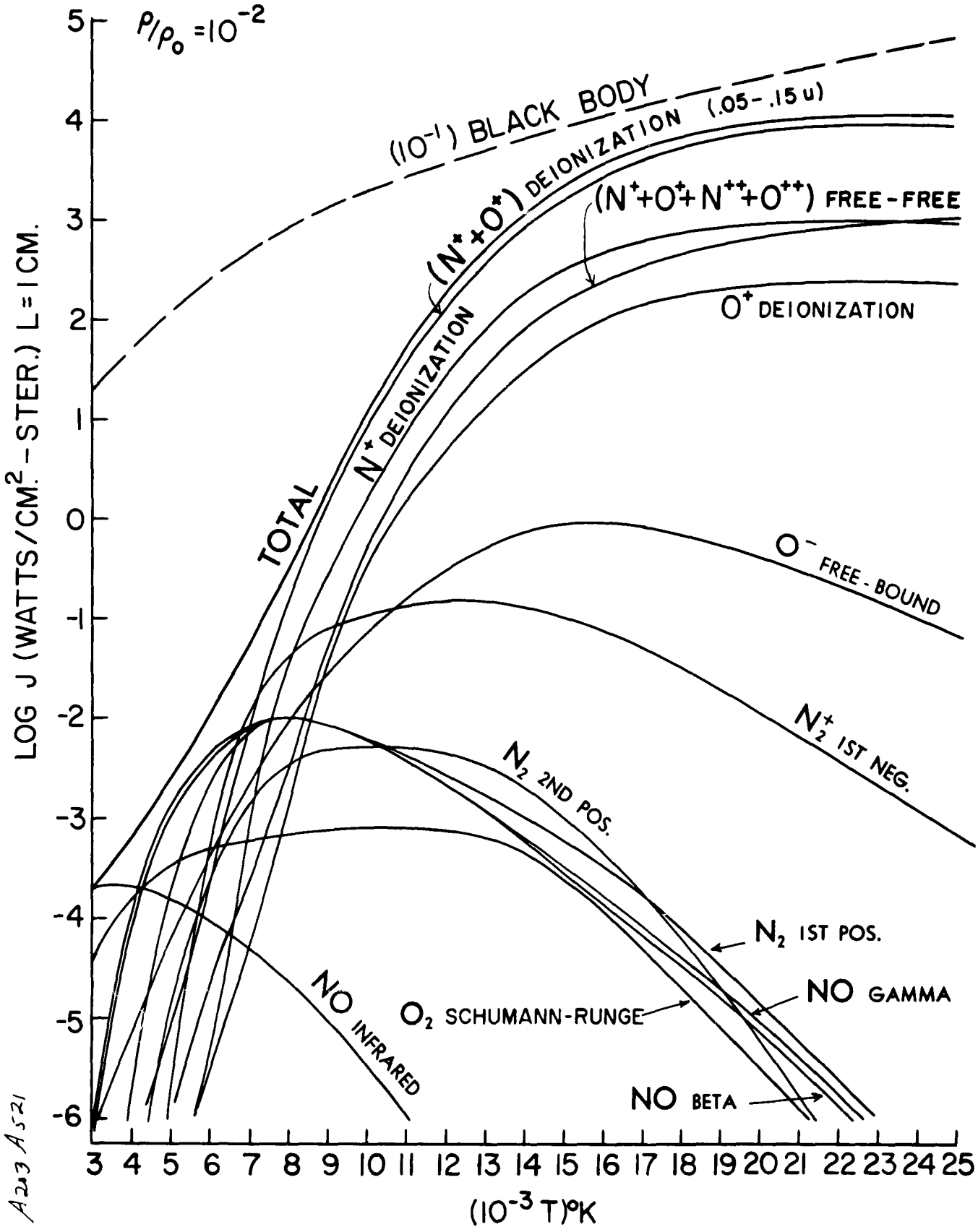

A23 A521

Figure 6. Radiance of Equilibrium Air vs. Temperature ($\rho/\rho_o = 10^{-1}$)

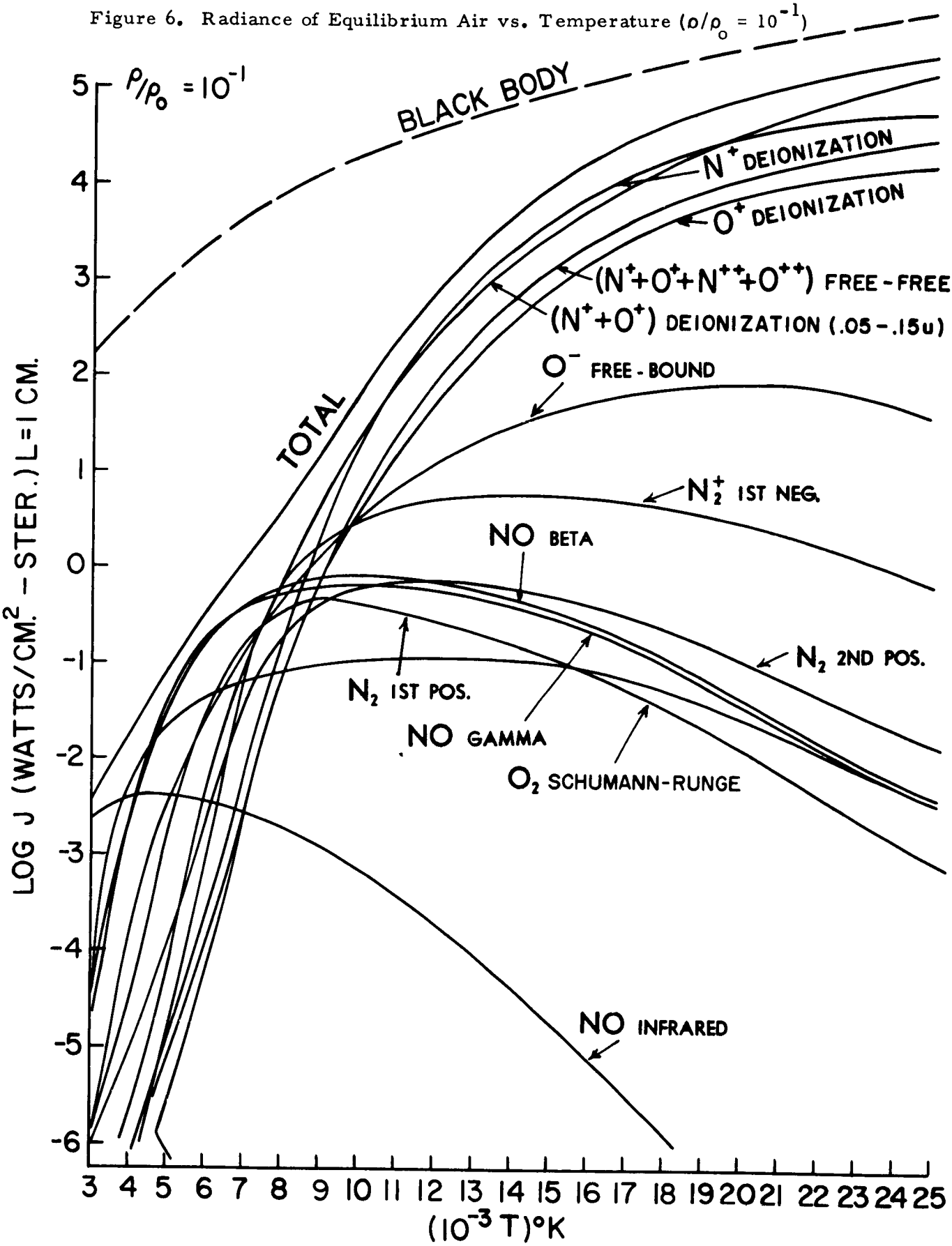

Figure 7. Radiance of Equilibrium Air vs. Temperature ($\rho / \rho_o = 10^o$)

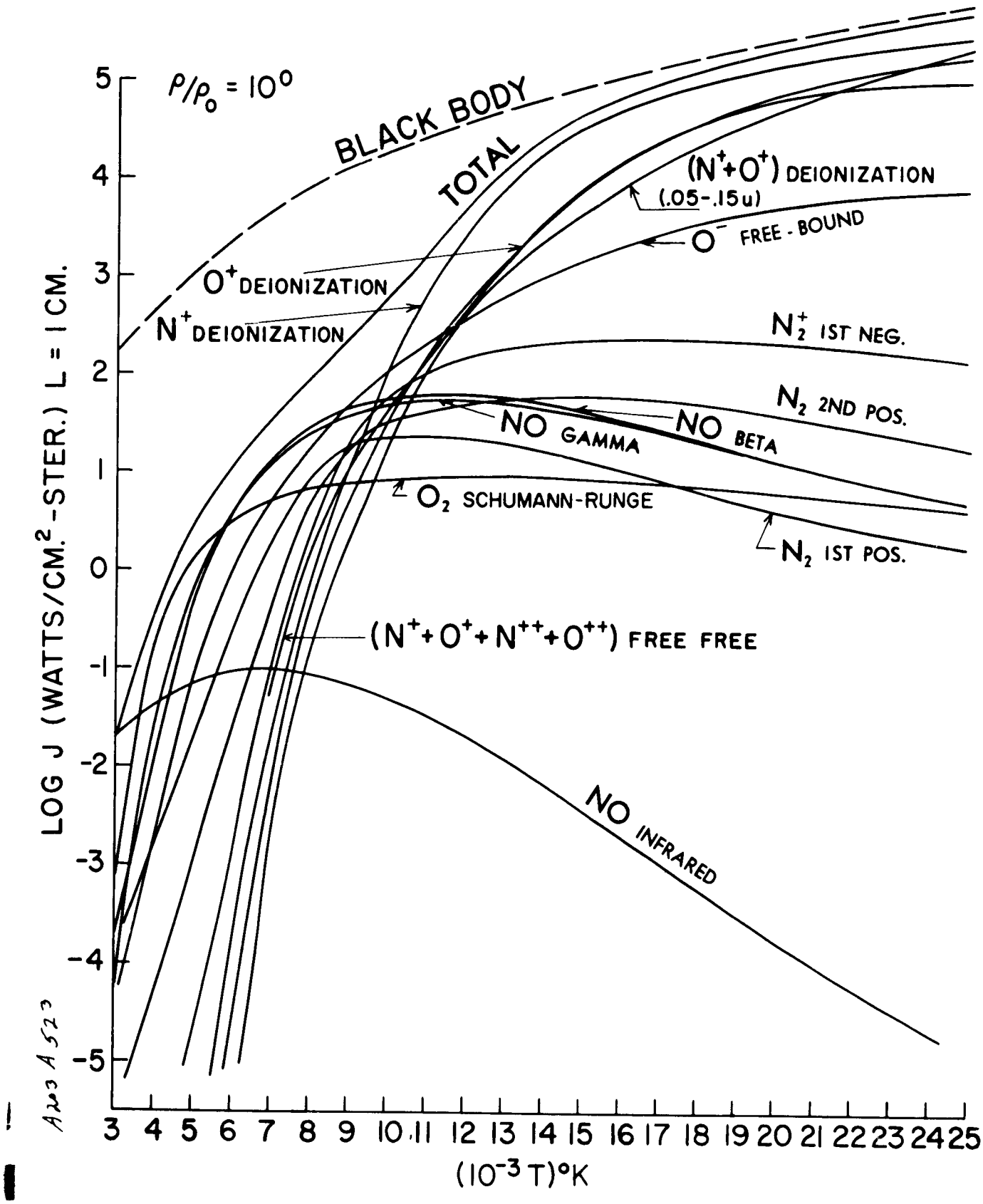

Figure 8. Radiance of Equilibrium Air vs. Temperature ($\rho/\rho_o = 10^1$)

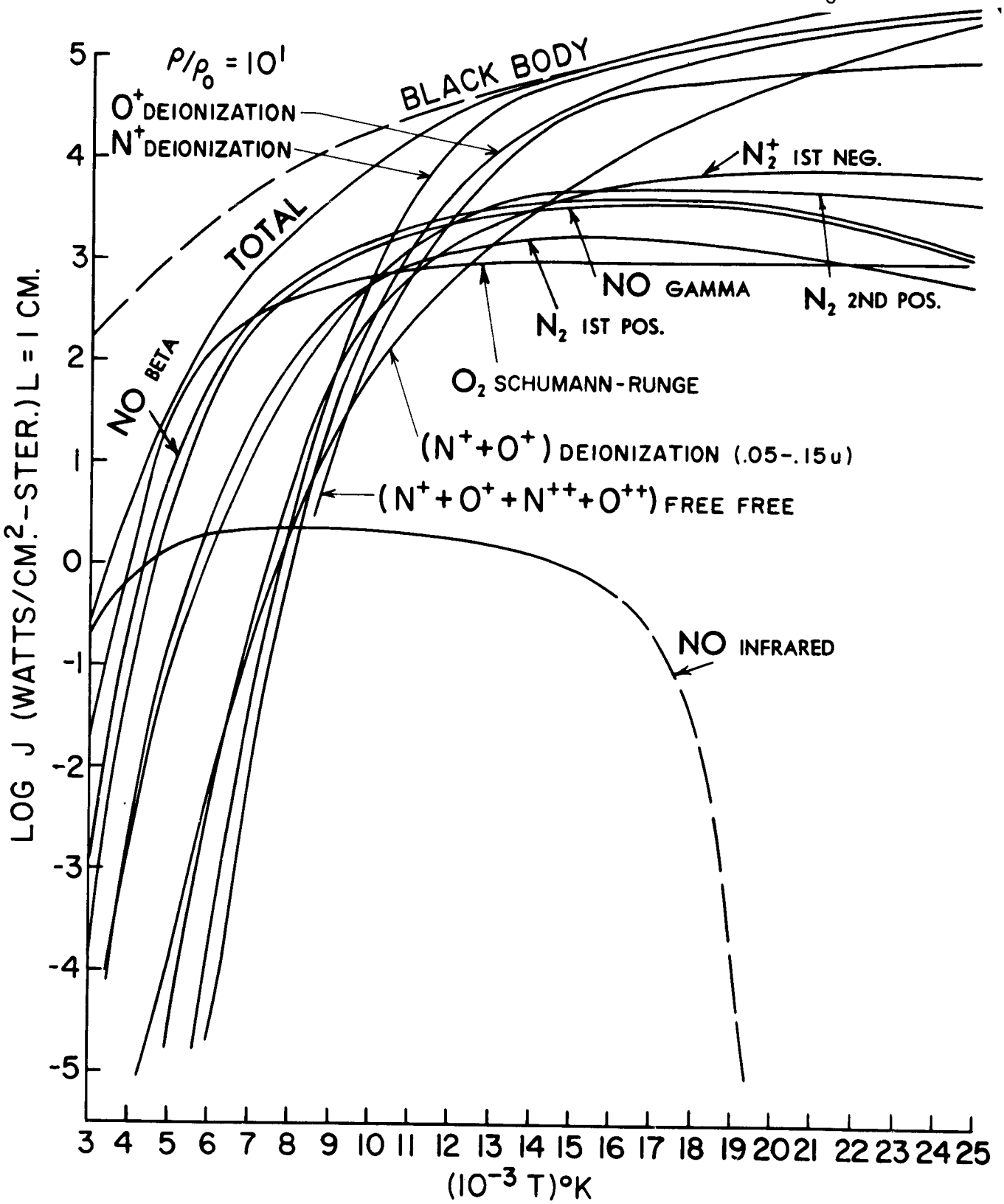

Figure 9. Comparison of Predictions: Total Radiance of Equilibrium Air (3000°K - 12,000°K)

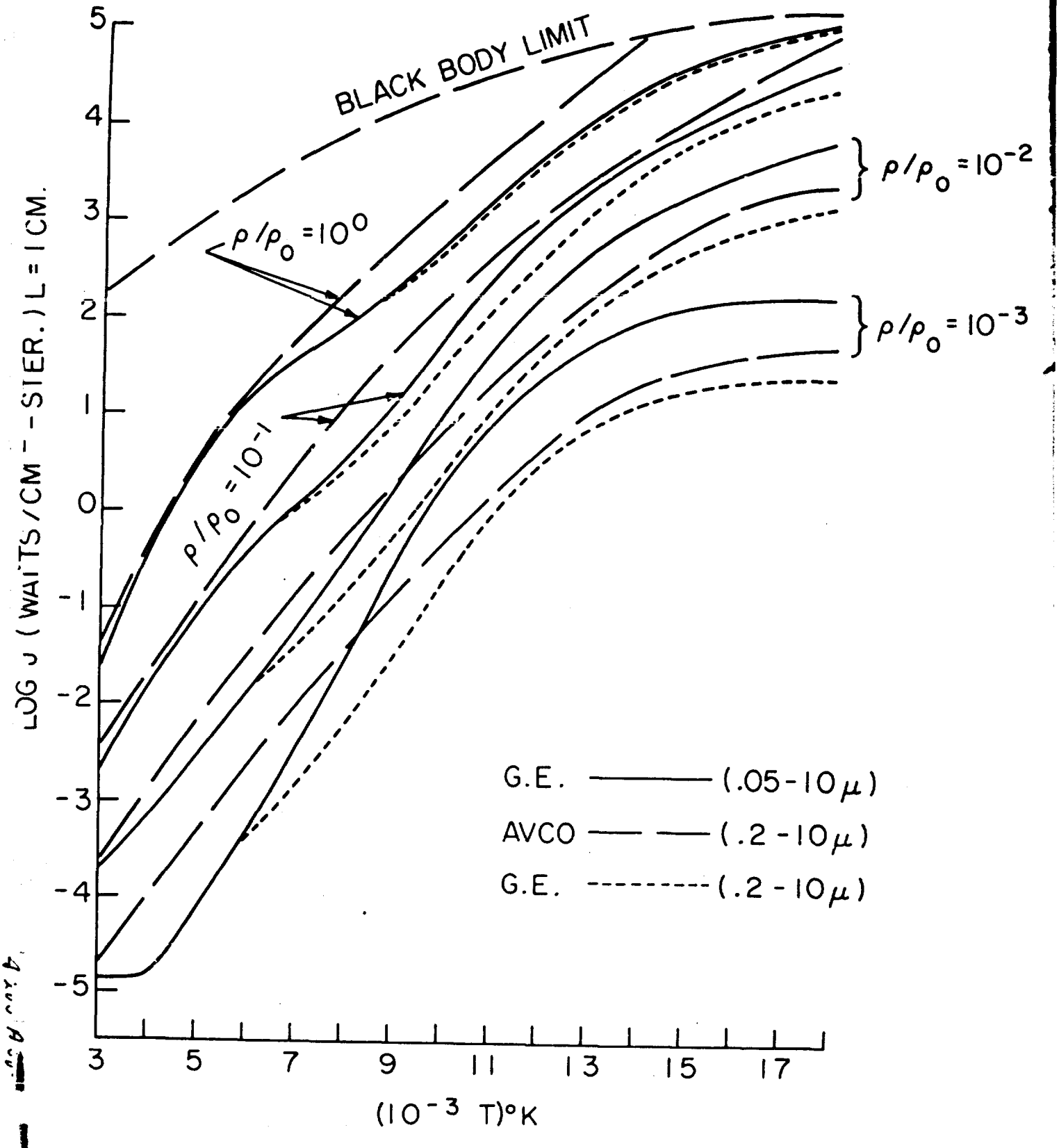

Figure 10. Comparison of Predictions: Radiance of Equilibrium Air (18,000°K)

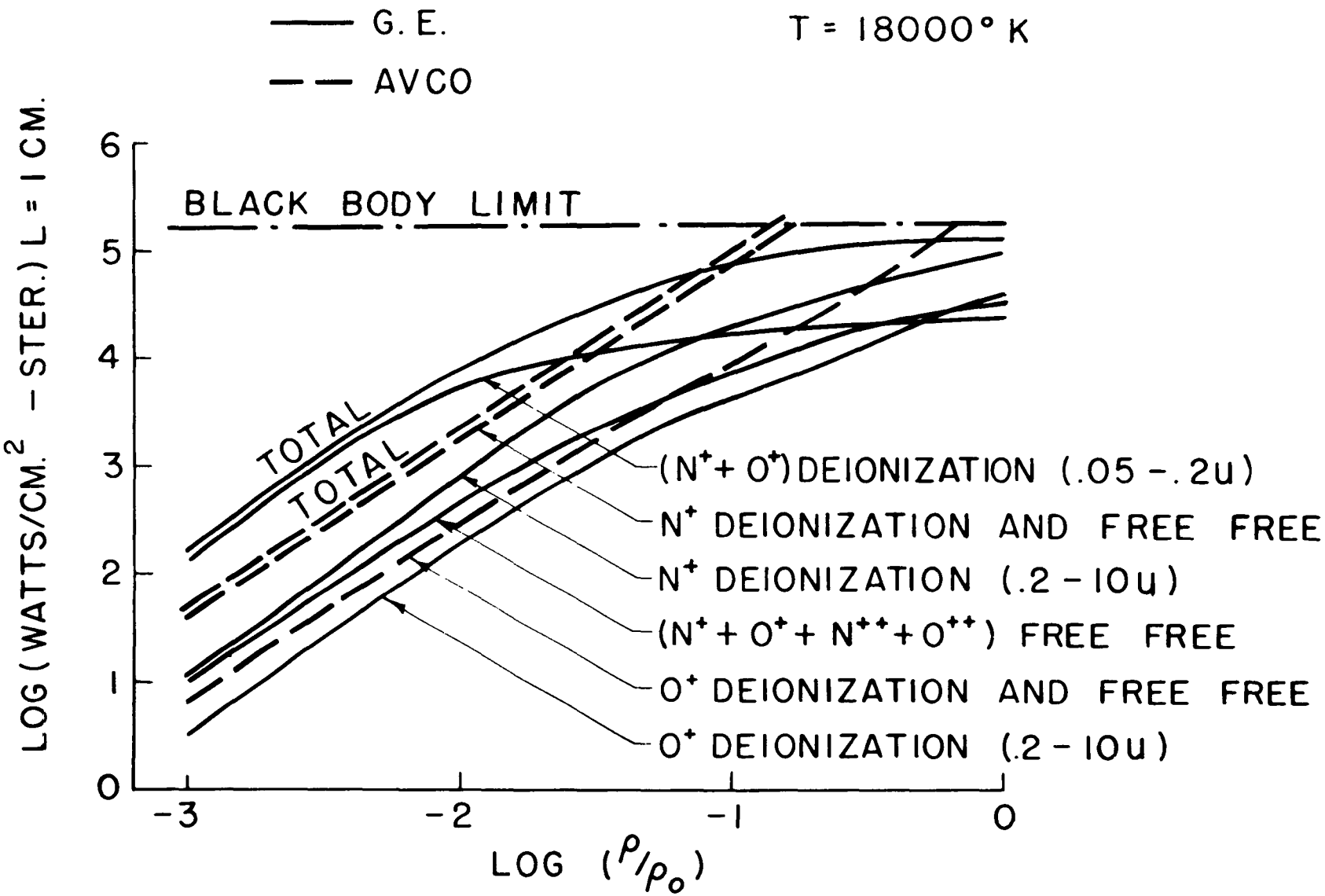

Figure 11. Spectral Radiance of Equilibrium Air (1000 - 100,000A)

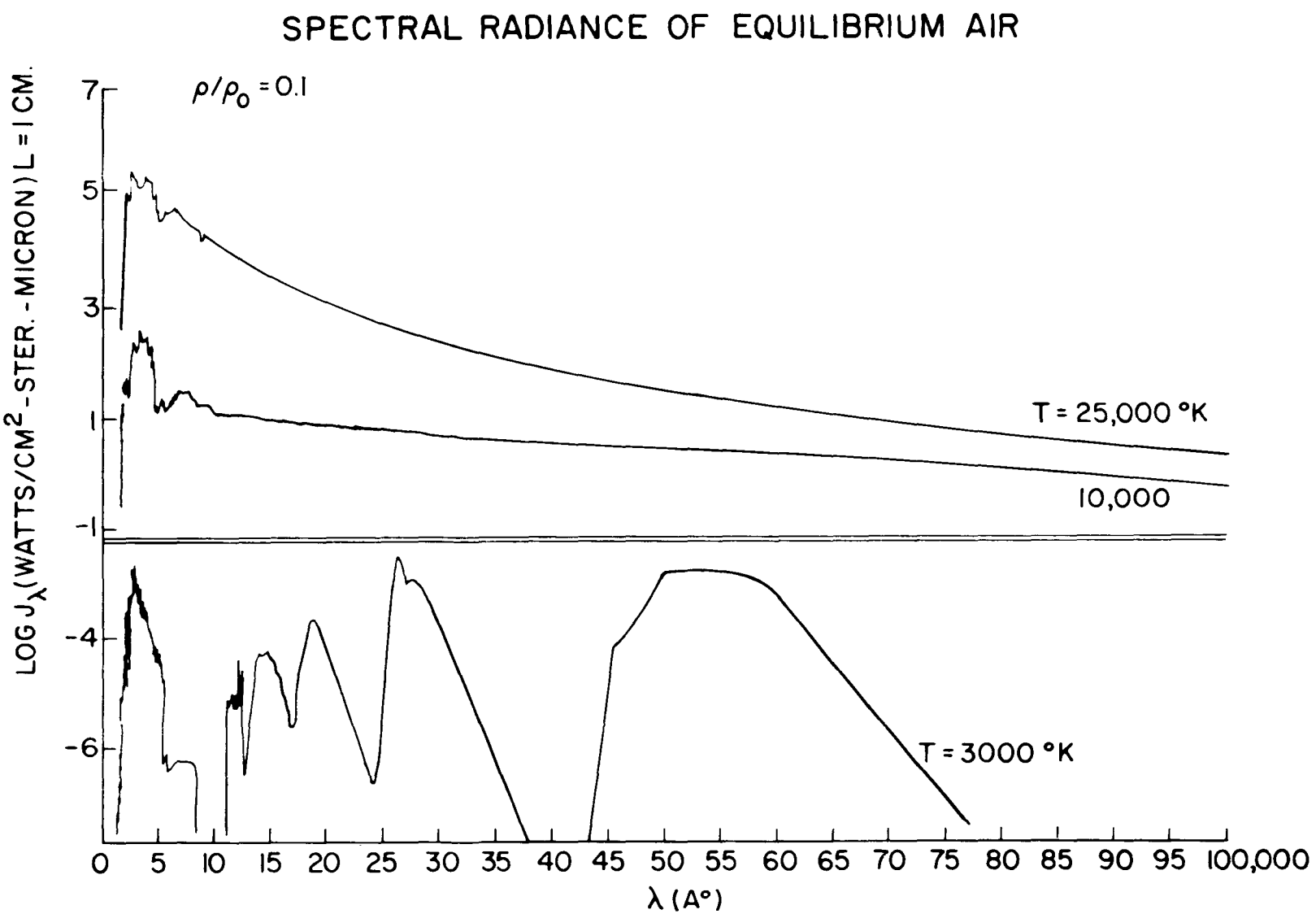

Figure 12. Spectral Radiance of Equilibrium Air (1000 - 13,000A)

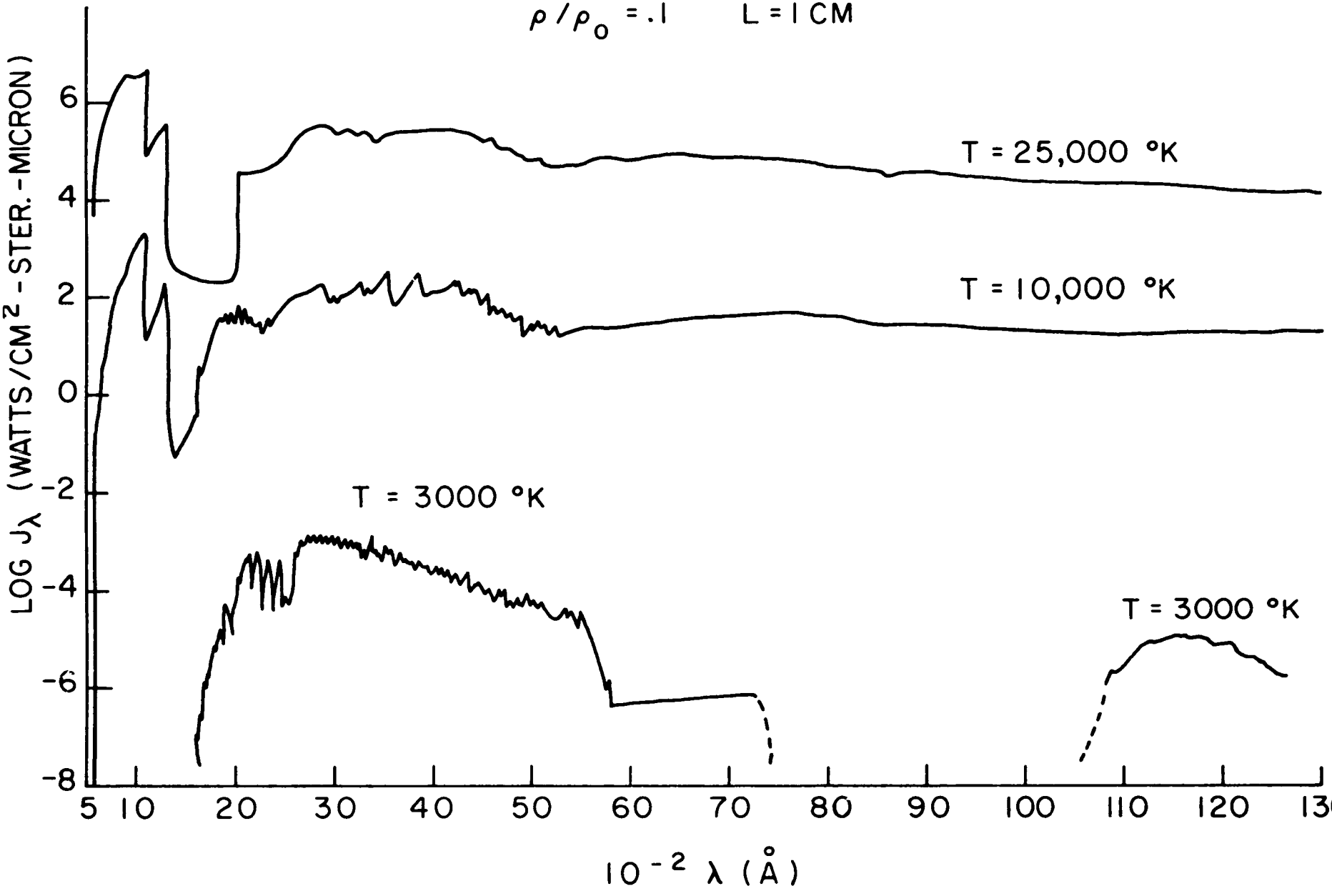

Figure 13. Comparison of Predictions: Spectral Radiance of Equilibrium Air (8000°K)

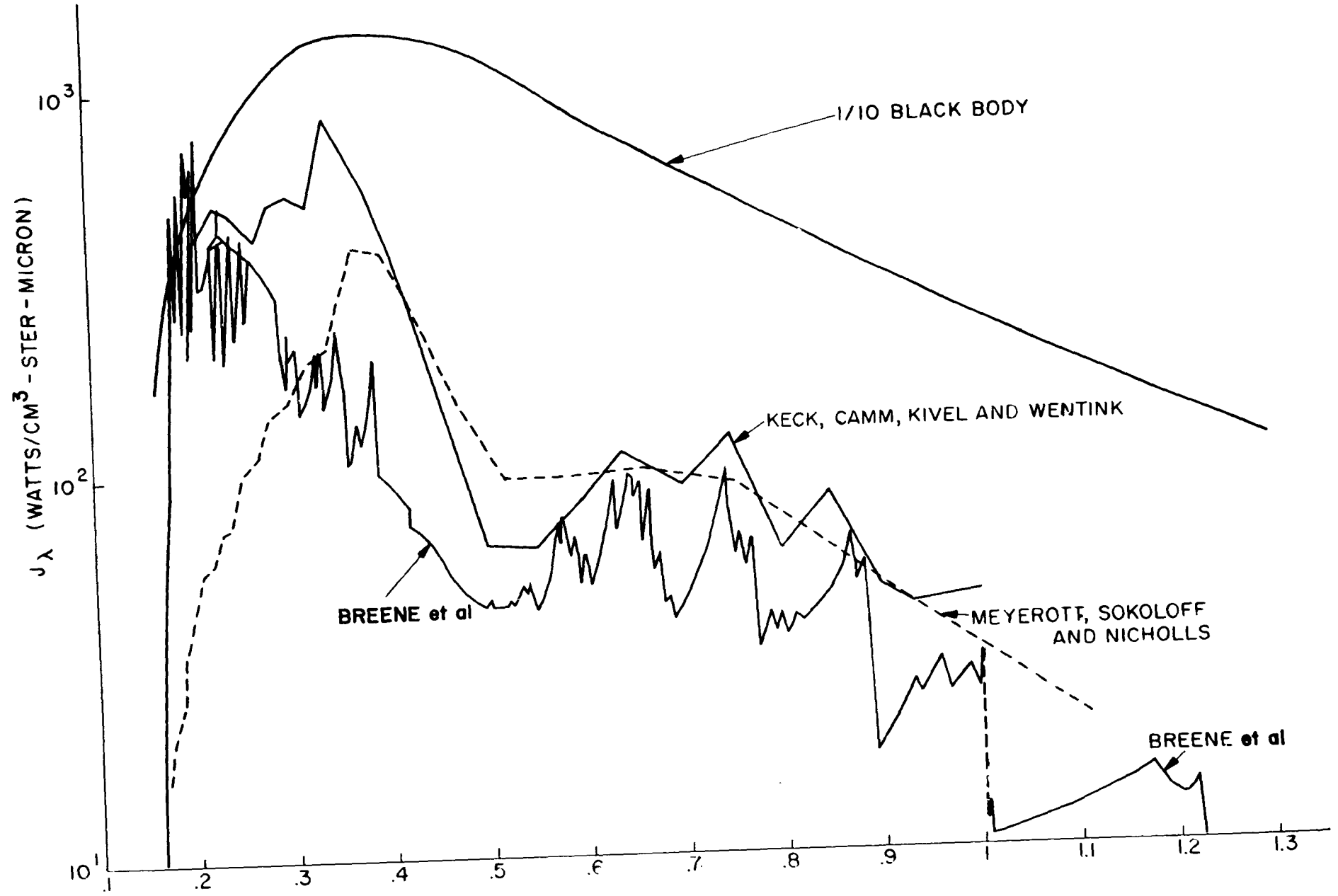

Figure 14. Comparison of Predictions: Spectral Absorption Coefficients of Equilibrium Air (12,000°K)

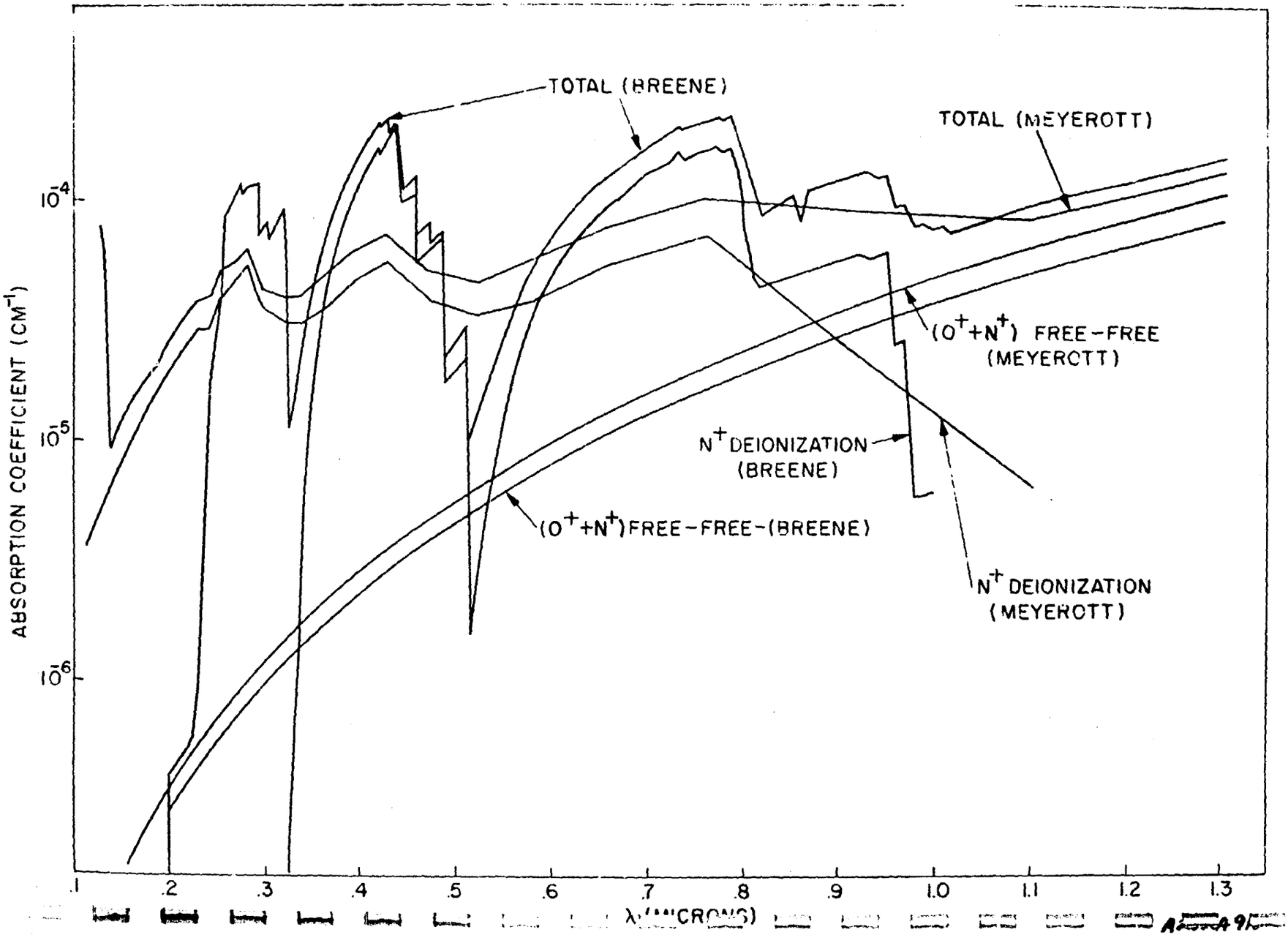

Figure 15. Radiance of O_2 Schumann-Runge Bands (3000°K - 9000°K)

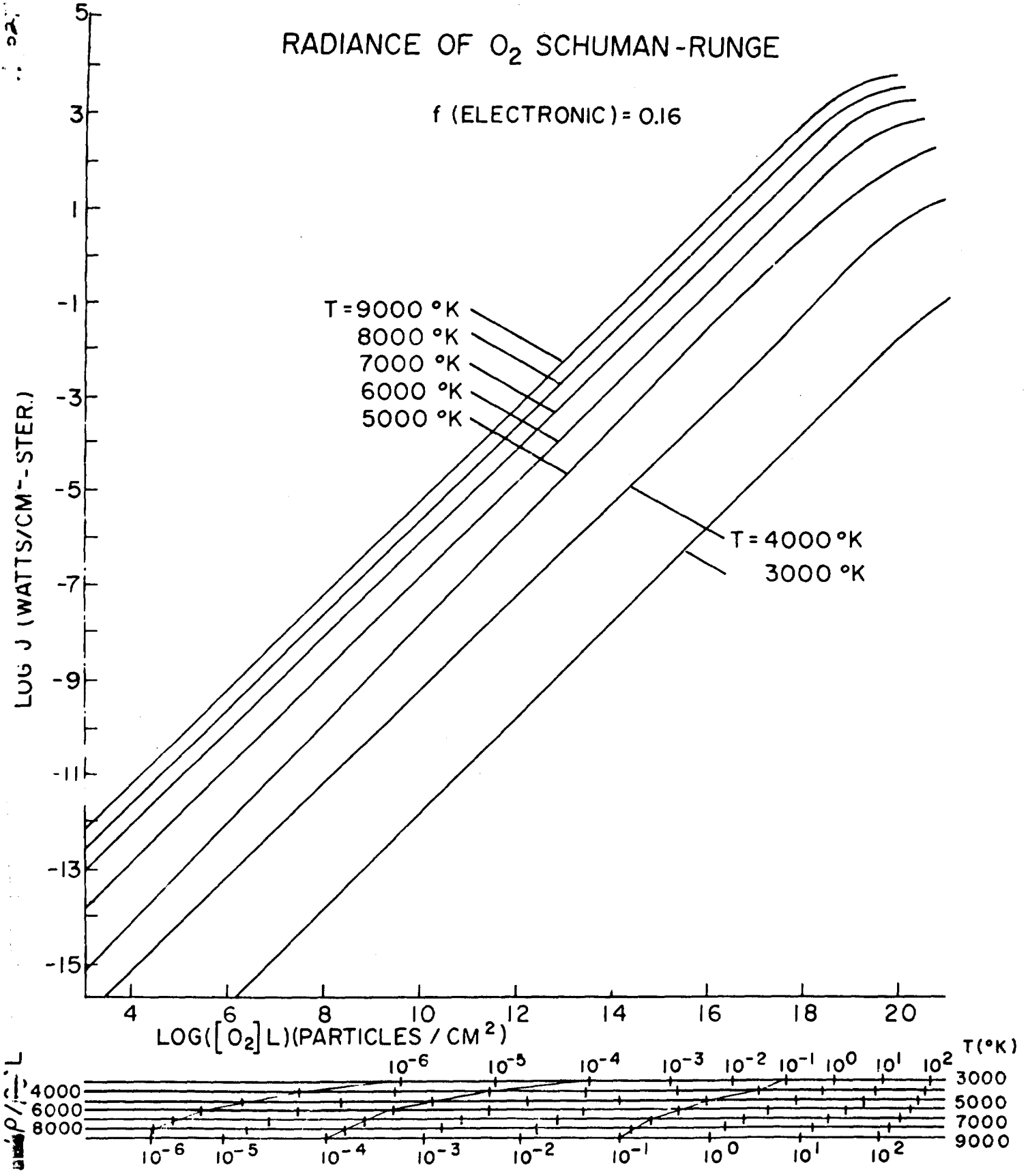

Figure 16. Radiance of O_2 Schumann-Runge Bands (10,000°K - 25,000°K)

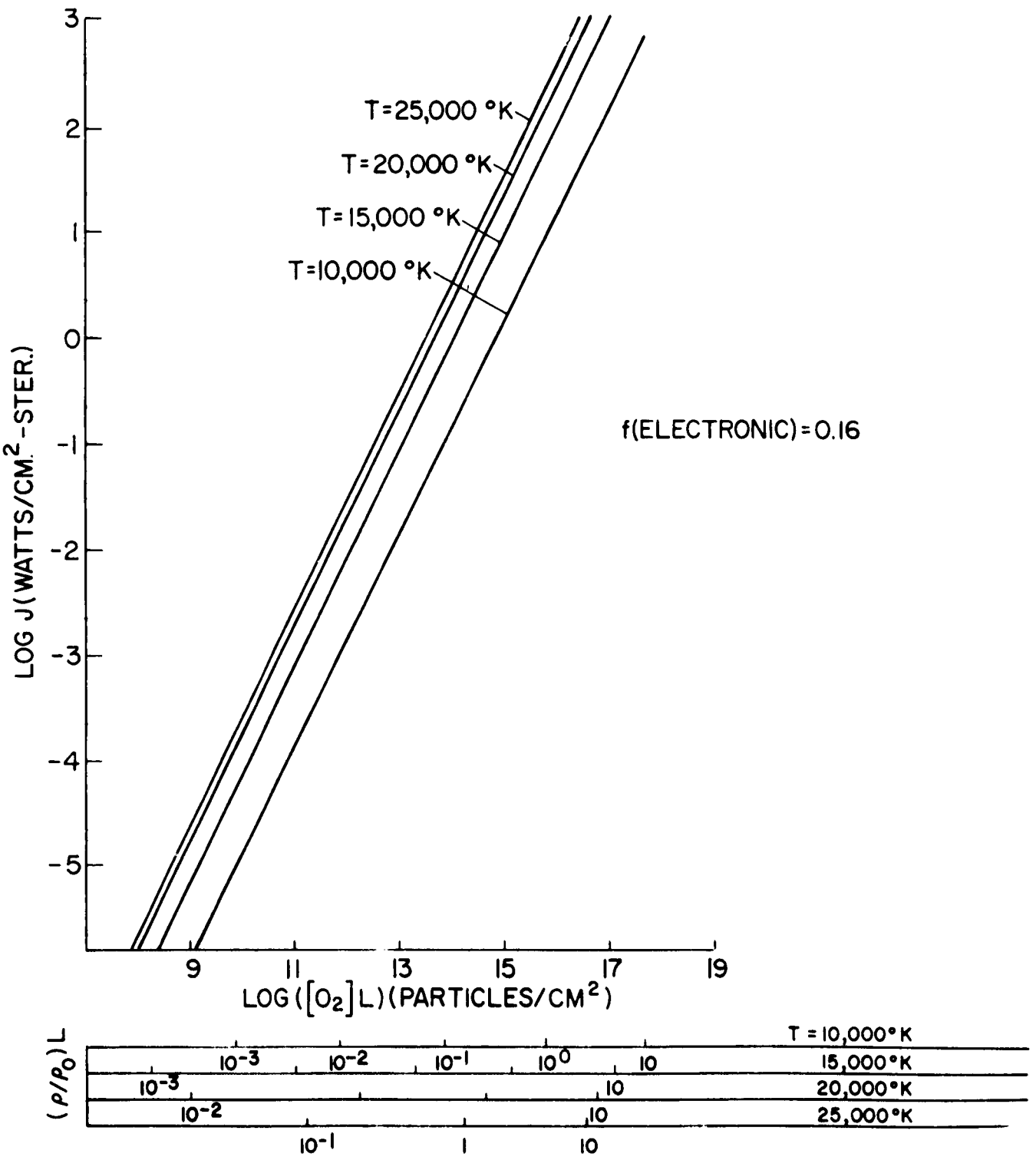

Figure 17. Radiance of O_2 Schumann-Runge Bands (O_2 Density 10^4 - 10^{18})

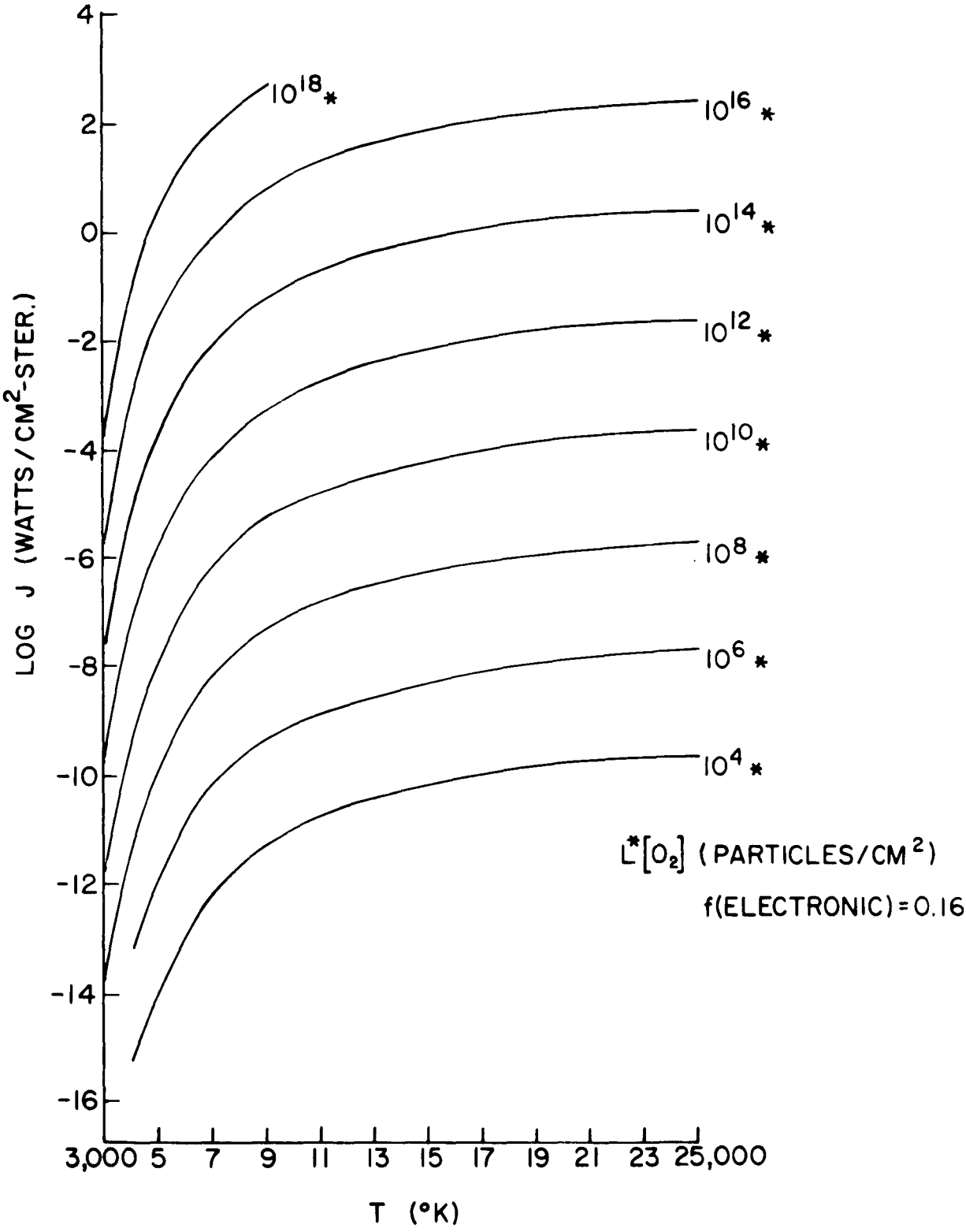

A202A5033

Figure 18. Comparison of Predictions: Radiance of O_2 Schumann-Runge Bands

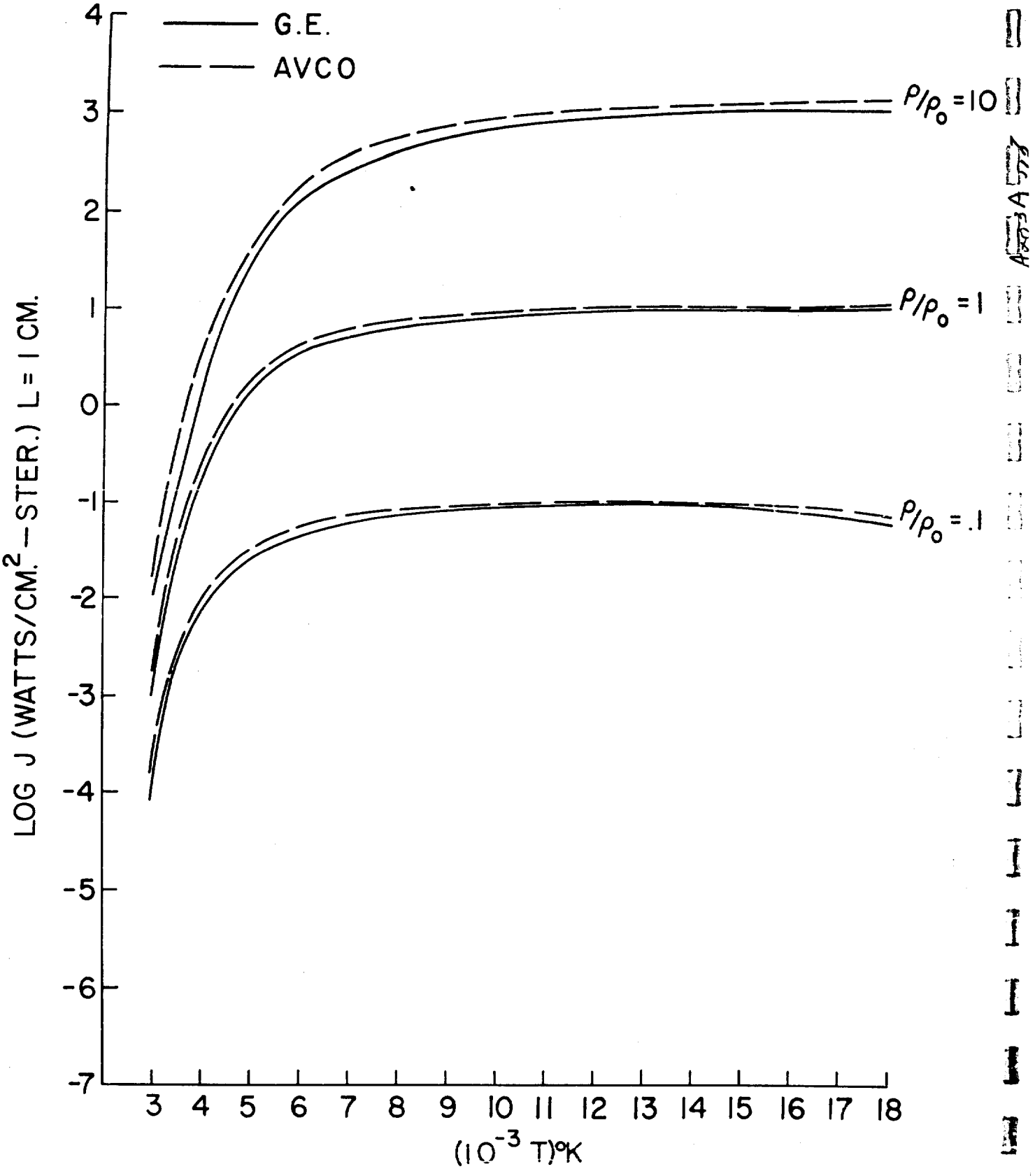

Figure 19. Spectral Radiance of O_2 Schumann-Runge Bands

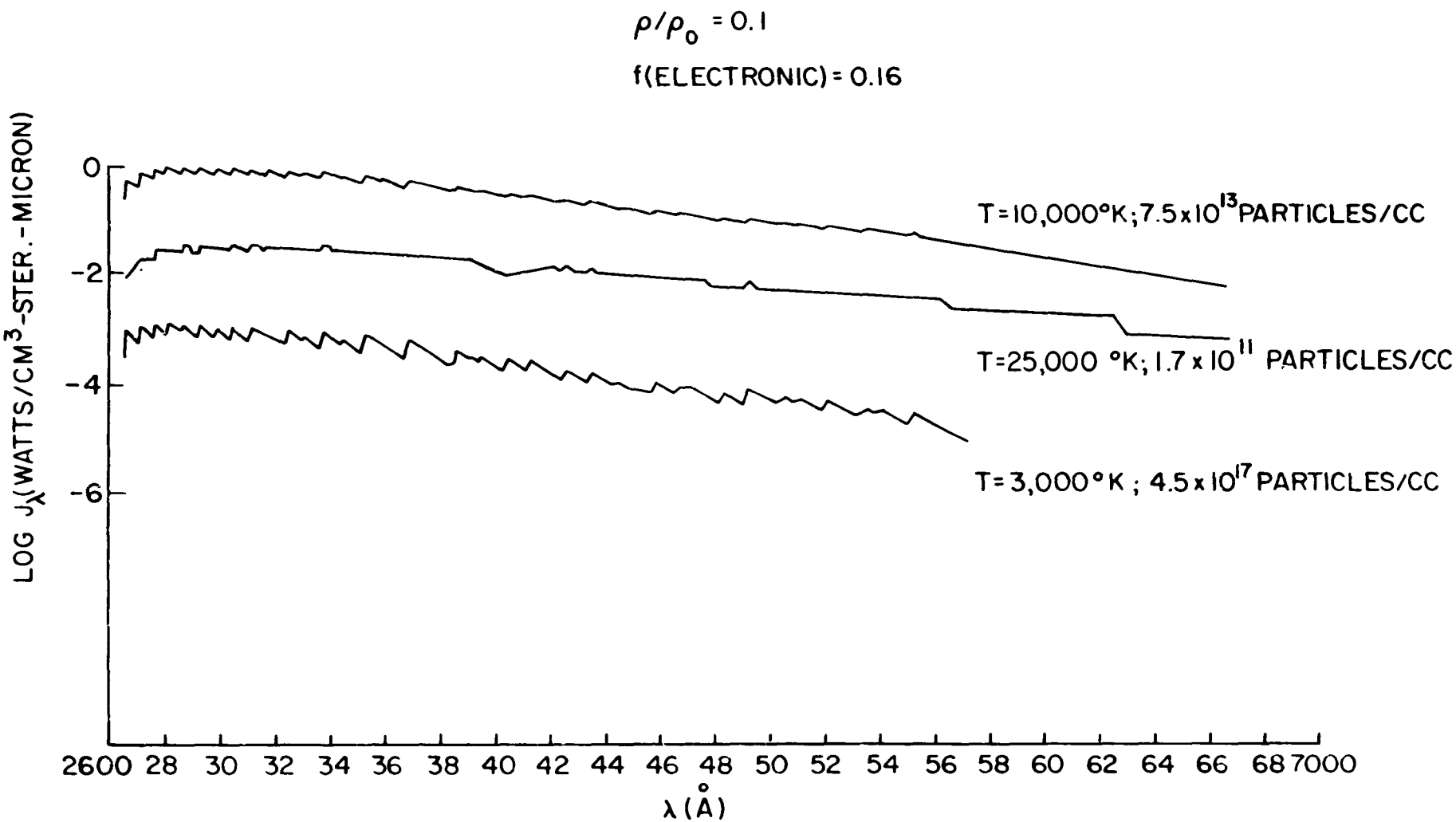

Figure 20. Radiance of N_2 First Positive Bands (3000°K - 9000°K)

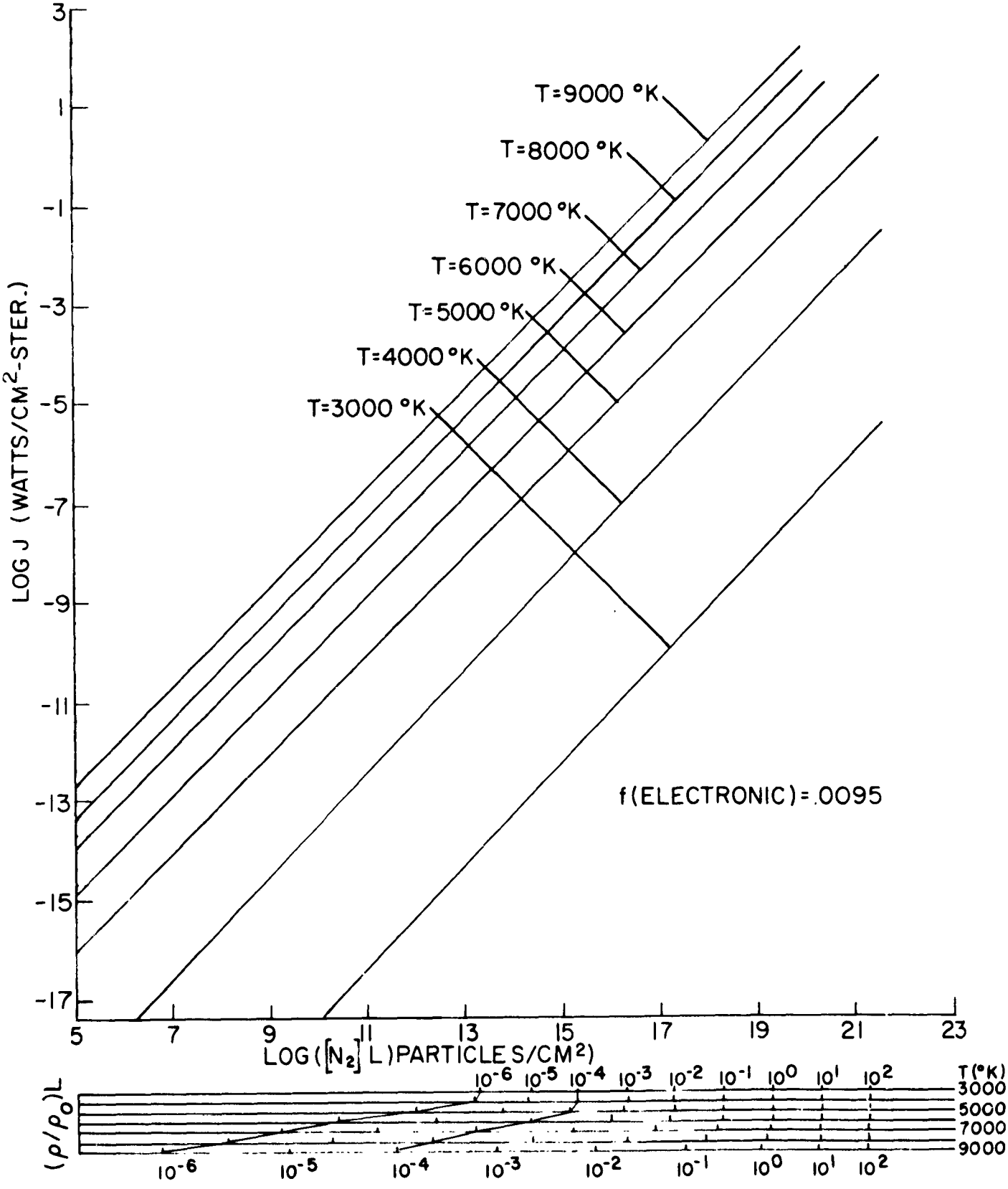

Figure 21. Radiance of N_2 First Positive Bands (10,000°K - 25,000°K)

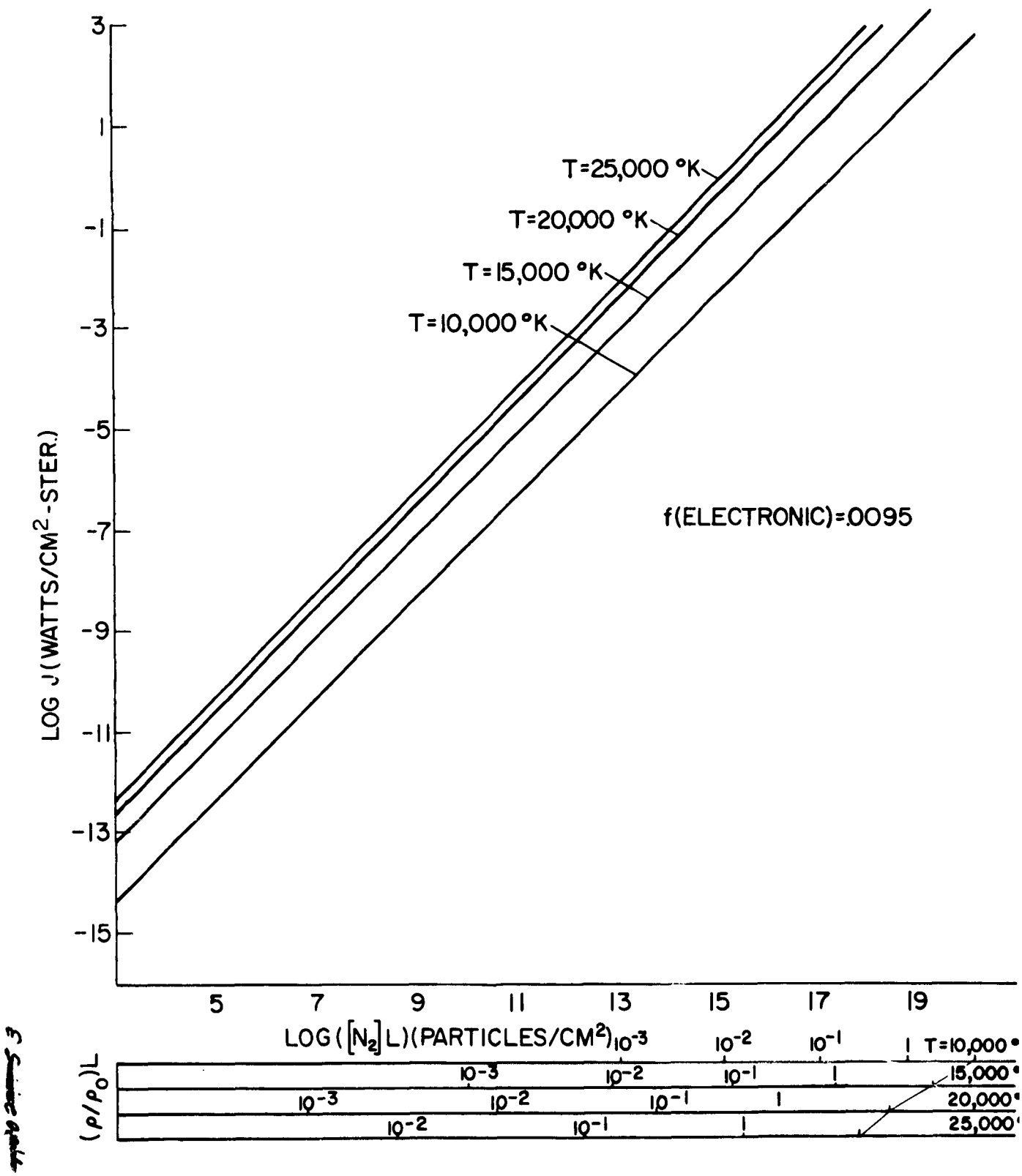

Figure 22. Radiance of N_2 First Positive Bands (N_2 Density 10^5 - 10^{21})

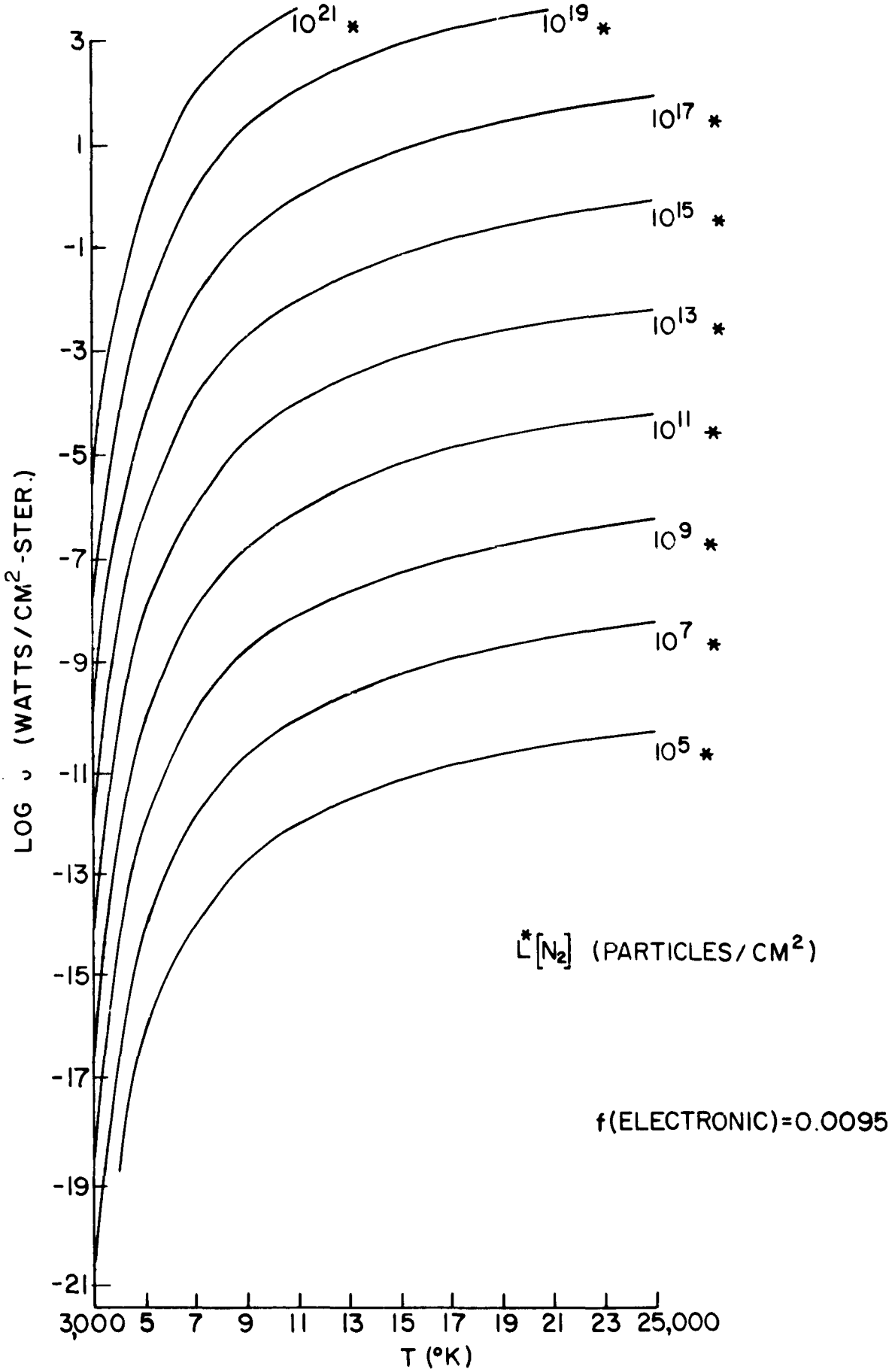

Figure 23. Comparison of Predictions: Radiance of N_2 First Positive Bands

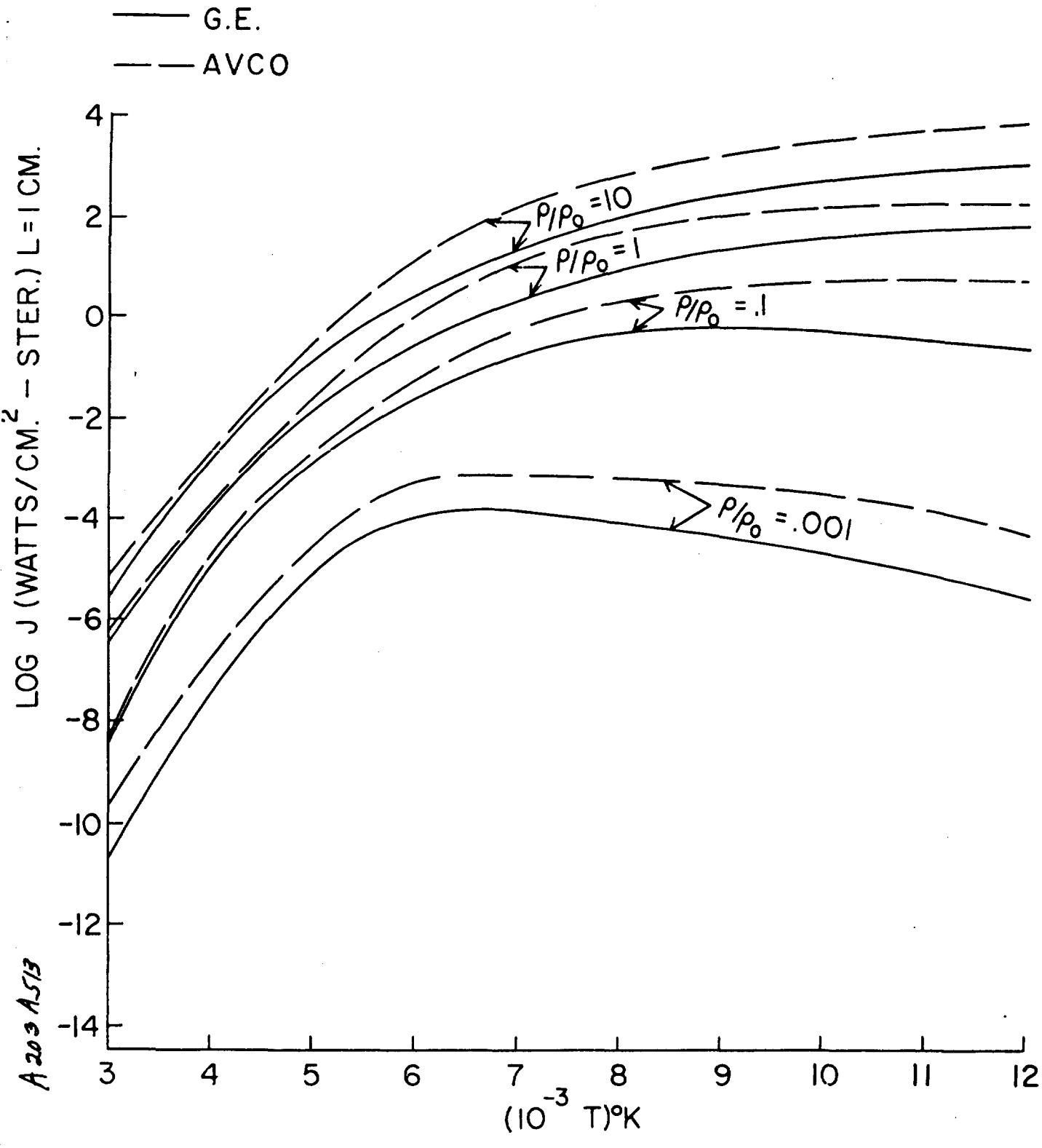

Figure 24. Spectral Radiance of N_2 First Positive Bands

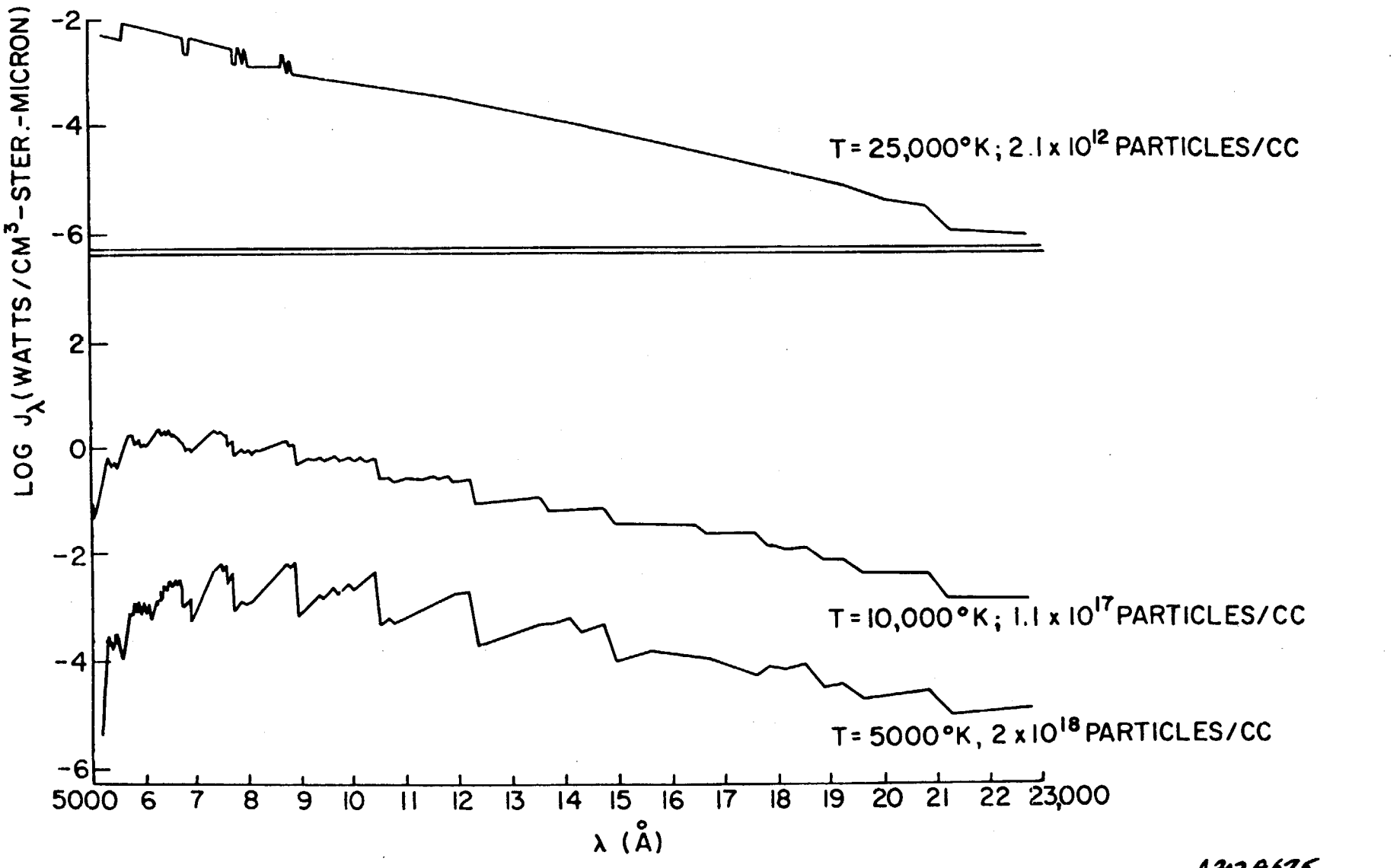

A202A675

Figure 25. Radiance of N_2 Second Positive Bands (4000°K - 9000°K)

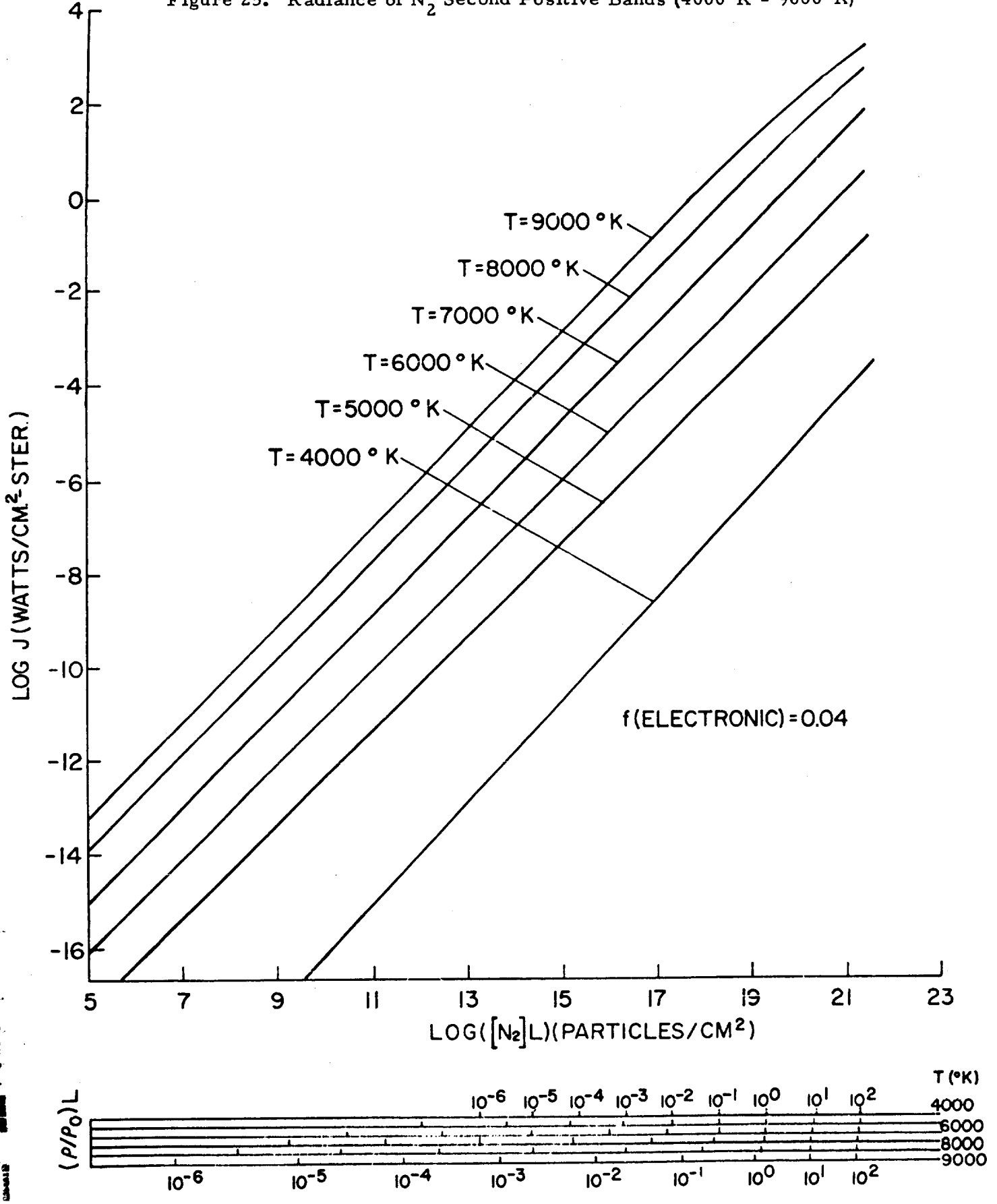

Figure 26. Radiance of N_2 Second Positive Bands (10,000°K - 25,000°K)

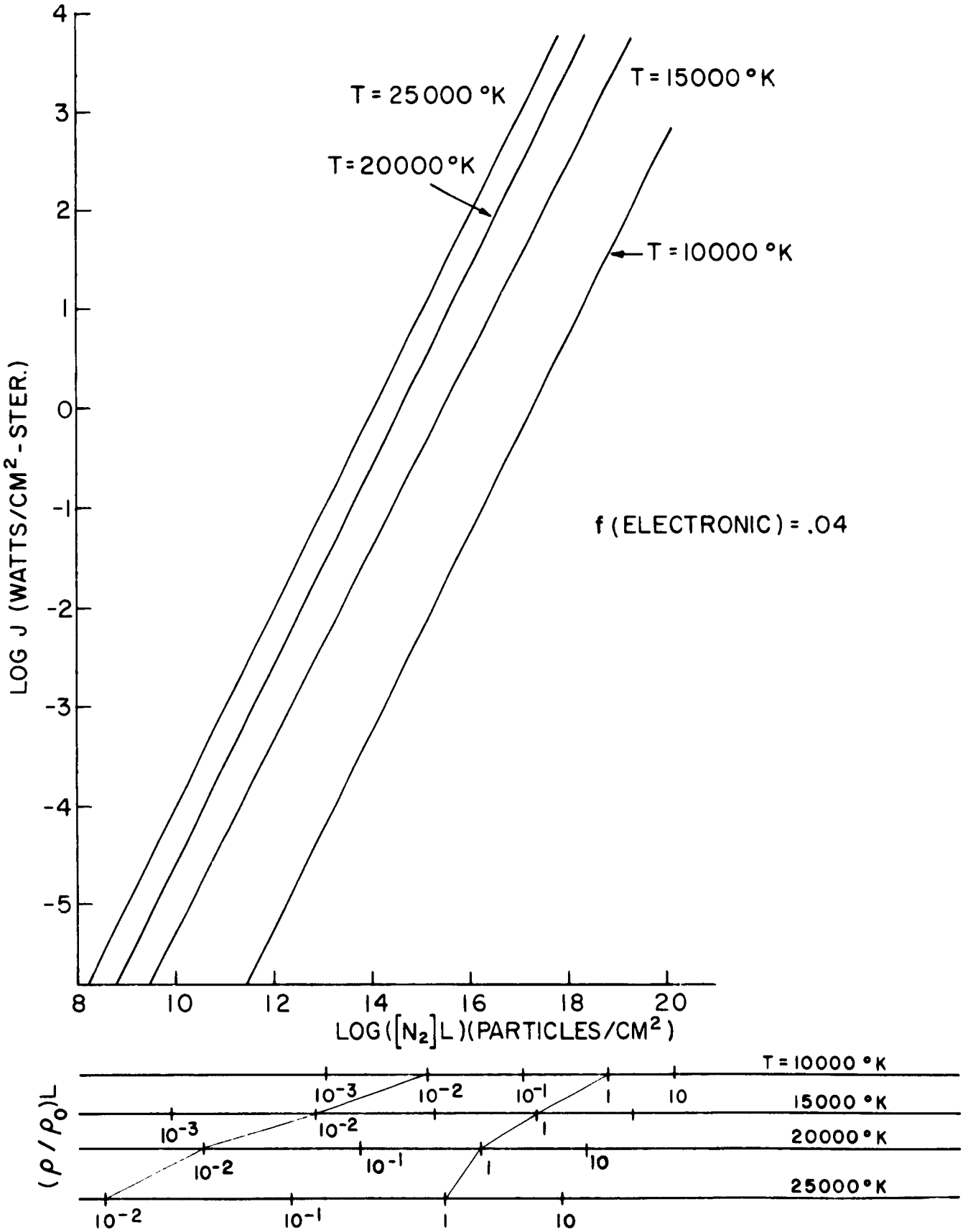

Figure 27. Radiance of N_2 Second Positive Bands (N_2 Density 10^8 - 10^{20})

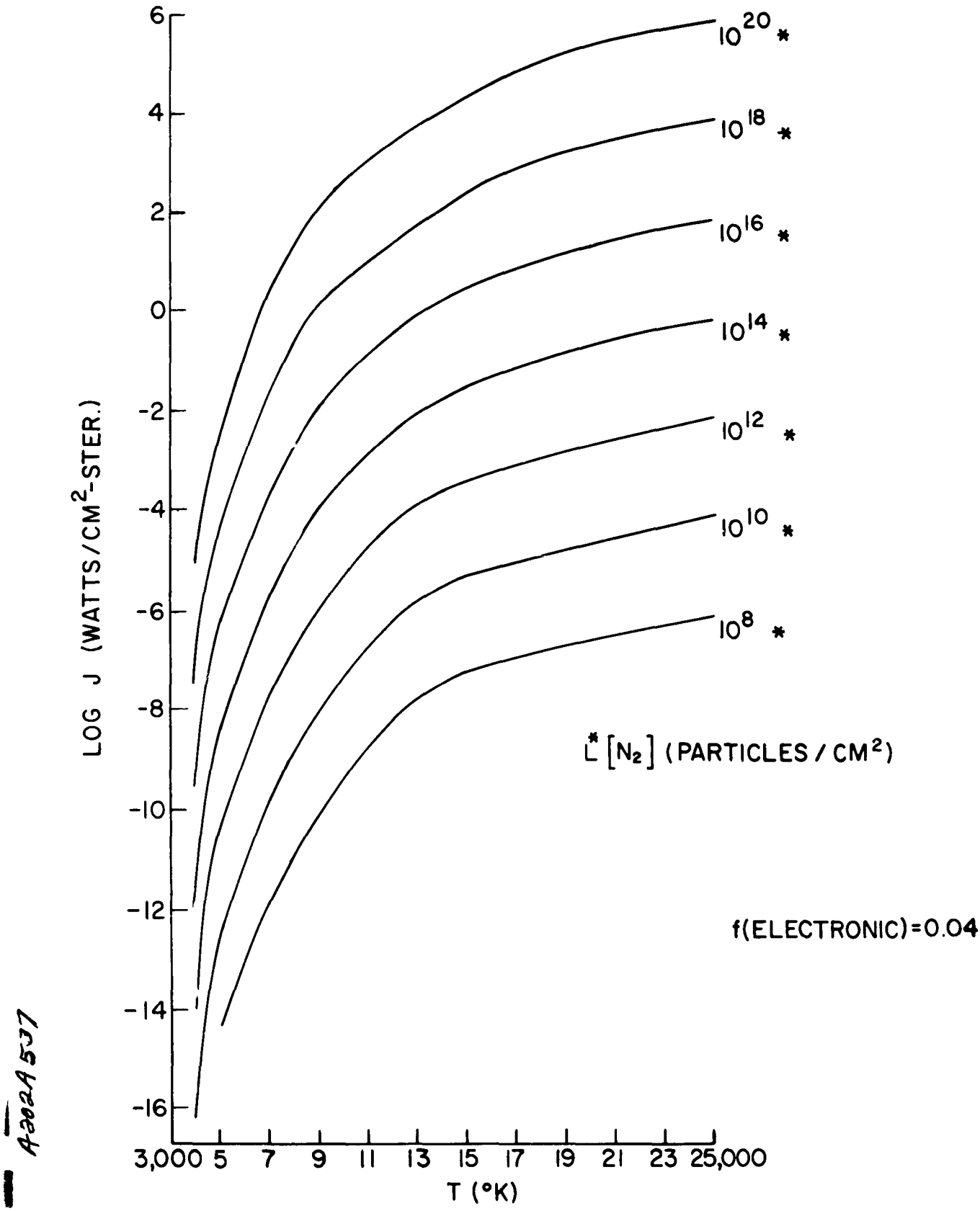

A2029537

Figure 28. Comparison of Predictions: Radiance of N_2 Second Positive Bands

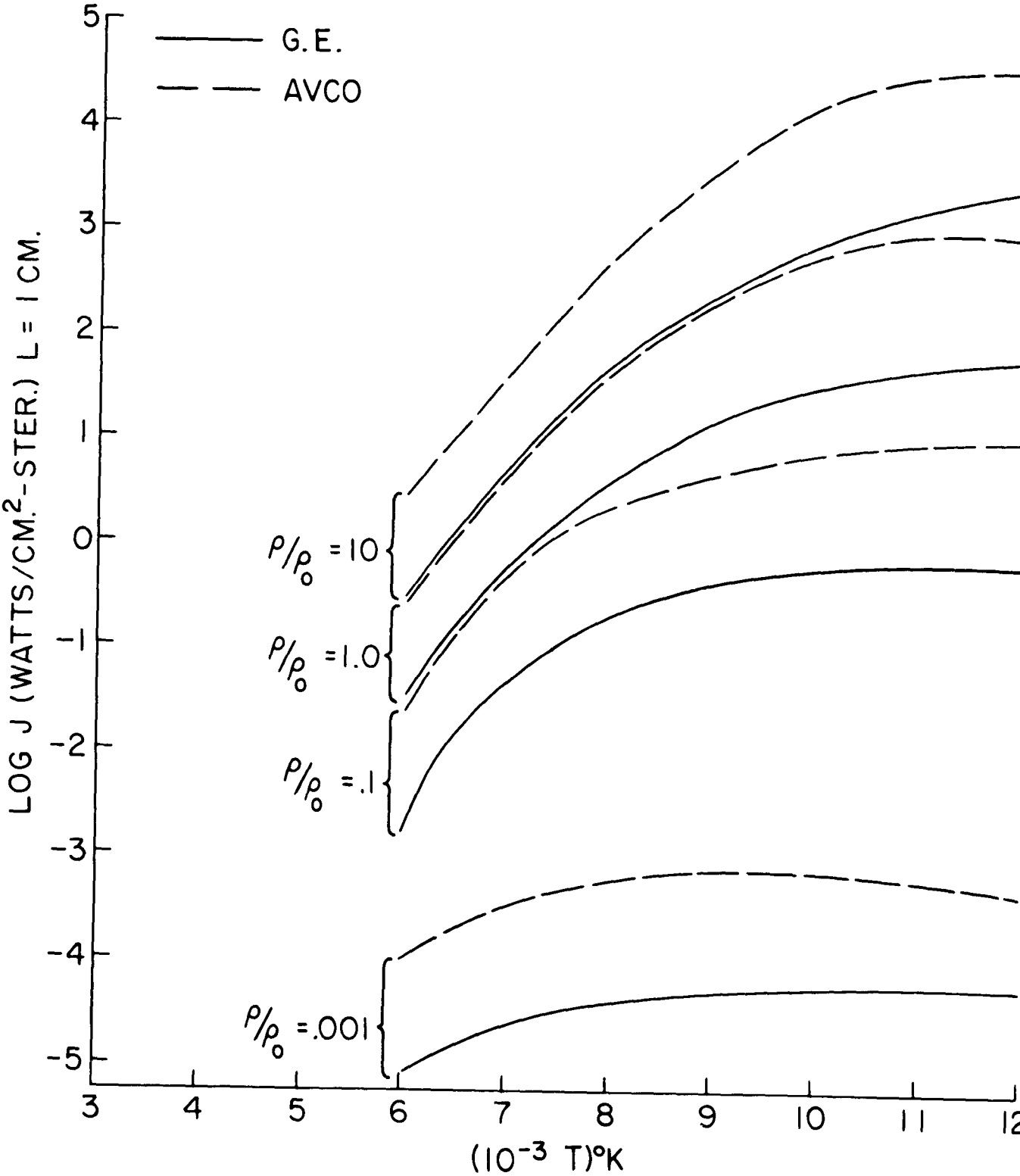

Figure 29. Spectral Radiance of N_2 Second Positive Bands

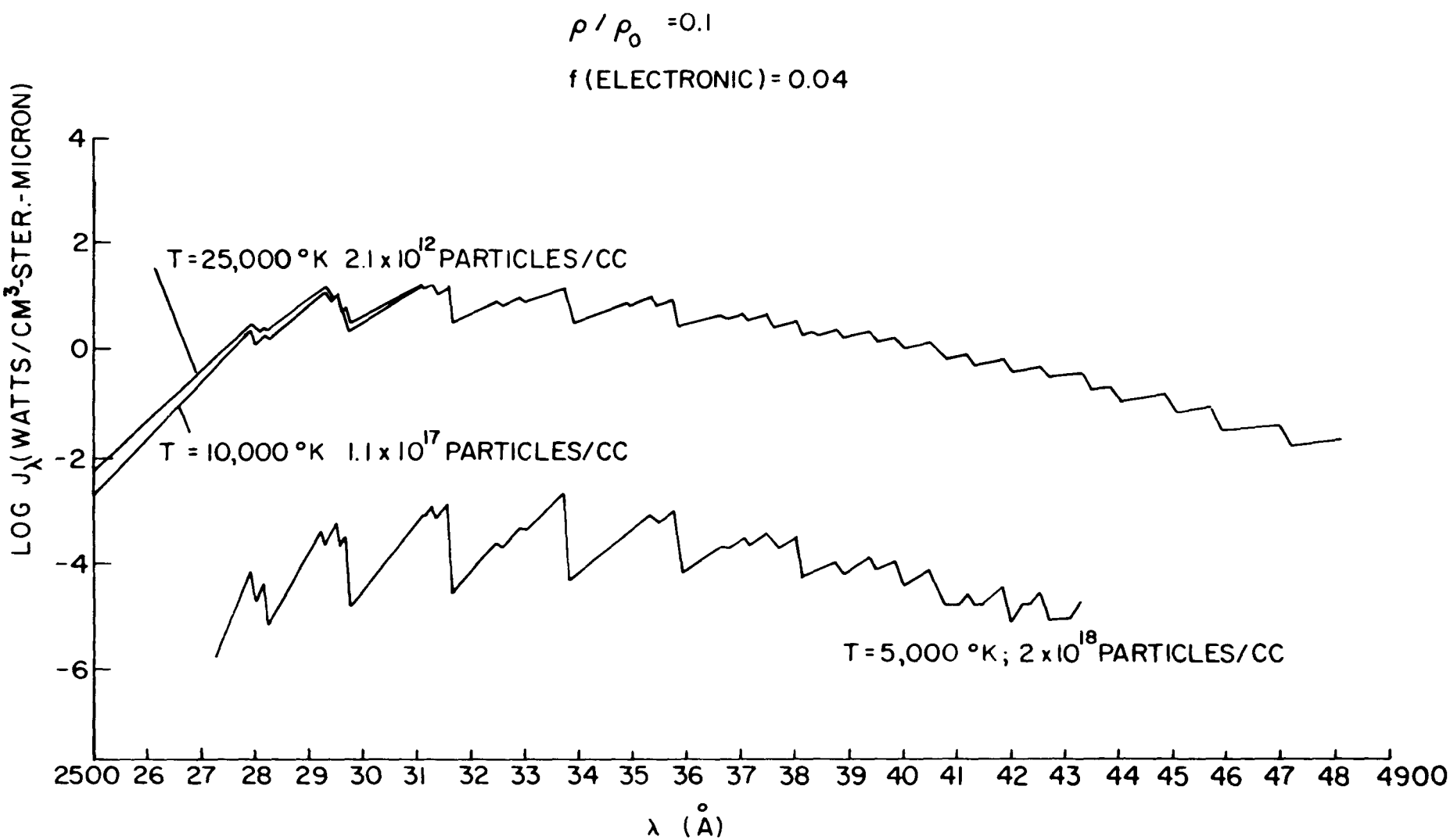

Figure 30. Radiance of N_2^+ First Negative Bands (4000°K - 9000°K)

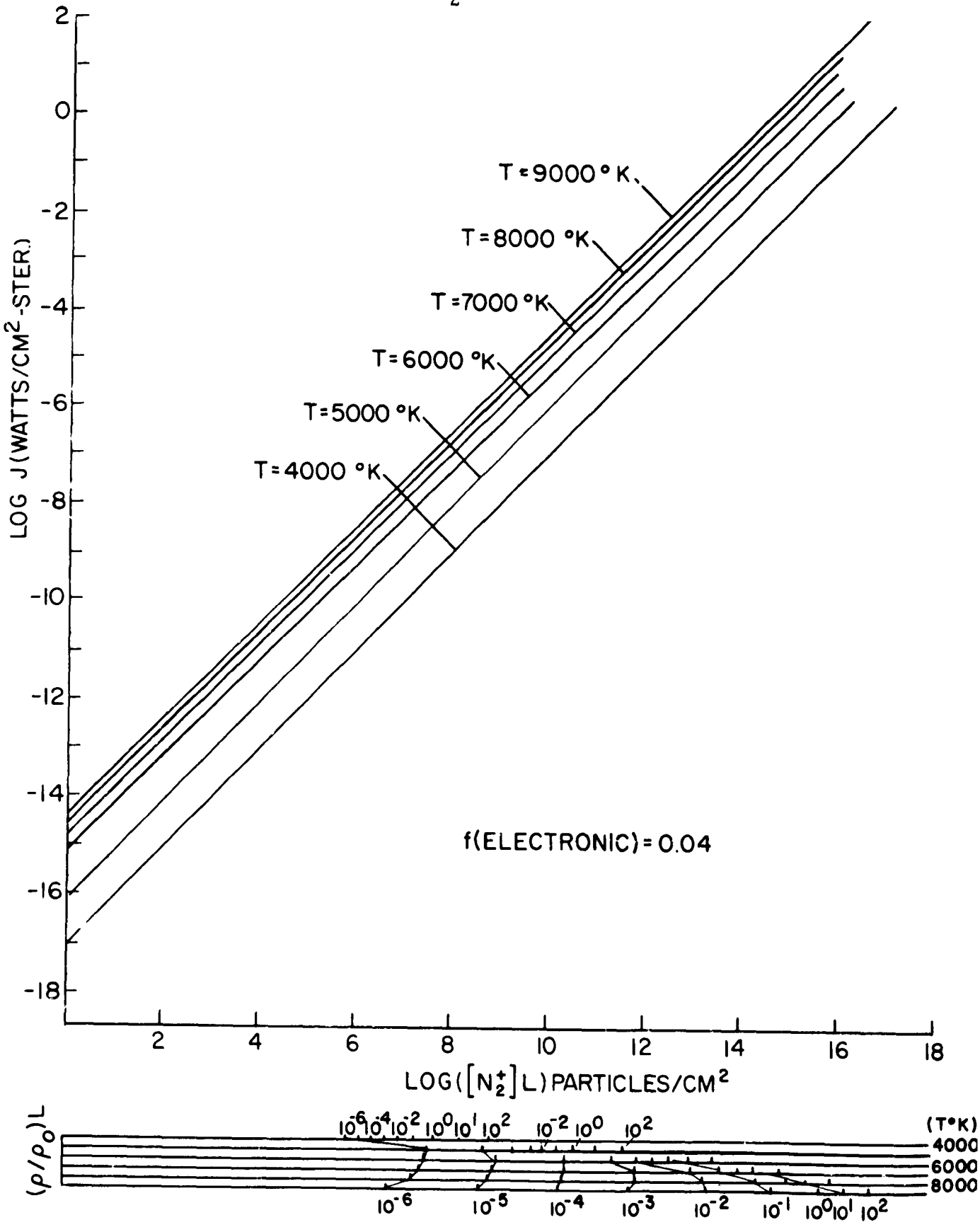

Figure 31. Radiance of N_2^+ First Negative Bands (10,000°K - 25,000°K)

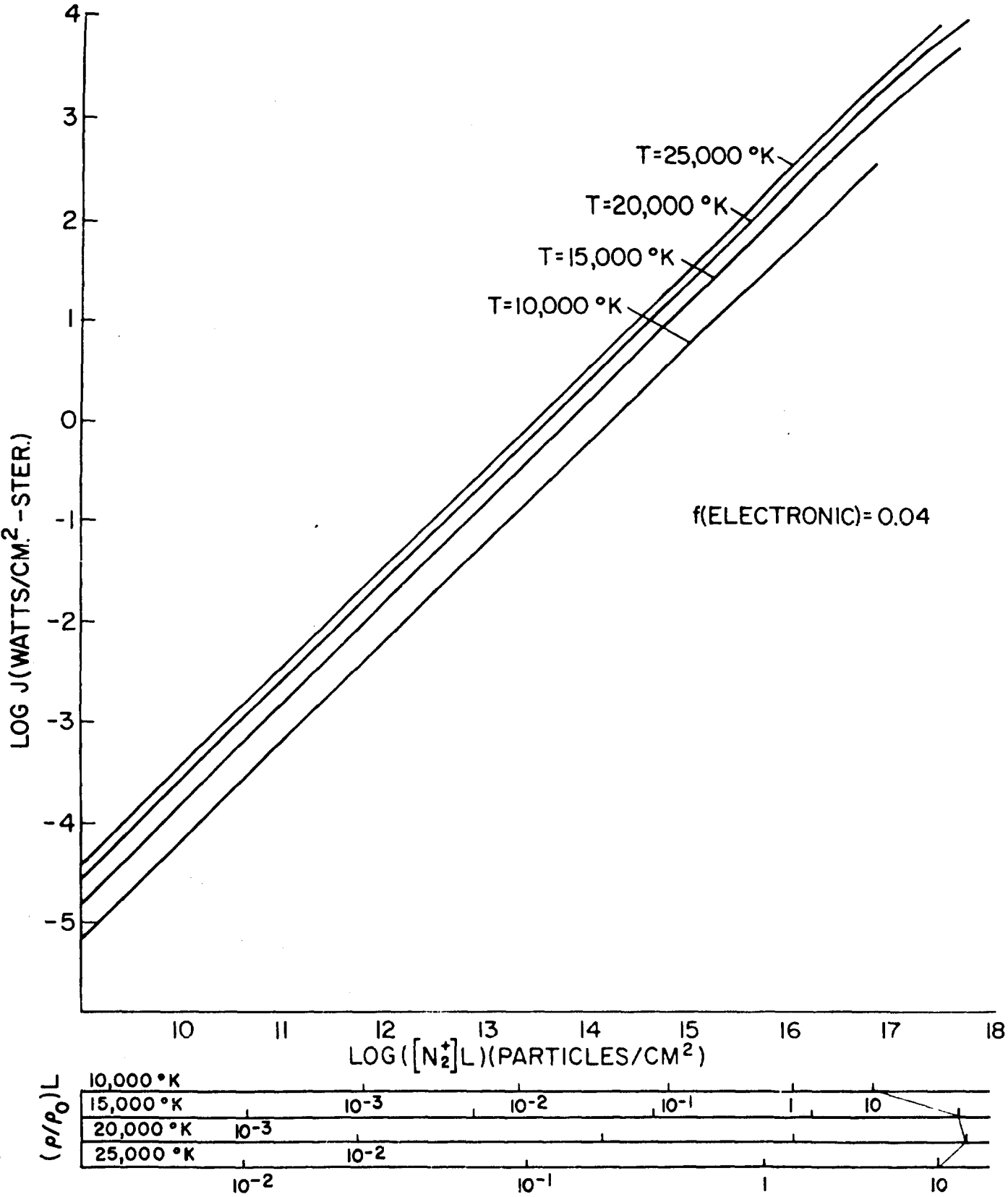

Figure 32. Radiance of N_2^+ First Negative Bands (N_2^+ Density 10^2 - 10^{16})

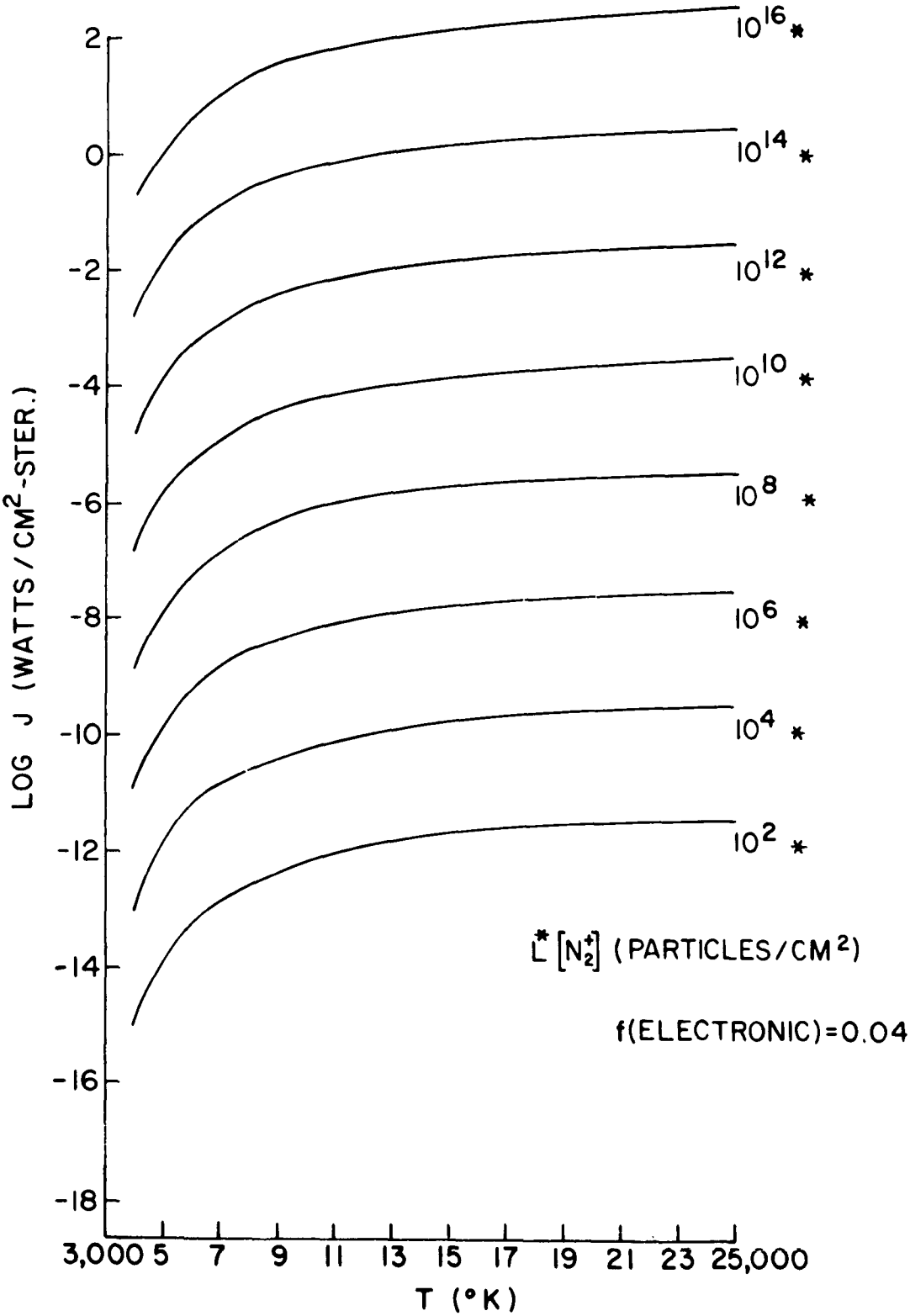

Figure 33. Comparison of Predictions: Radiance of N_2^+ First Negative Bands

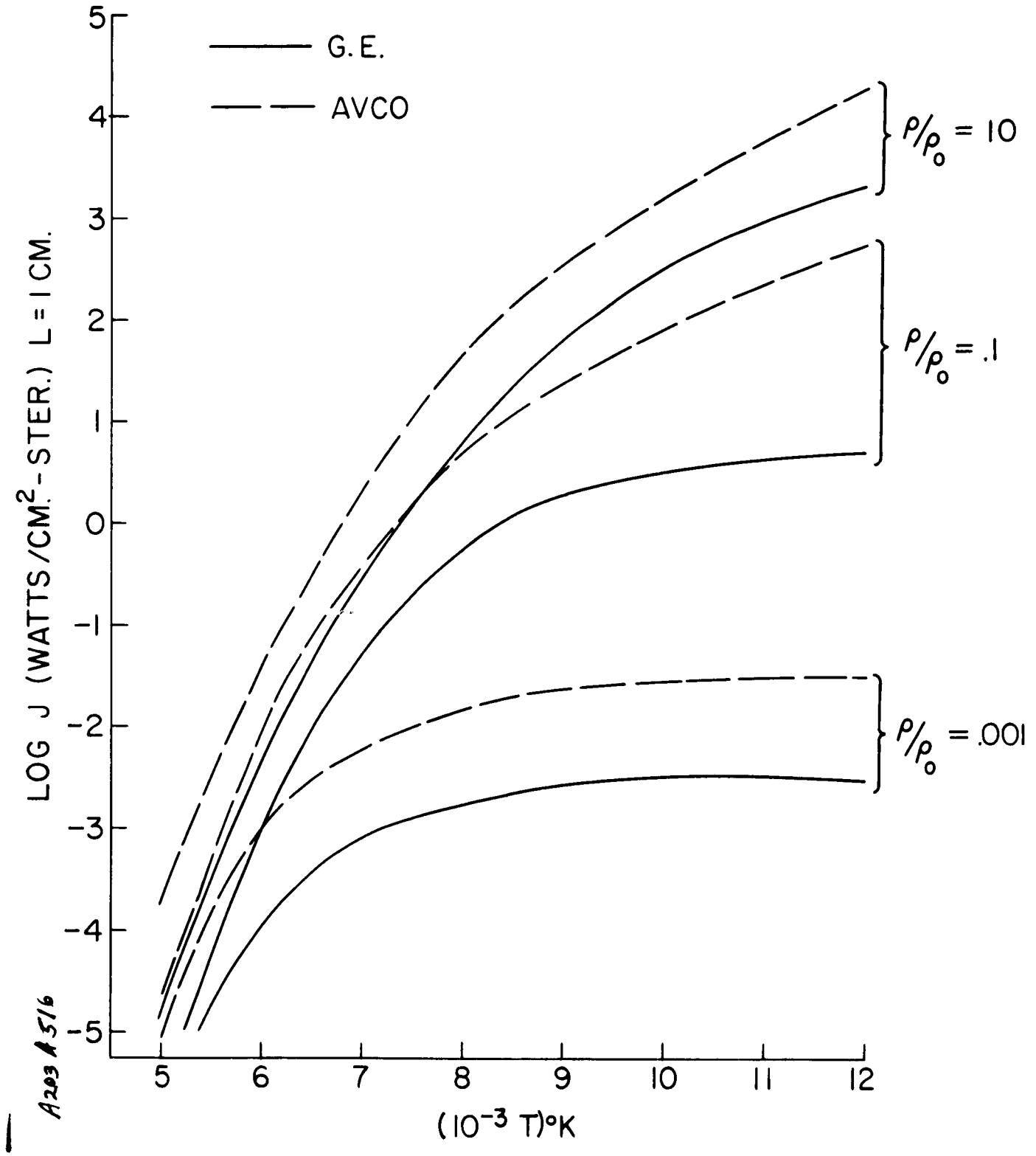

Figure 34. Spectral Radiance of N_2^+ First Negative Bands

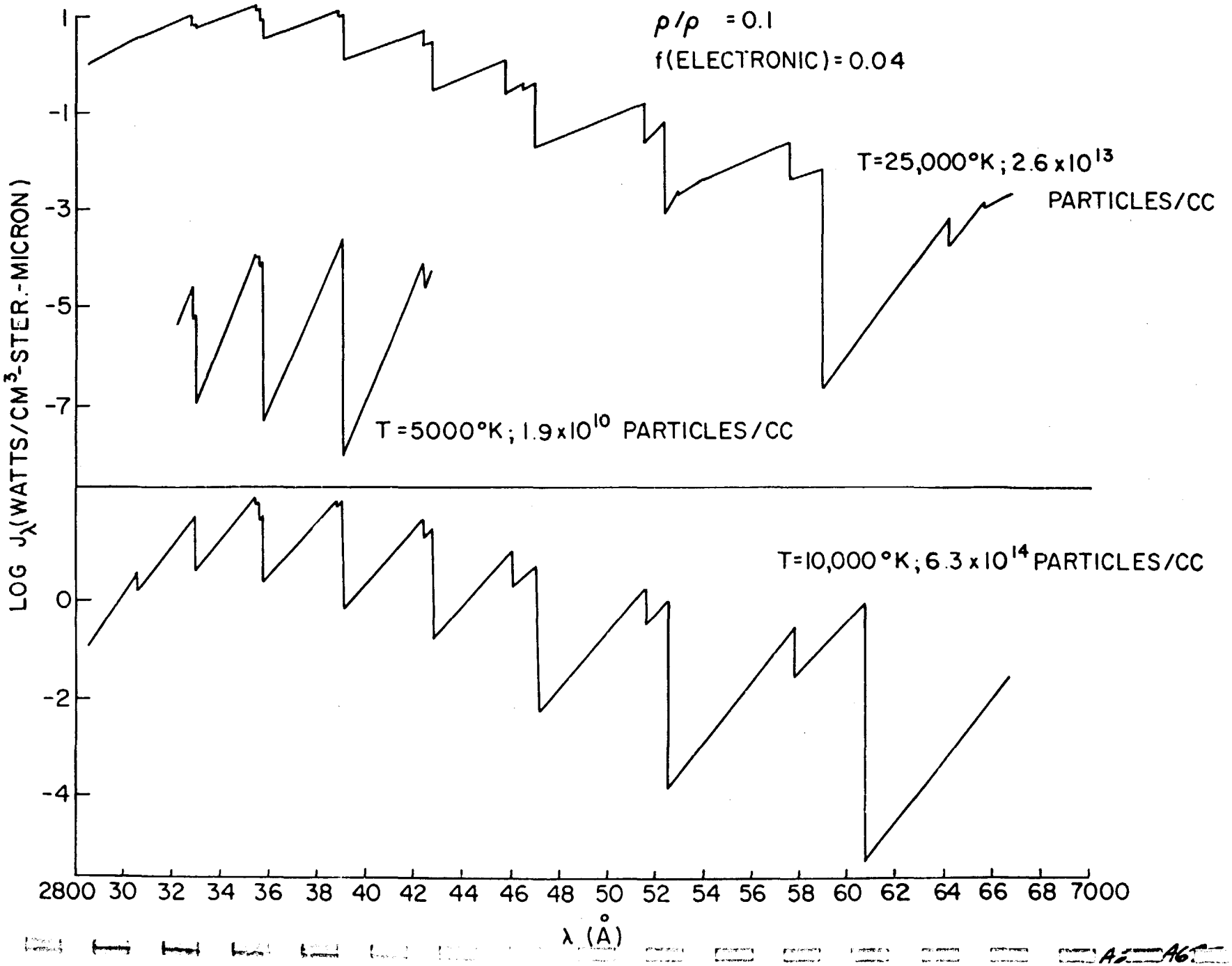

Figure 35. Radiance of NO Beta Bands (3000°K - 9000°K)

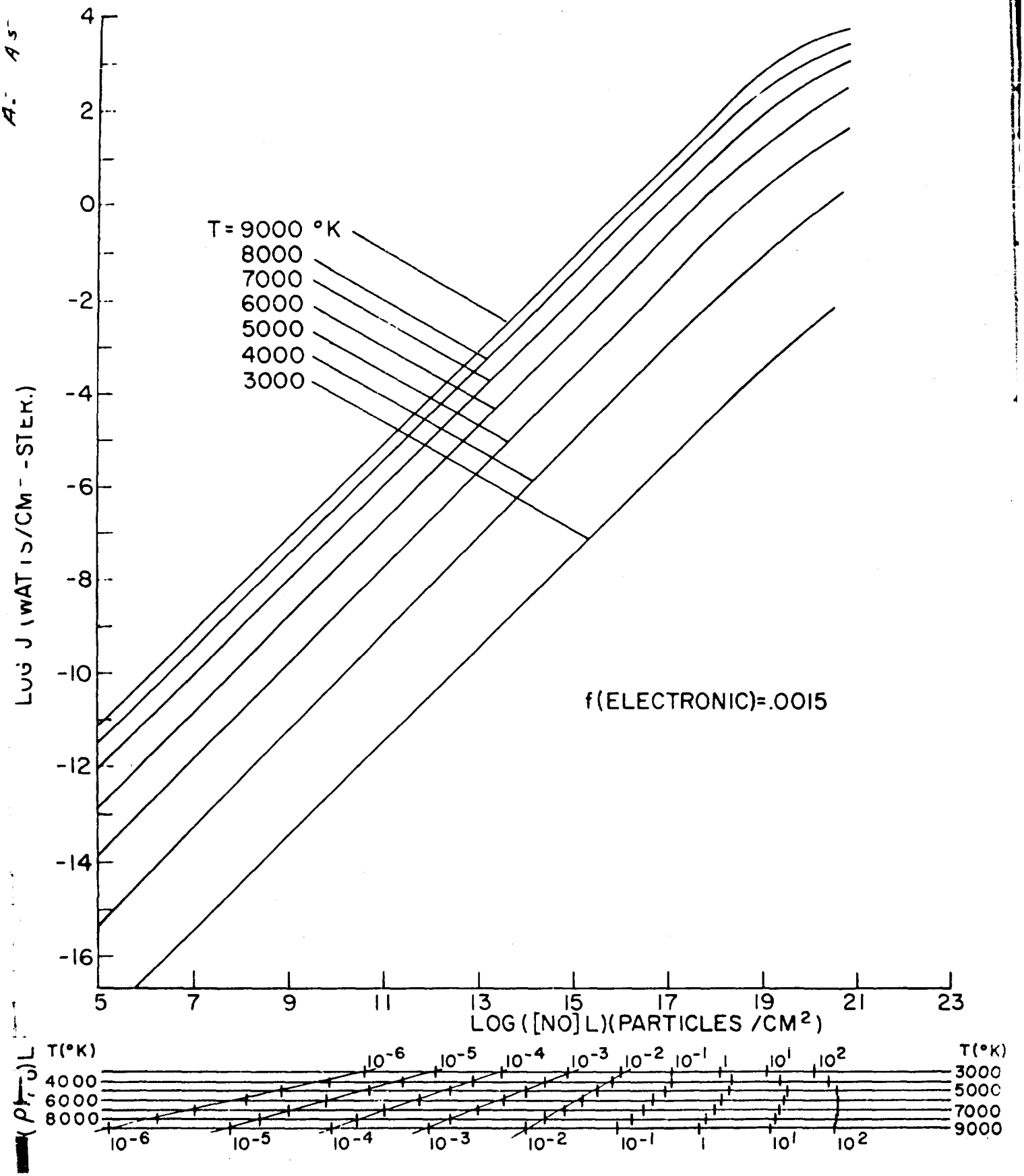

Figure 36. Radiance of NO Beta Bands (10,000°K - 25,000°K)

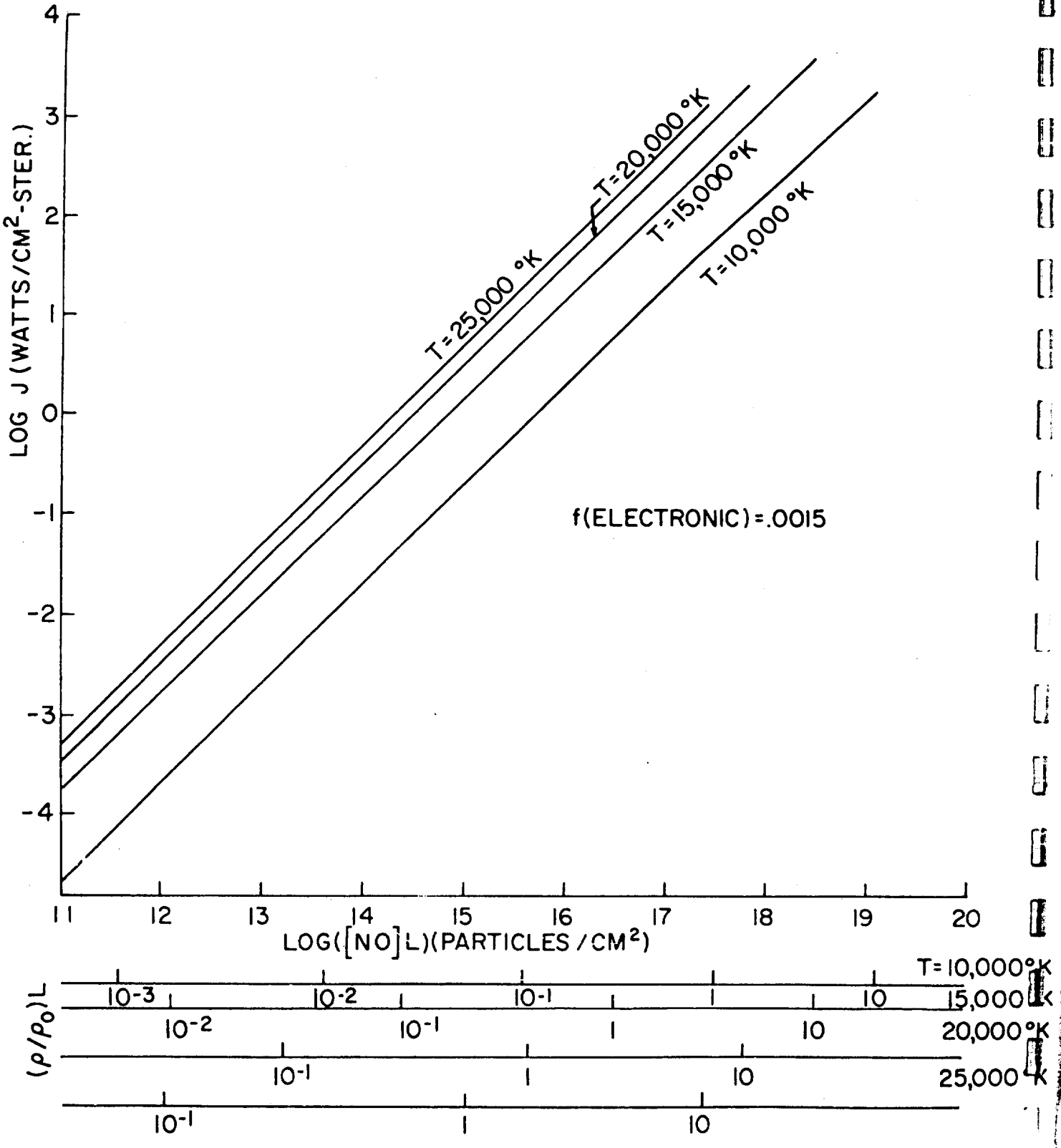

Figure 37. Radiance of NO Beta Bands (NO Density 10^5 - 10^{19})

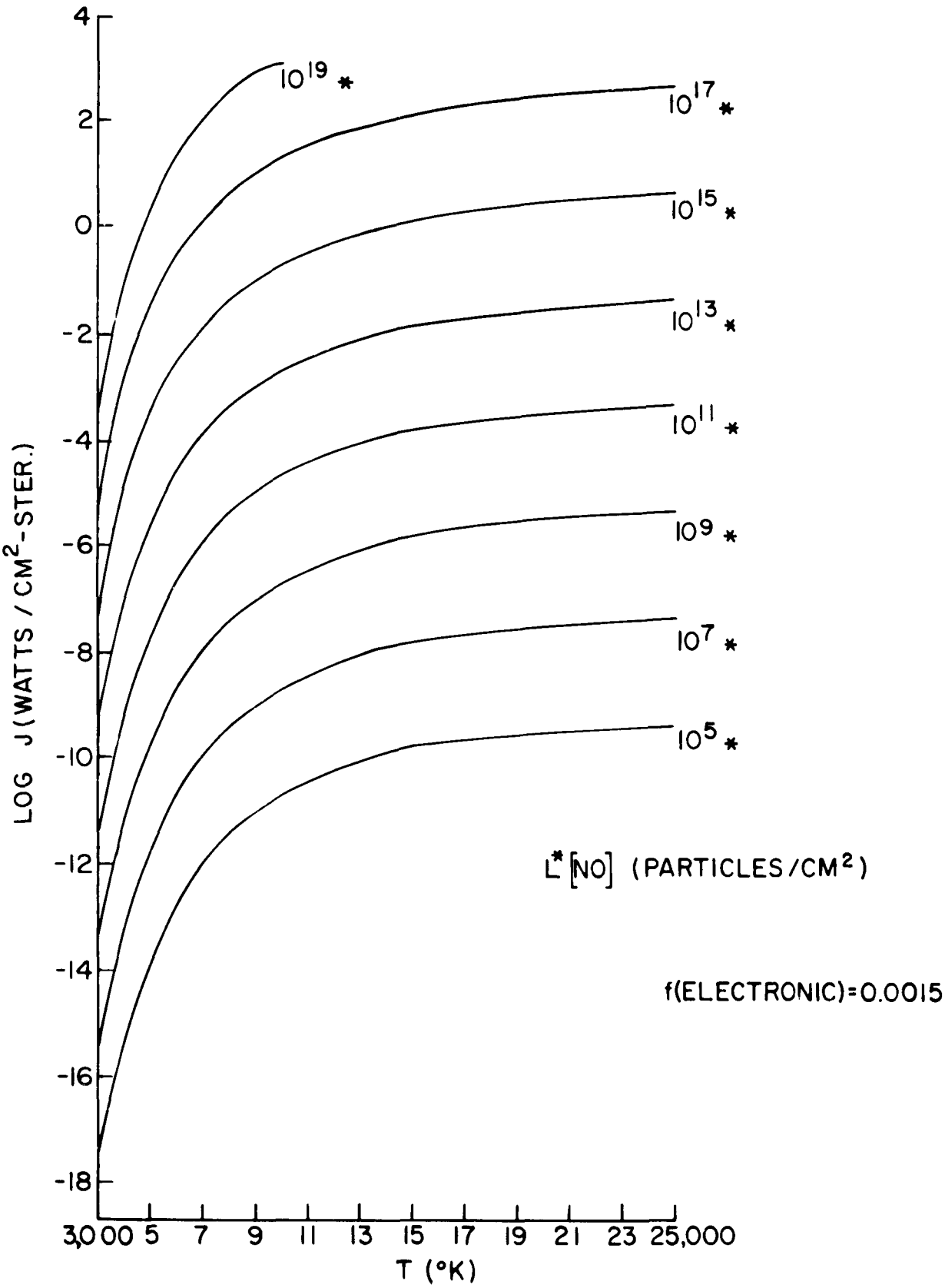

Figure 38. Spectral Radiance of NO Beta Bands

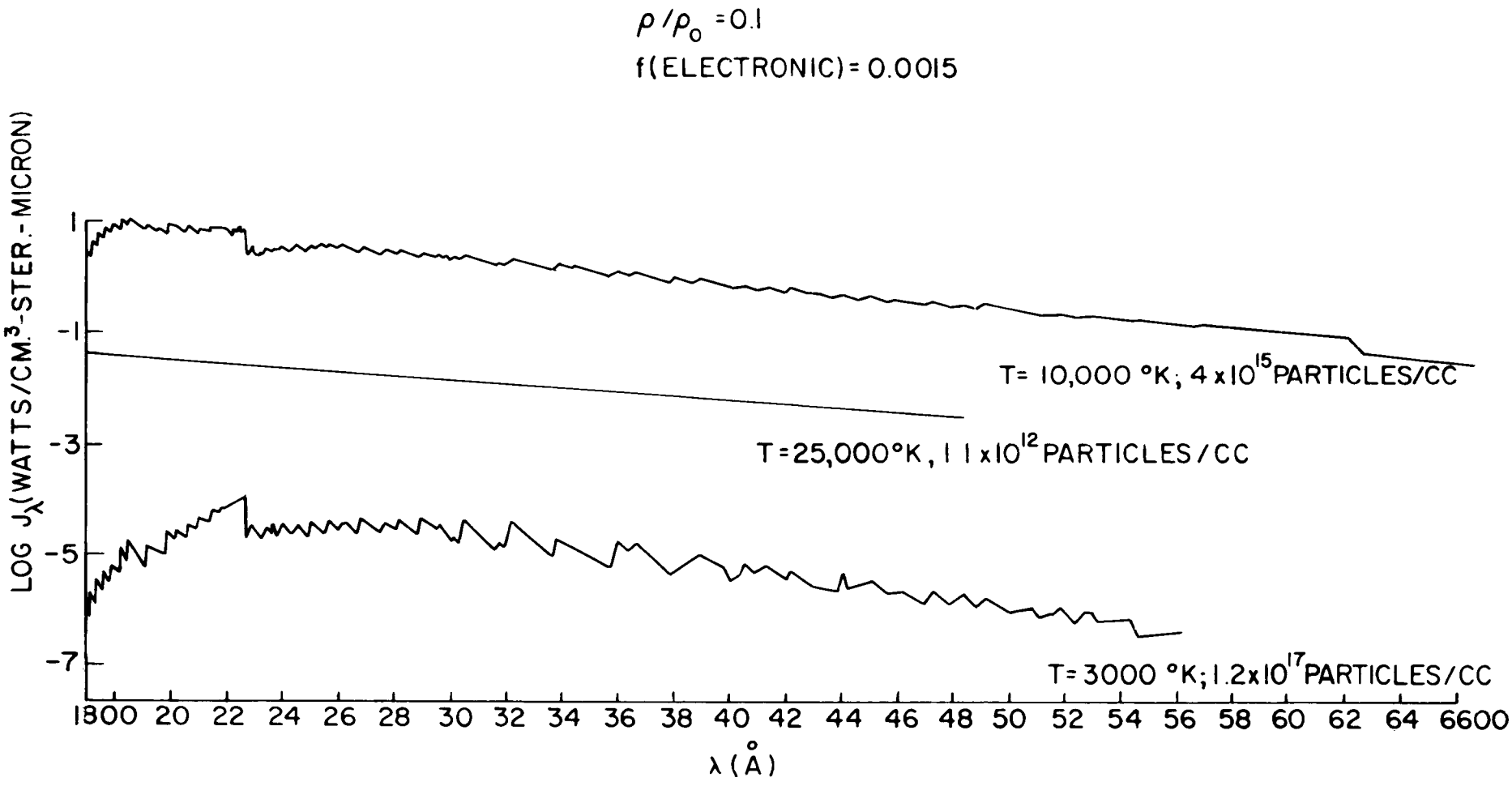

Figure 39. Radiance of NO Gamma Bands (3000°K - 9000°K)

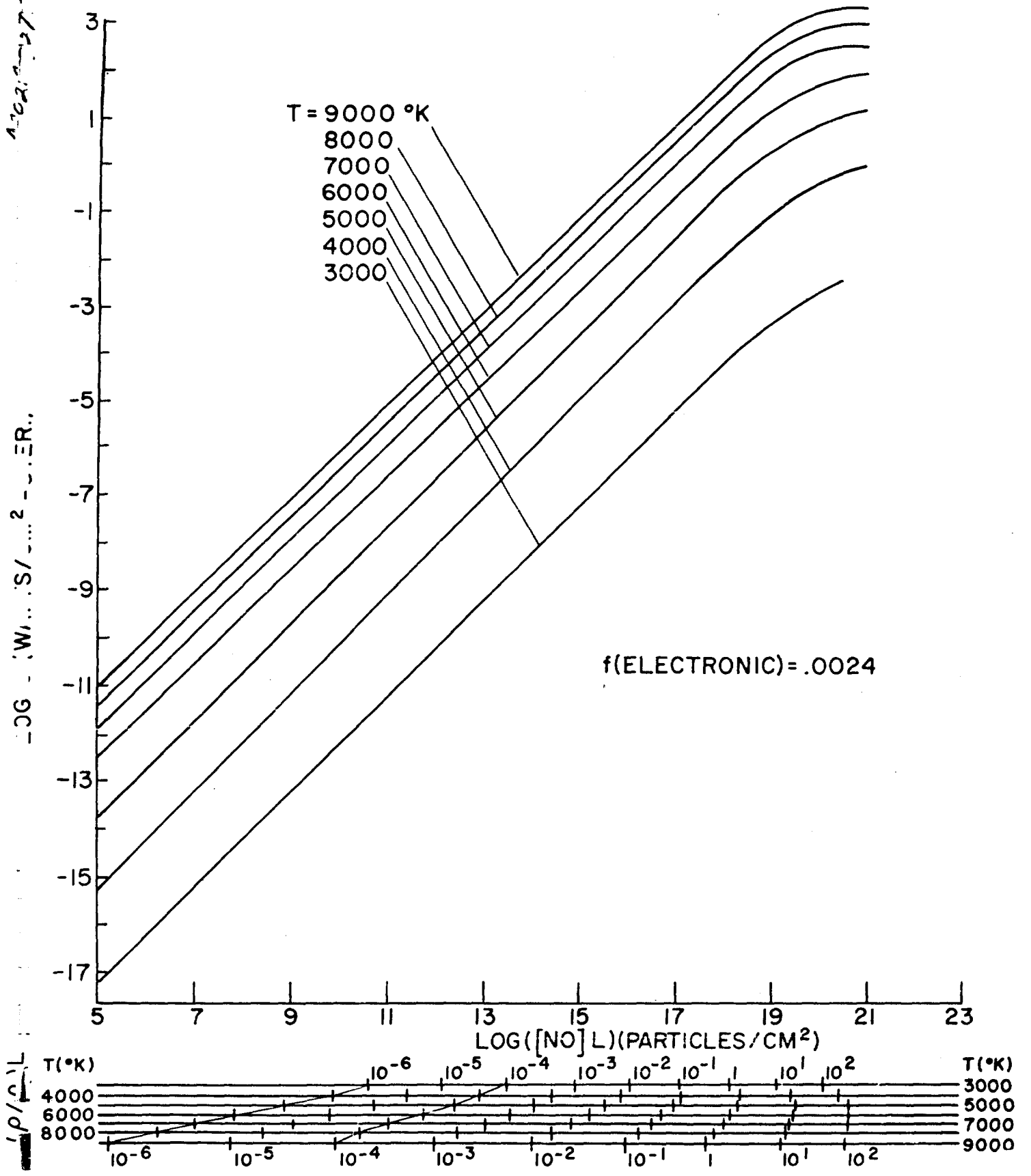

Figure 40. Radiance of NO Gamma Bands (10,000°K - 25,000°K)

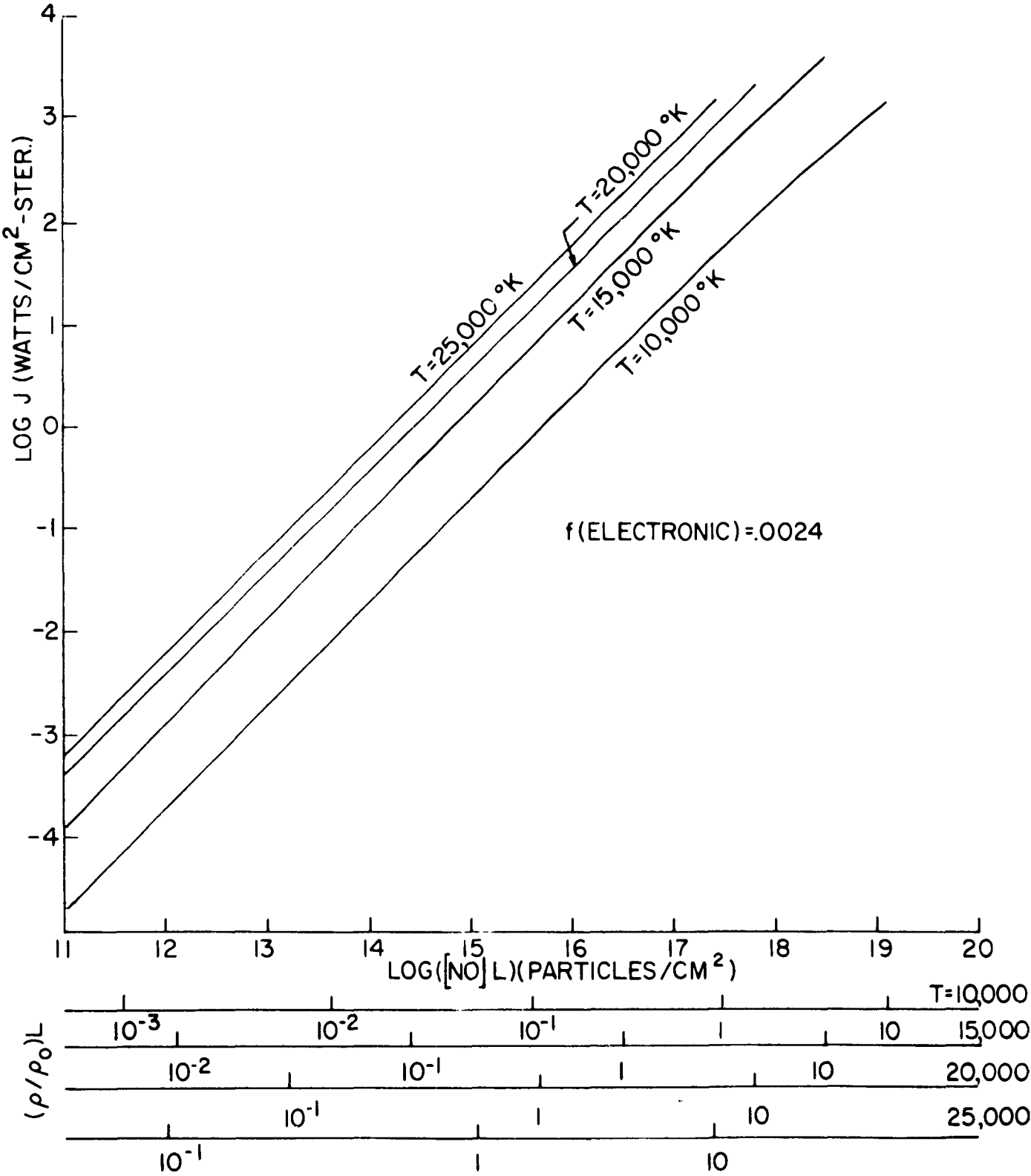

Figure 41. Radiance of NO Gamma Bands (NO Density 10^5 - 10^{19})

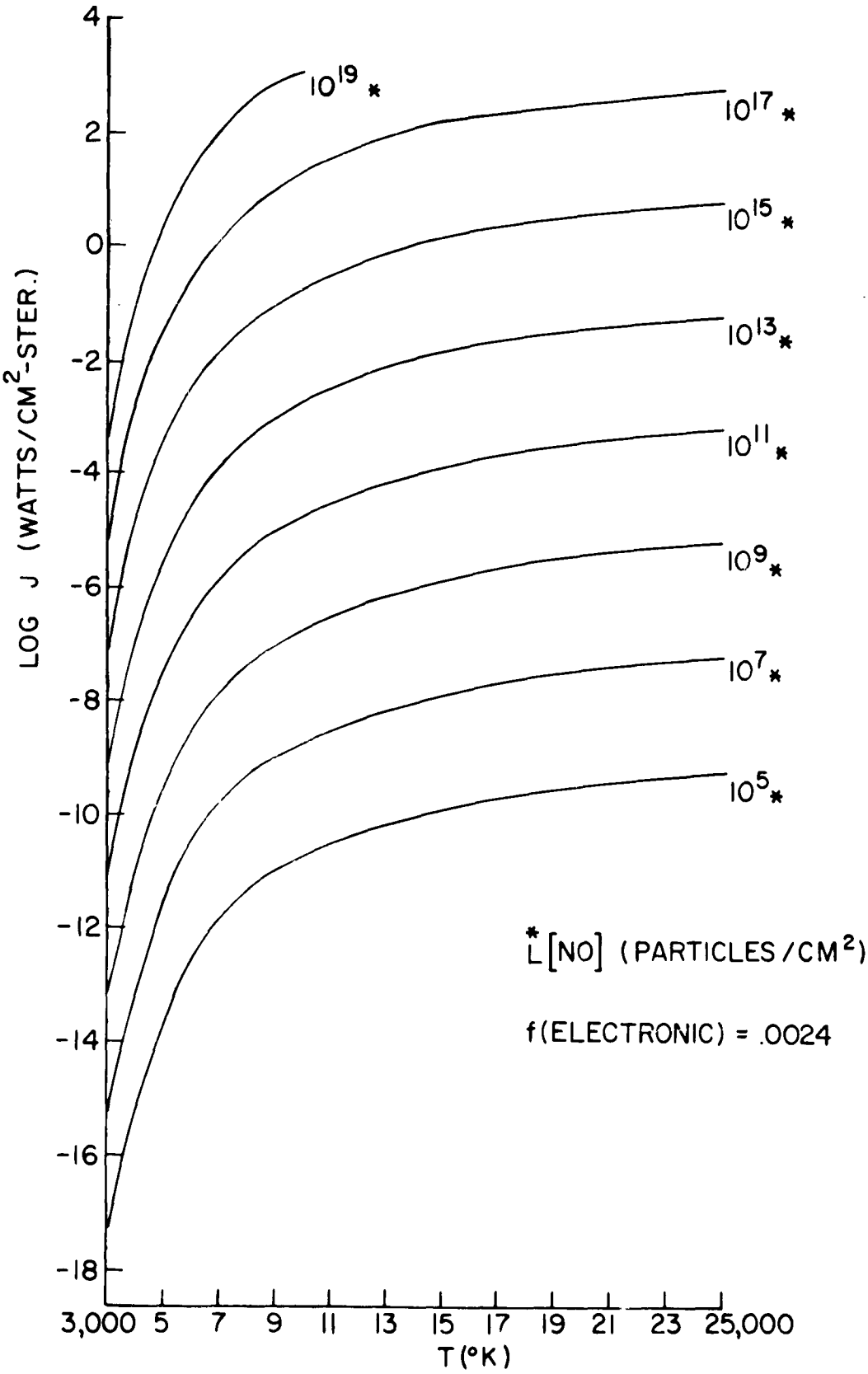

A202A529

Figure 42. Spectral Radiance of NO Gamma Bands

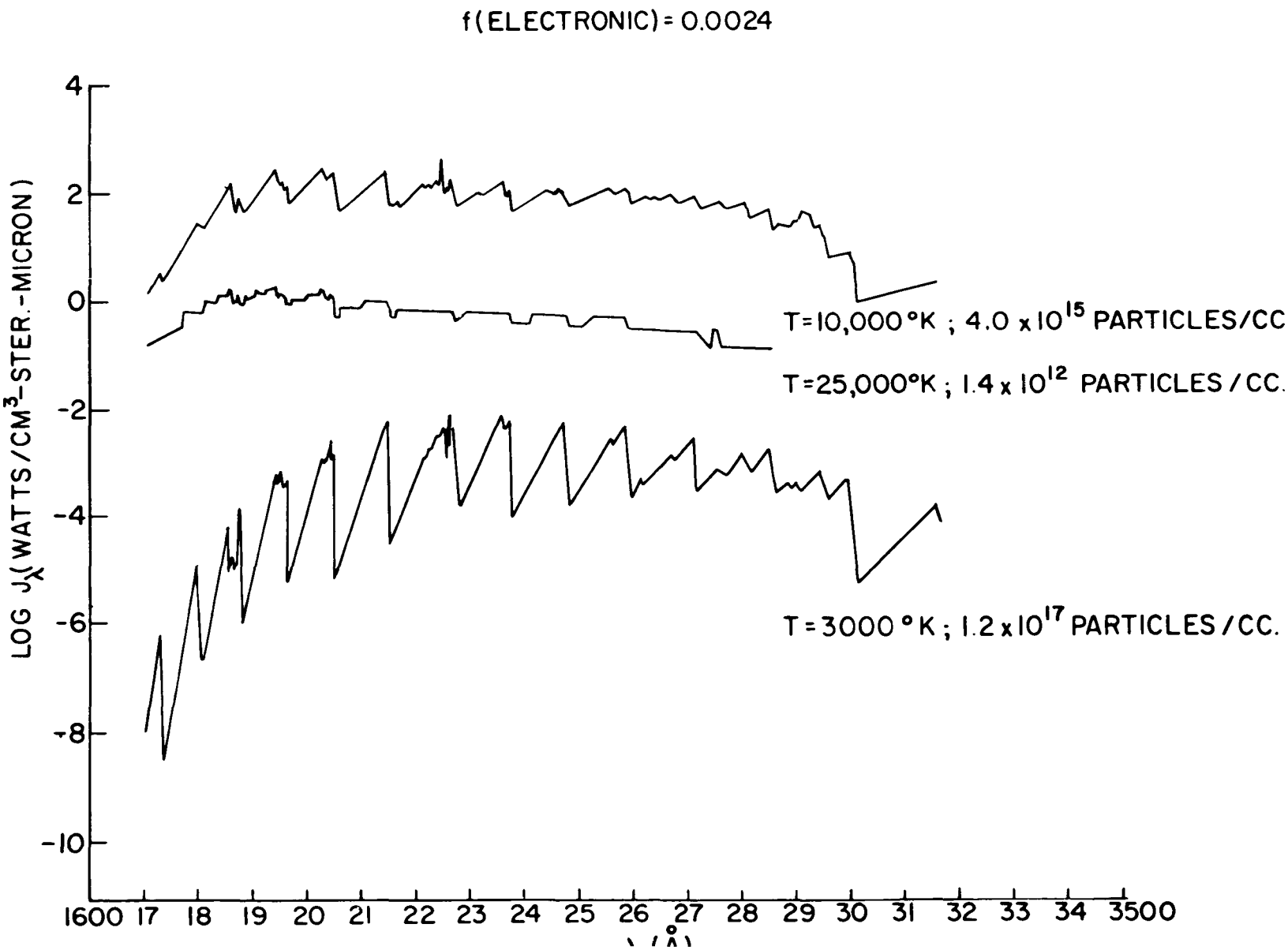

Figure 43. Comparison of Predictions: Radiance of NO ($\beta + \gamma$) Bands

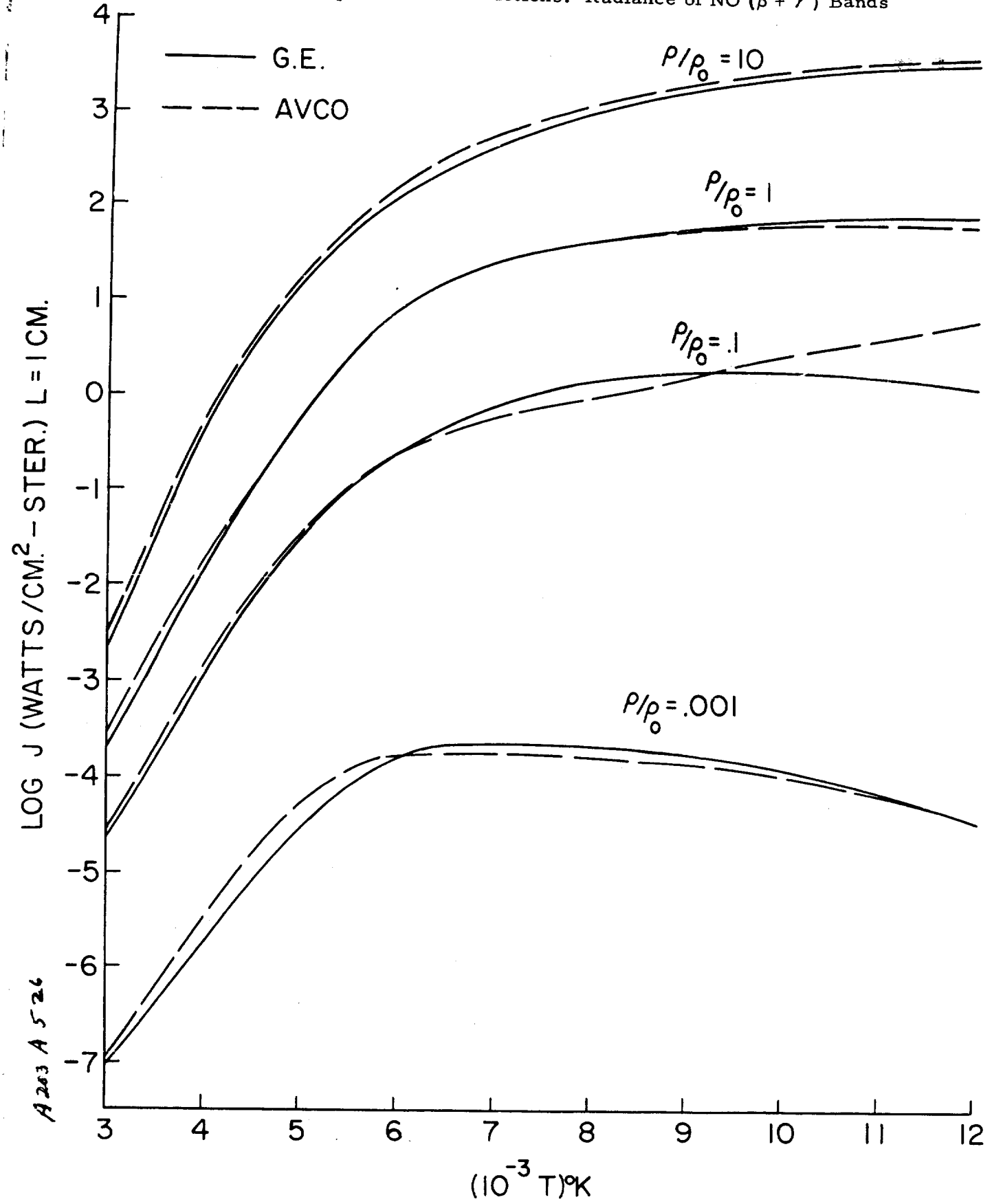

Figure 44. Radiance of NO Infrared Bands (1000°K - 25,000°K)

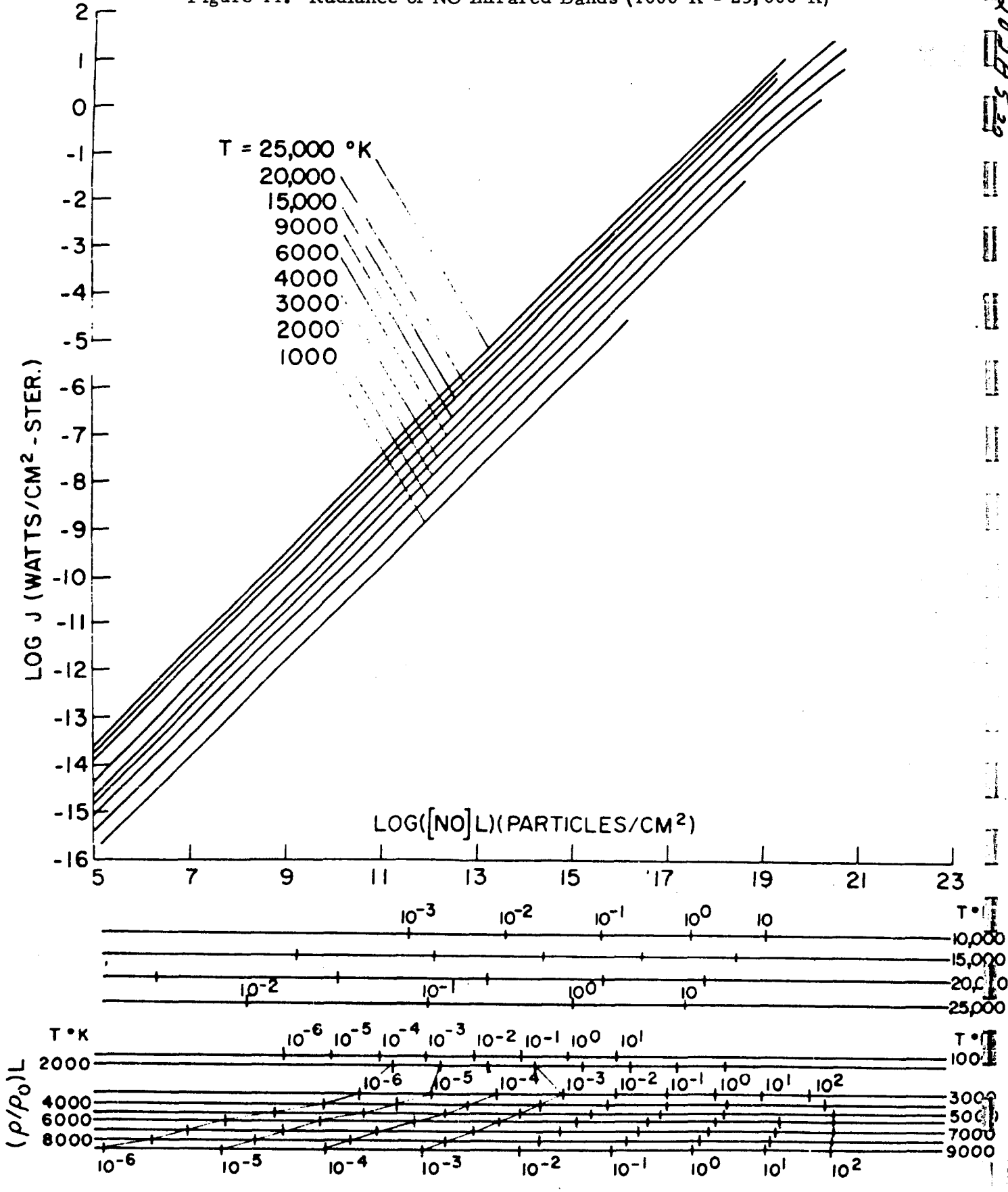

Figure 45. Radiance of NO Infrared Bands (NO Density 10^5 - 10^{19})

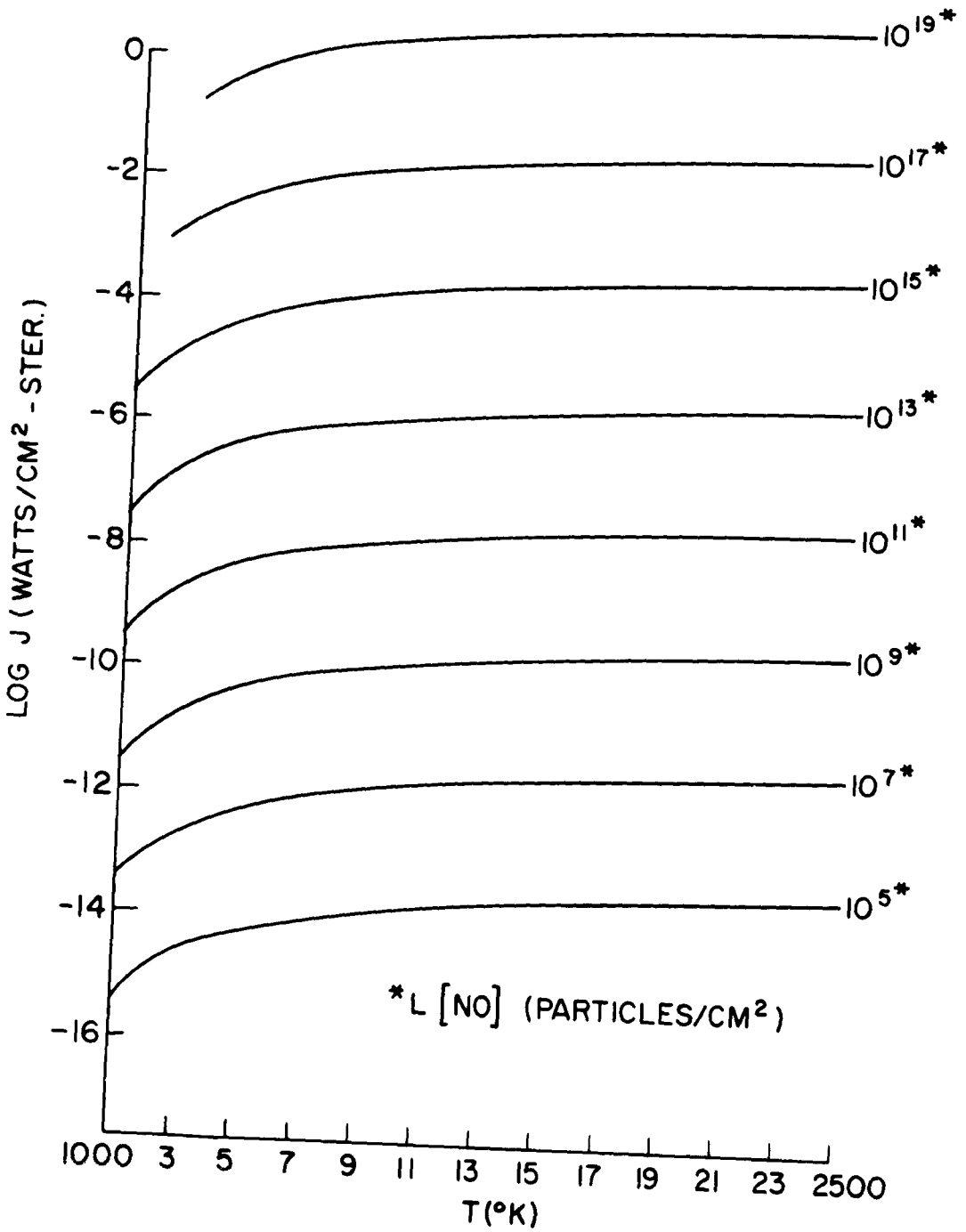

A2024531

Figure 46. Spectral Radiance of NO Infrared Bands

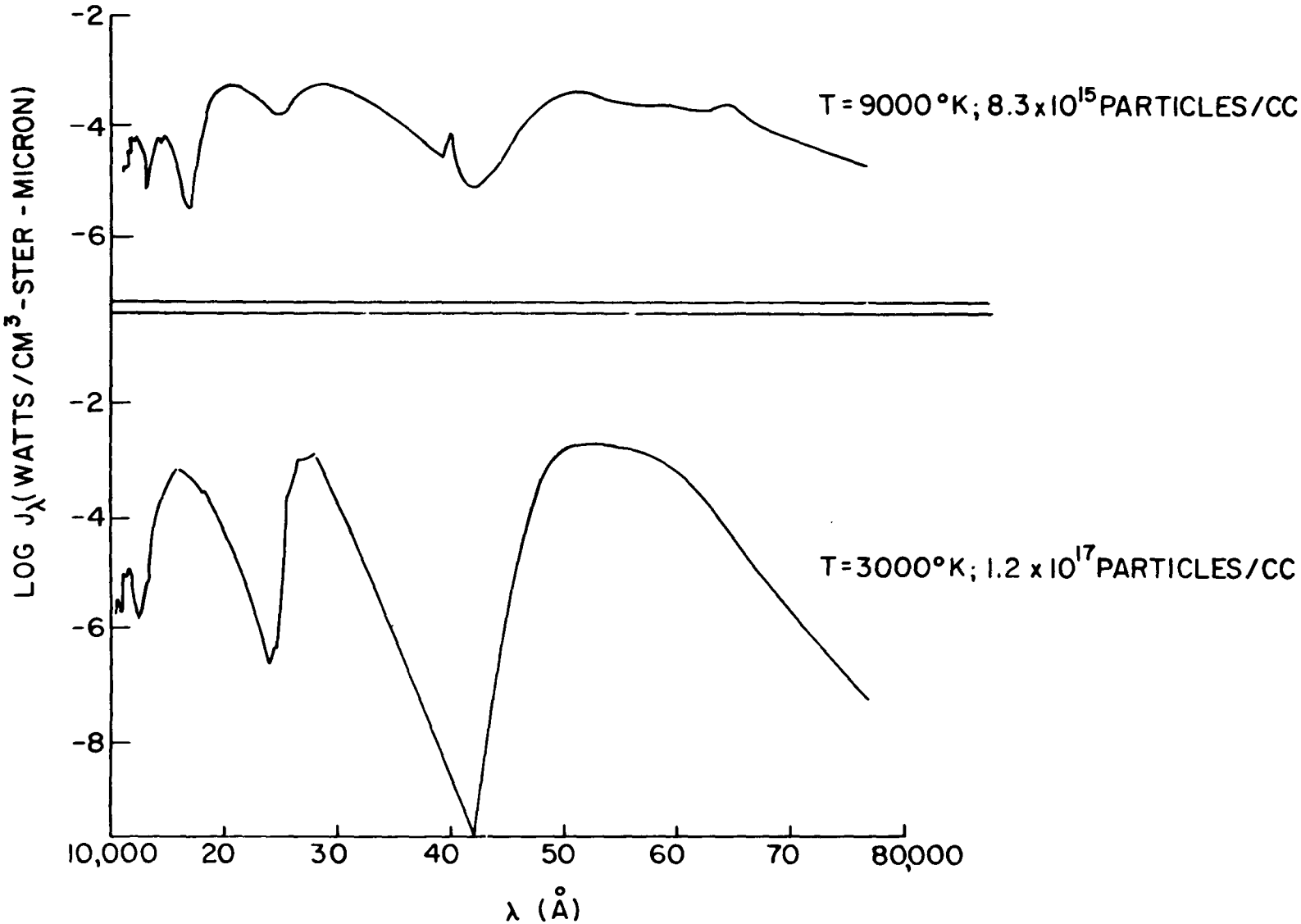

Figure 47. Radiance of O Free-Bound Continuum (3000°K - 9000°K)

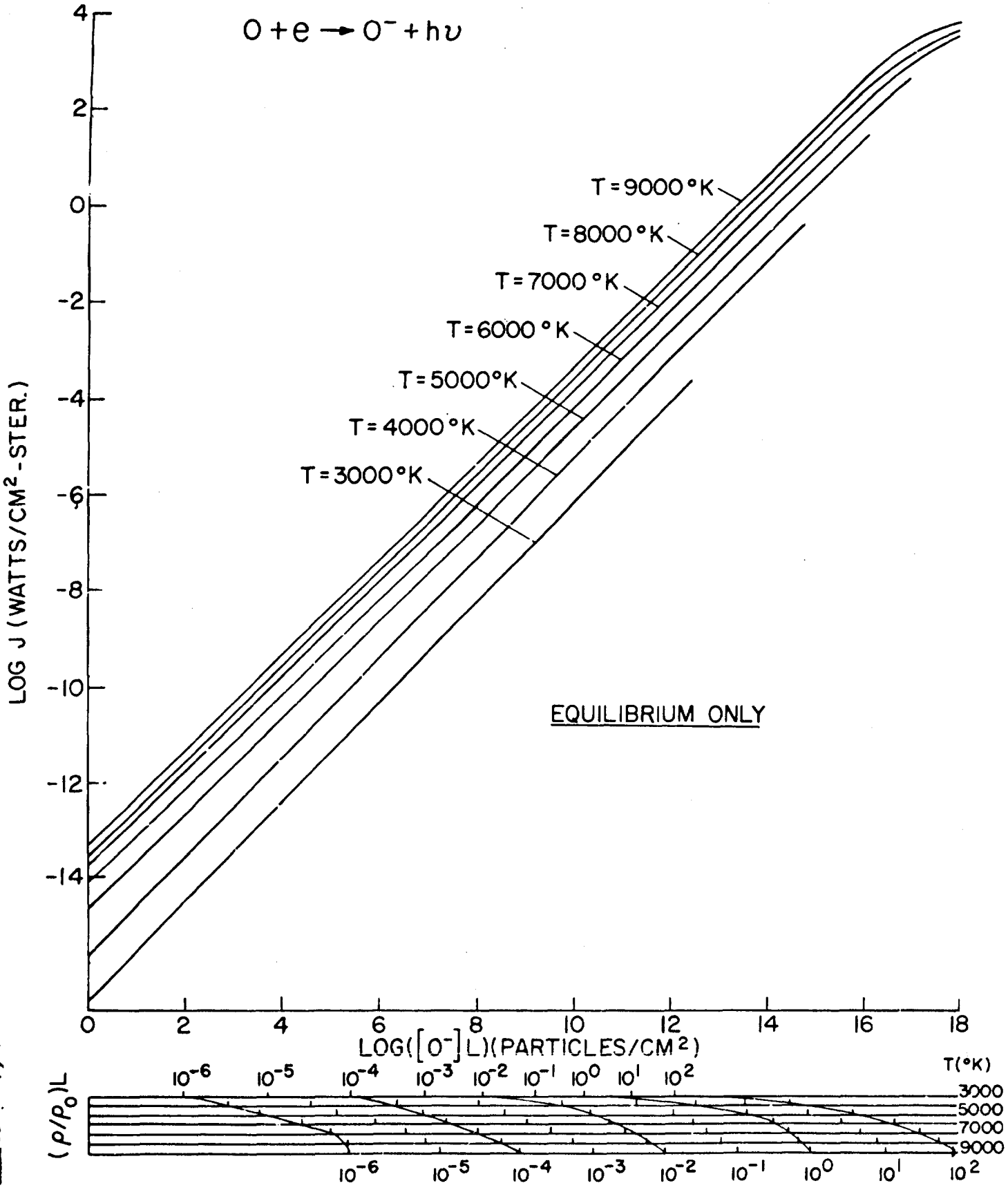

Figure 48. Radiance of O Free Bound Continuum (10,000°K - 25,000°K)

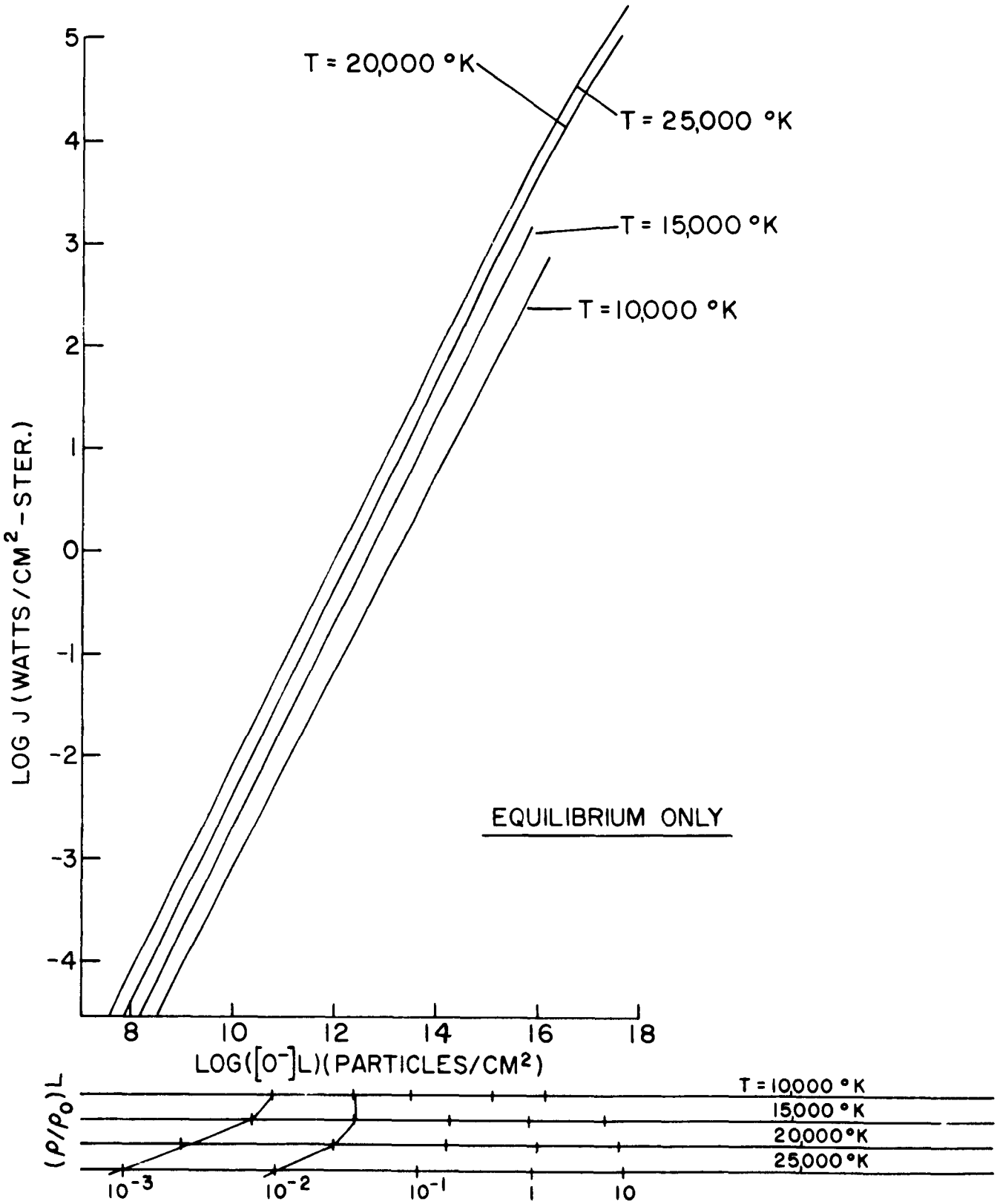

Figure 49. Radiance of O Free-Bound Continuum (0^- Density 10^4 - 10^{16})

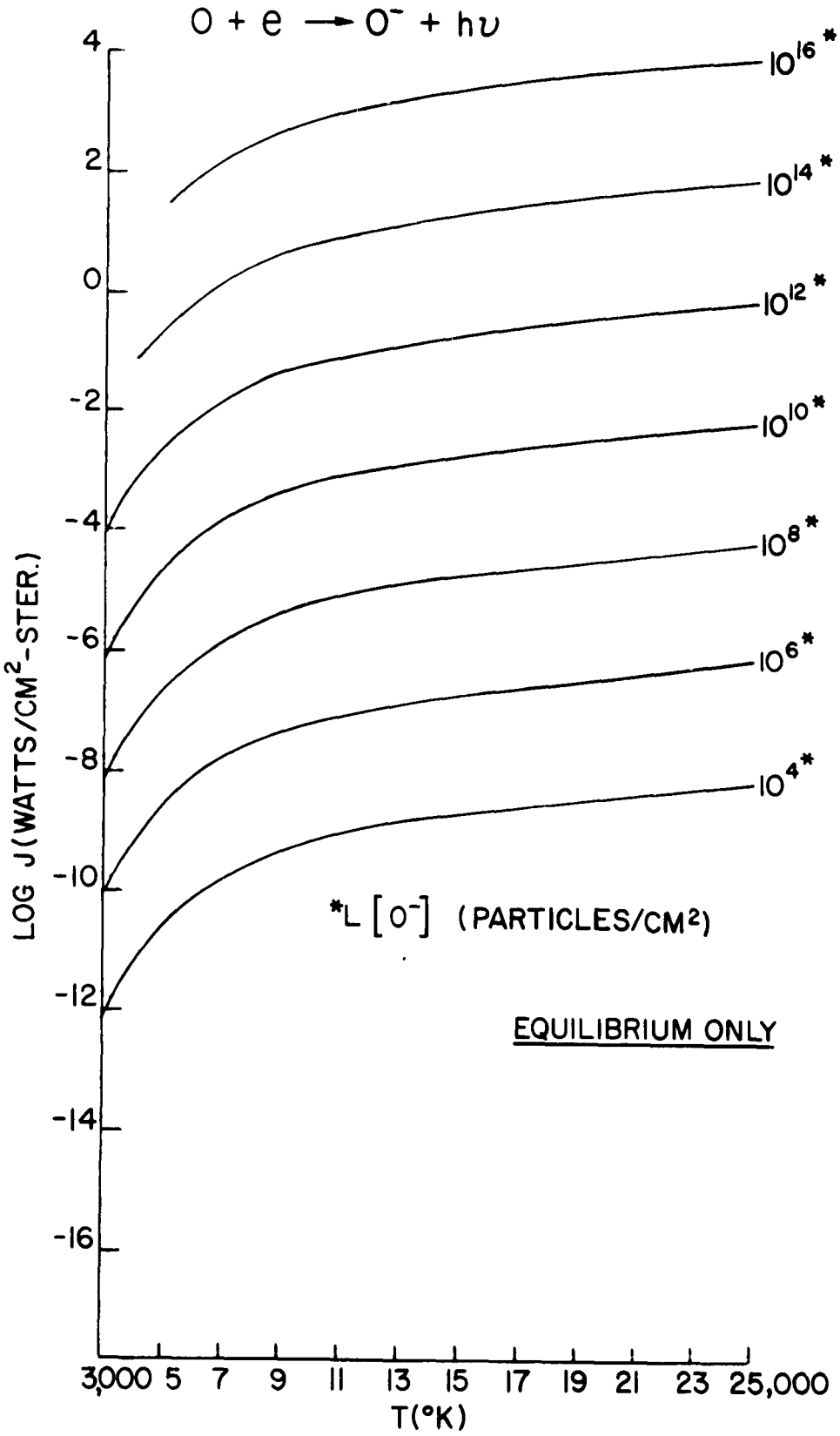

Figure 50. Spectral Radiance of O Free-Bound Continuum

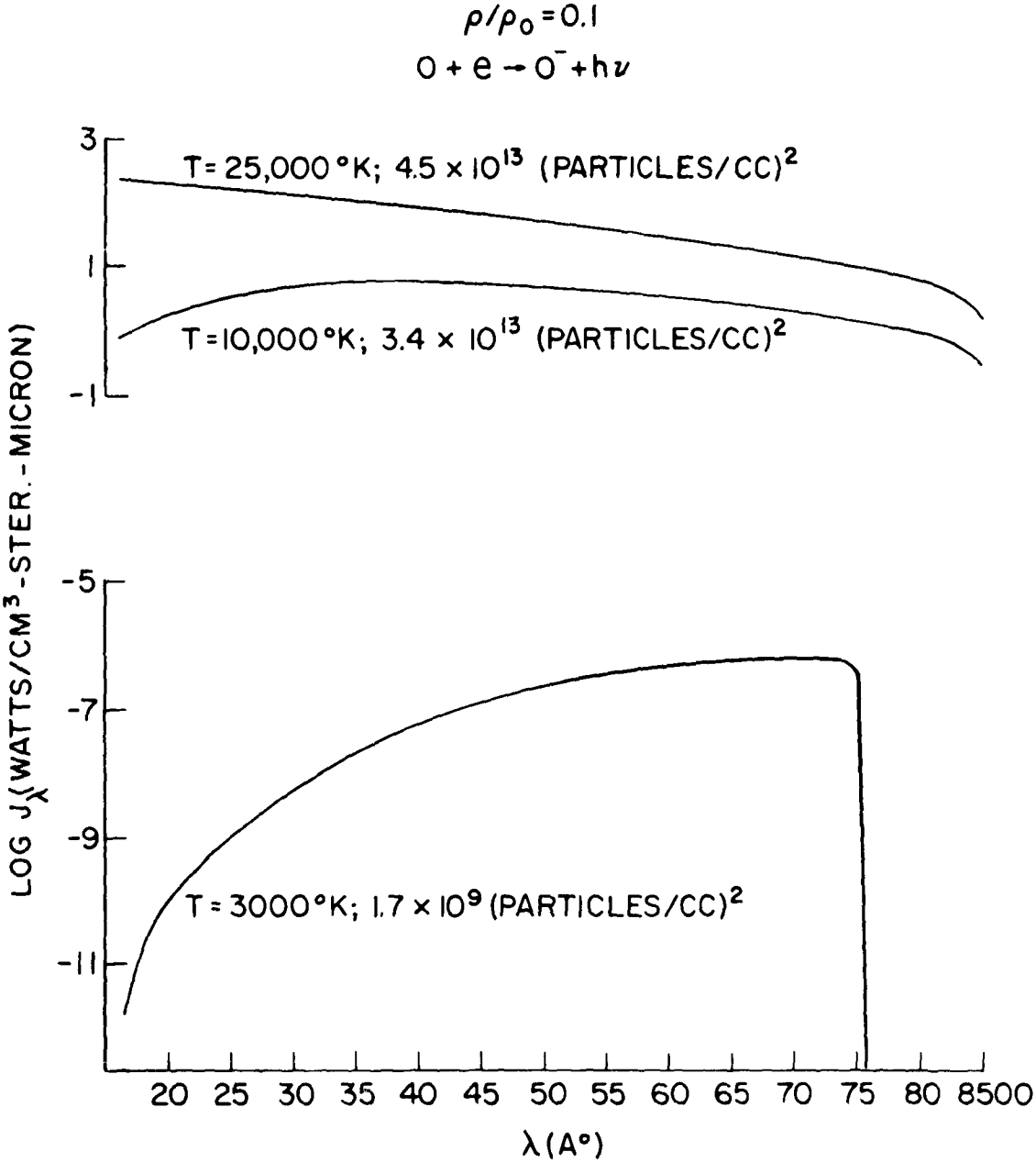

A402A553

Figure 51. Radiance of N Free - Free (4000°K - 9000°K)

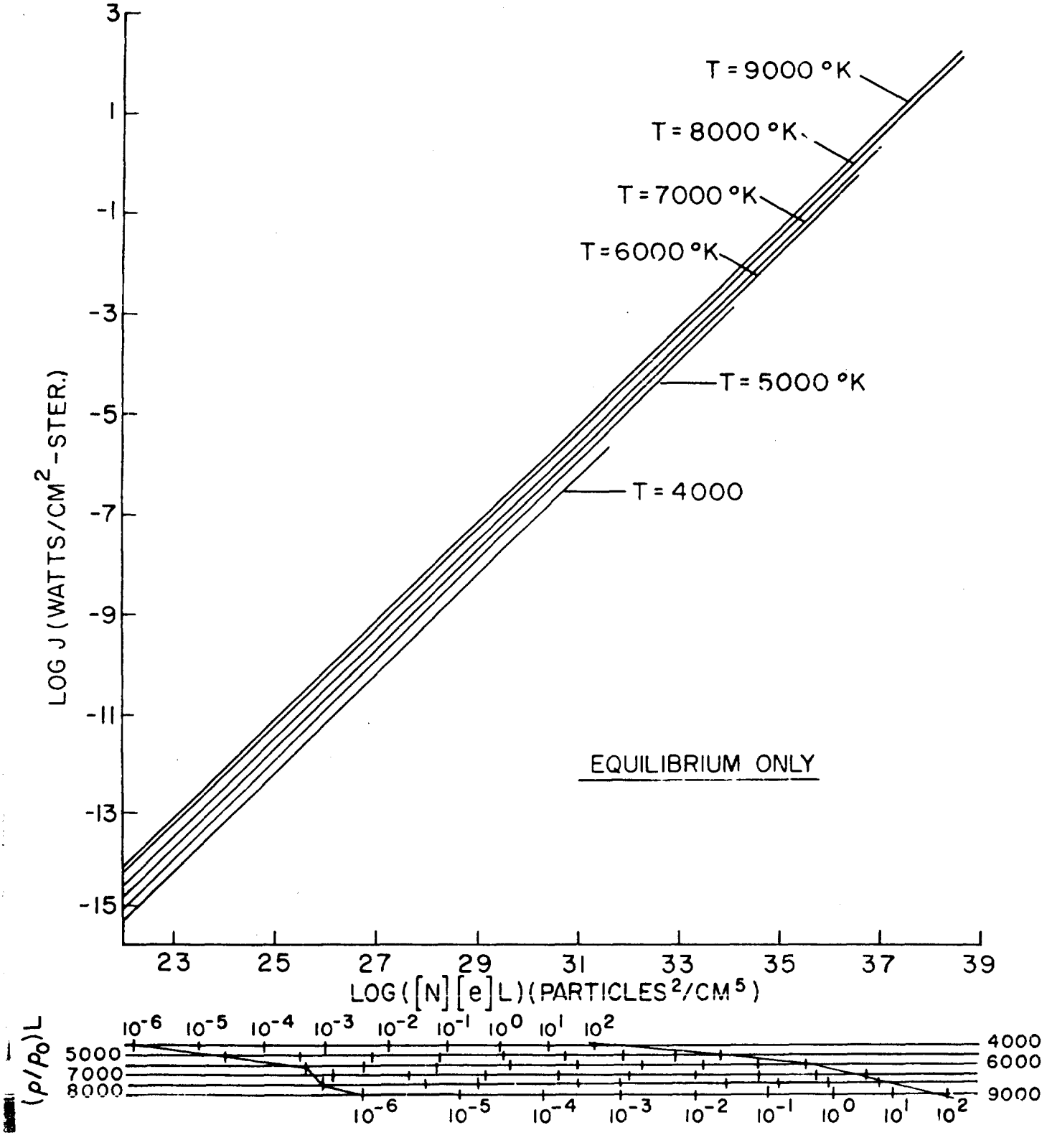

Figure 52. Radiance of N Free - Free (10,000°K - 25,000°K)

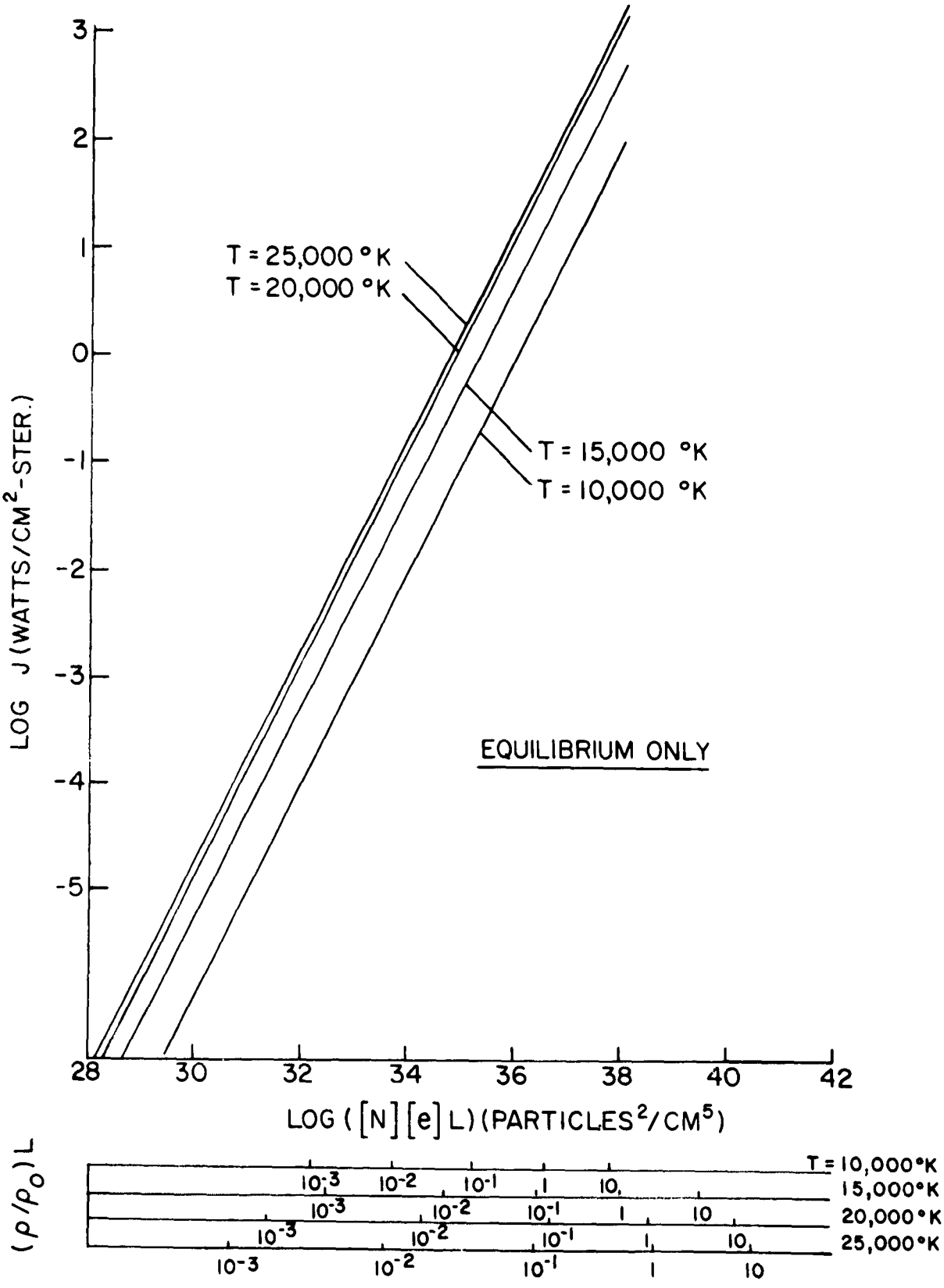

Figure 53. Radiance of N Free - Free ([N] [e] density product 10^{24} - 10^{38})

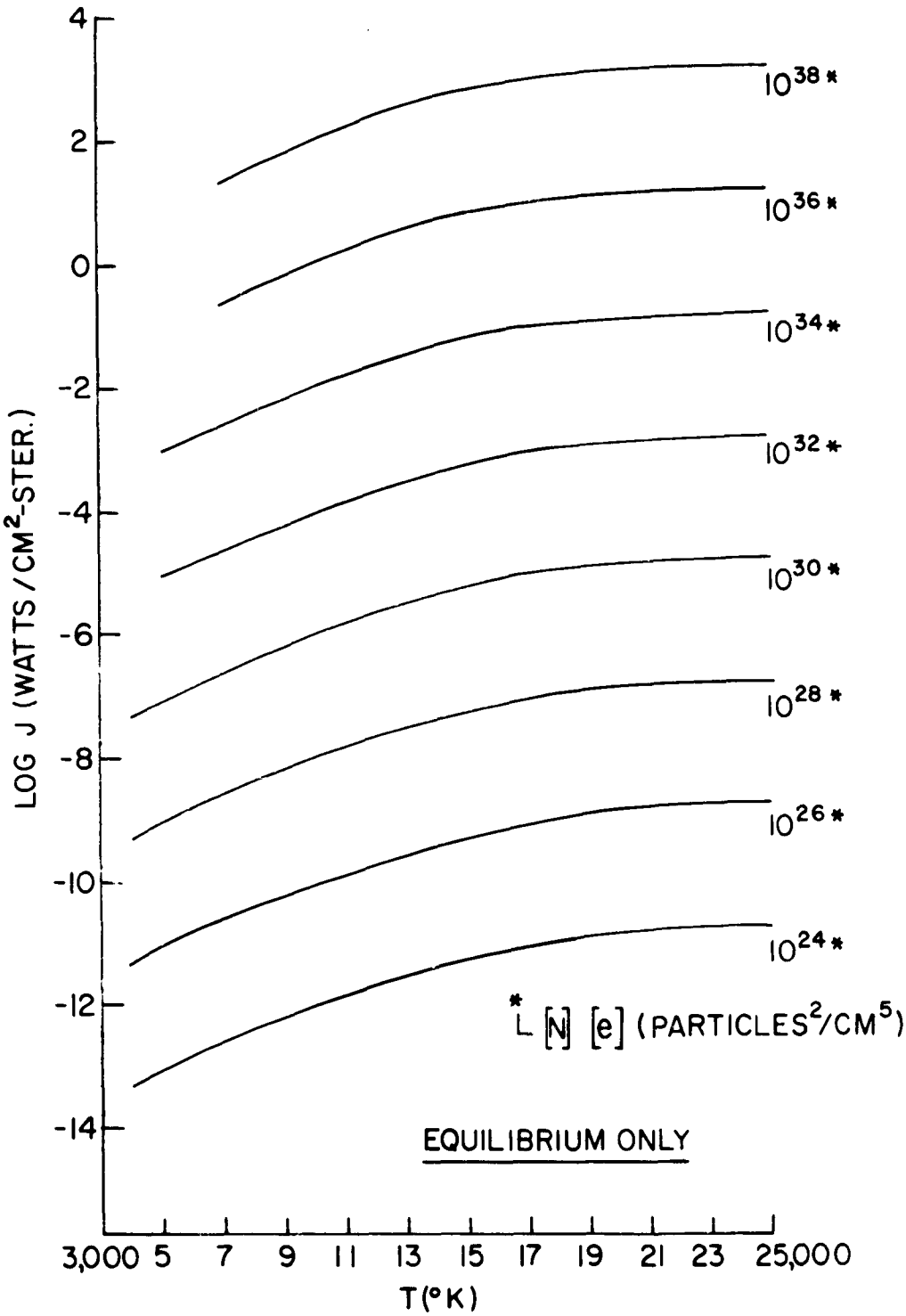

A302 A 553

Figure 54. Spectral Radiance of N Free - Free Continuum

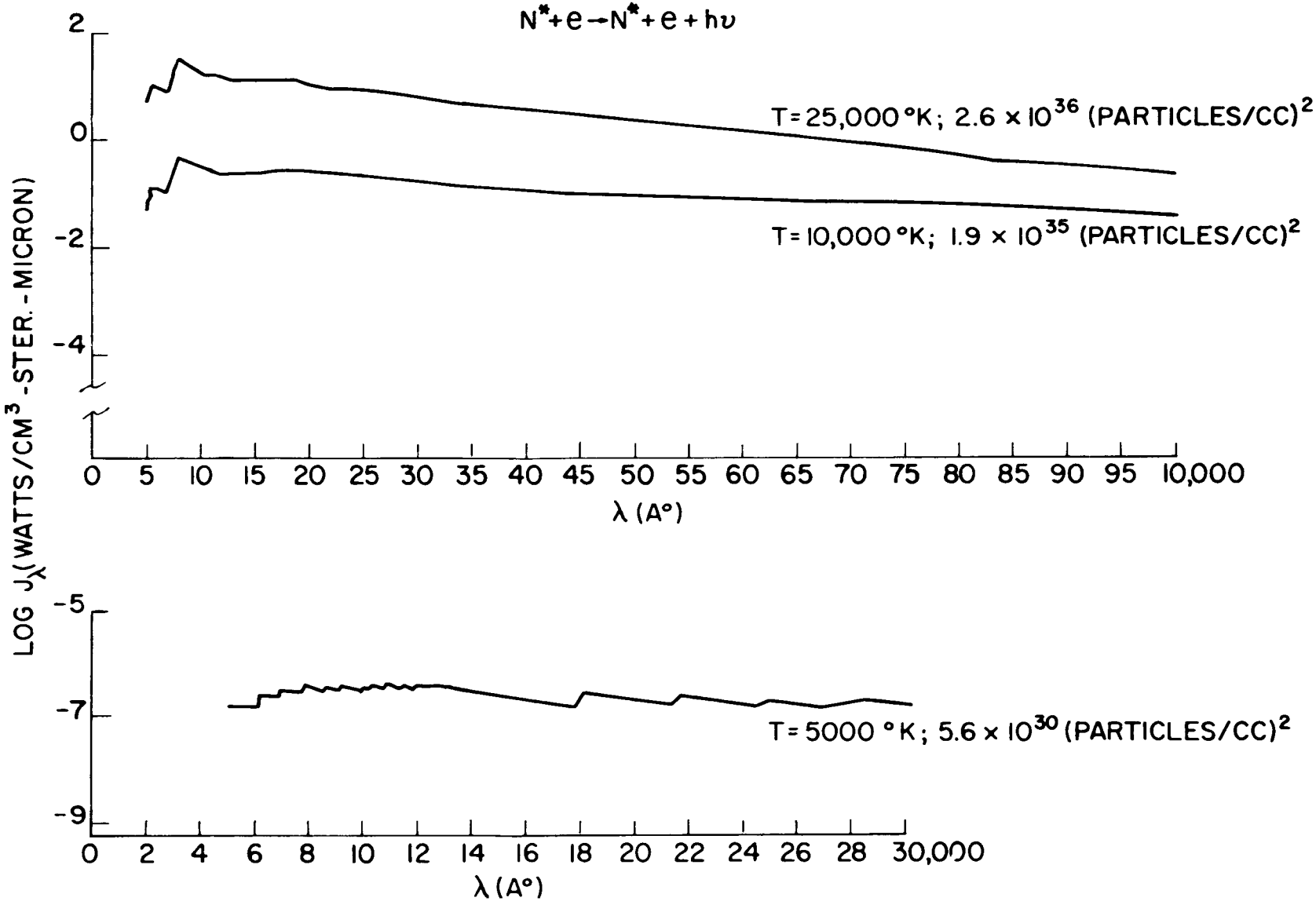

Figure 55. Radiance of O Free - Free (3000°K - 9000°K)

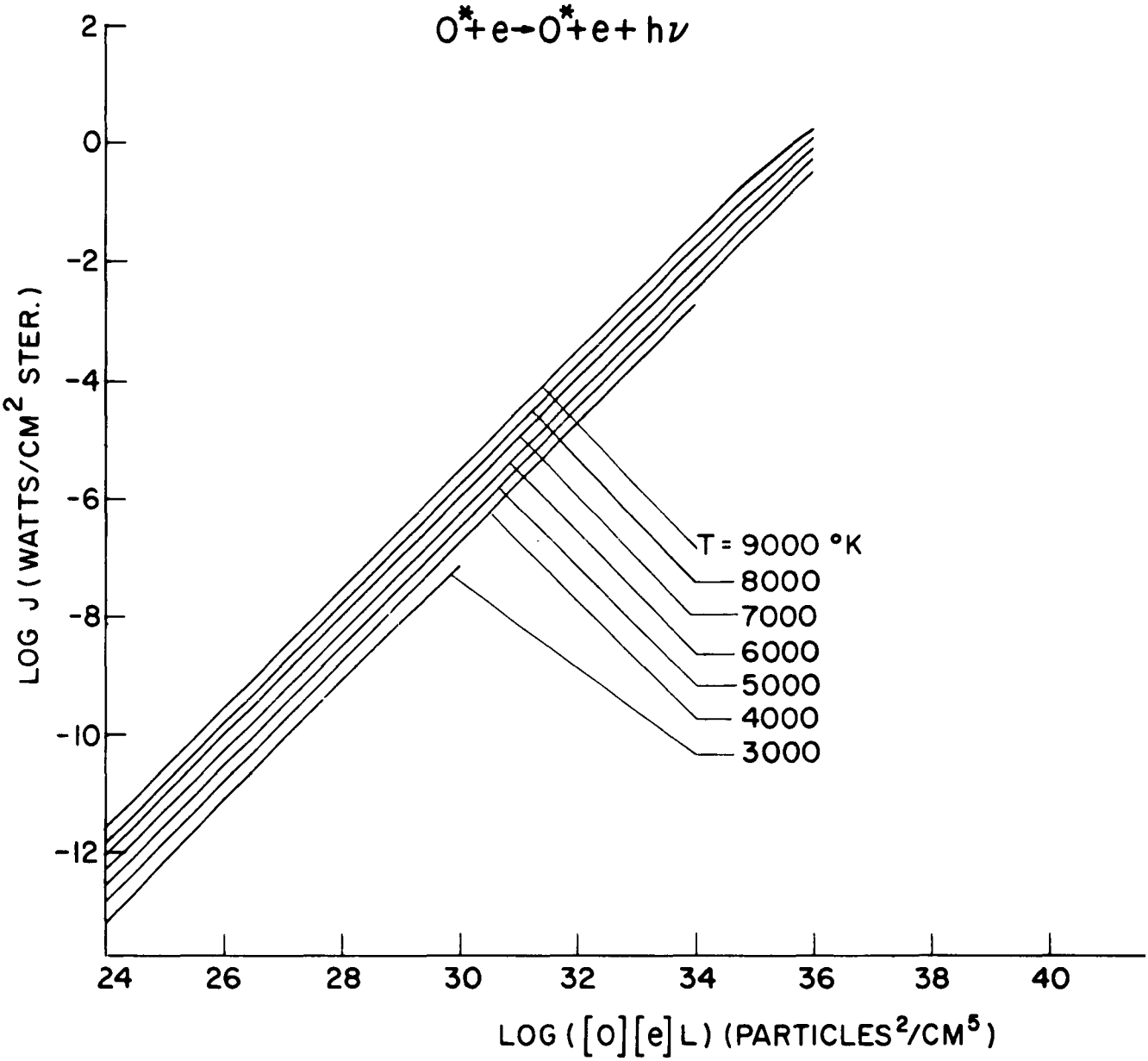

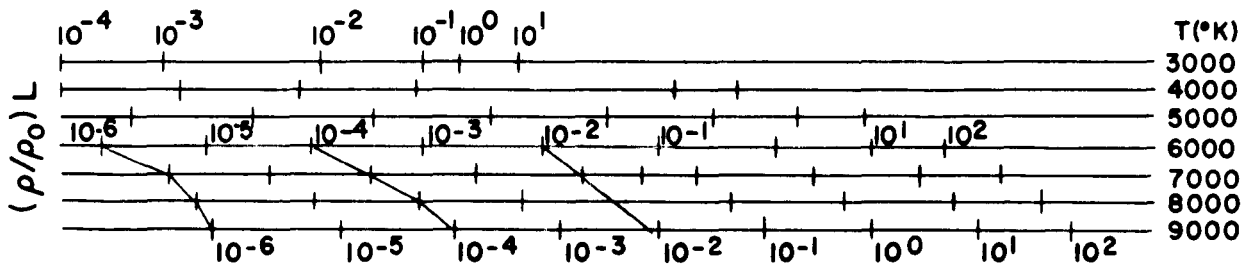

A202A550

Figure 56. Radiance of O Free - Free (10,000°K - 25,000°K)

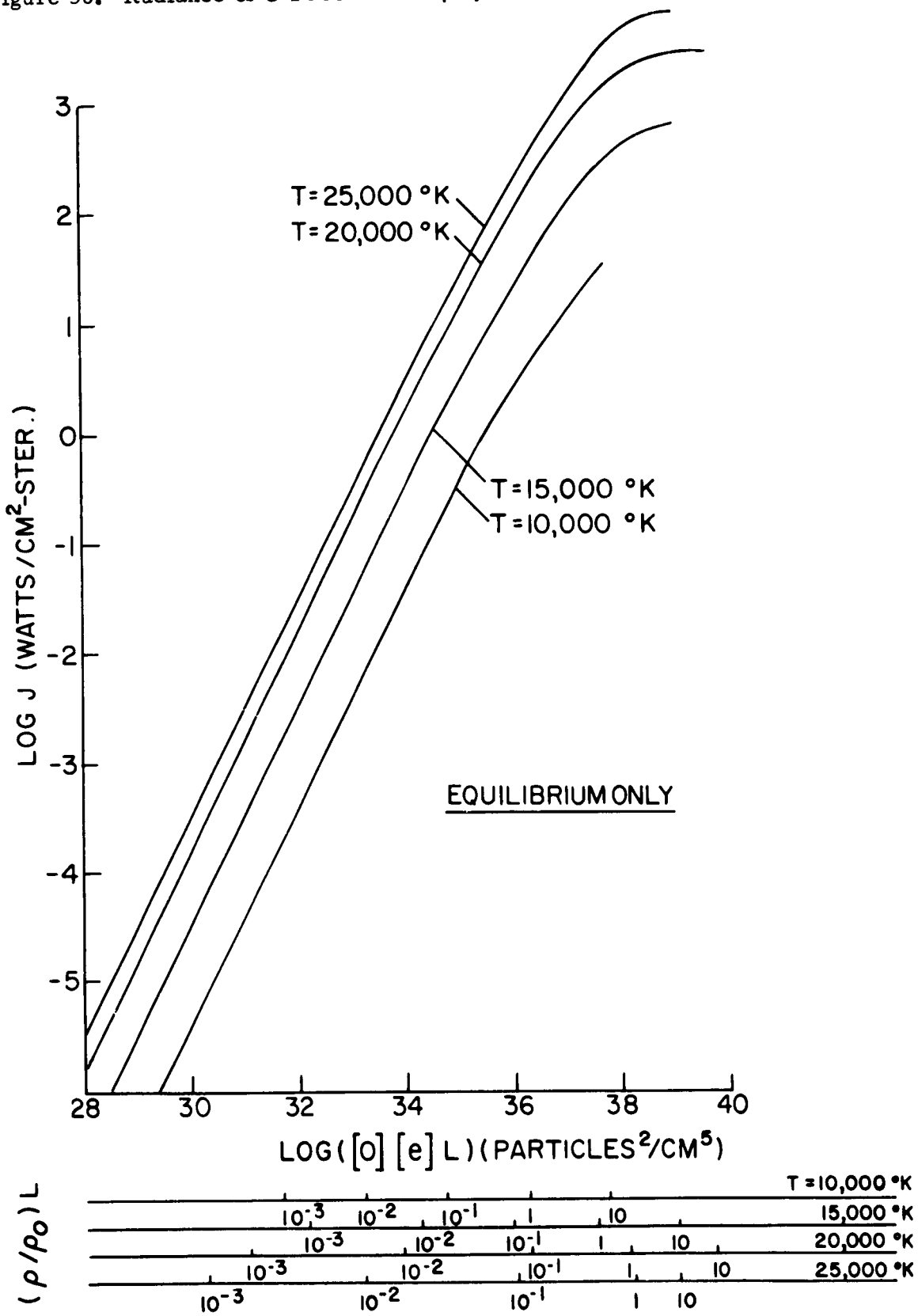

Figure 57. Radiance of O Free - Free ([N][e] Density Product 10^{24} - 10^{38})

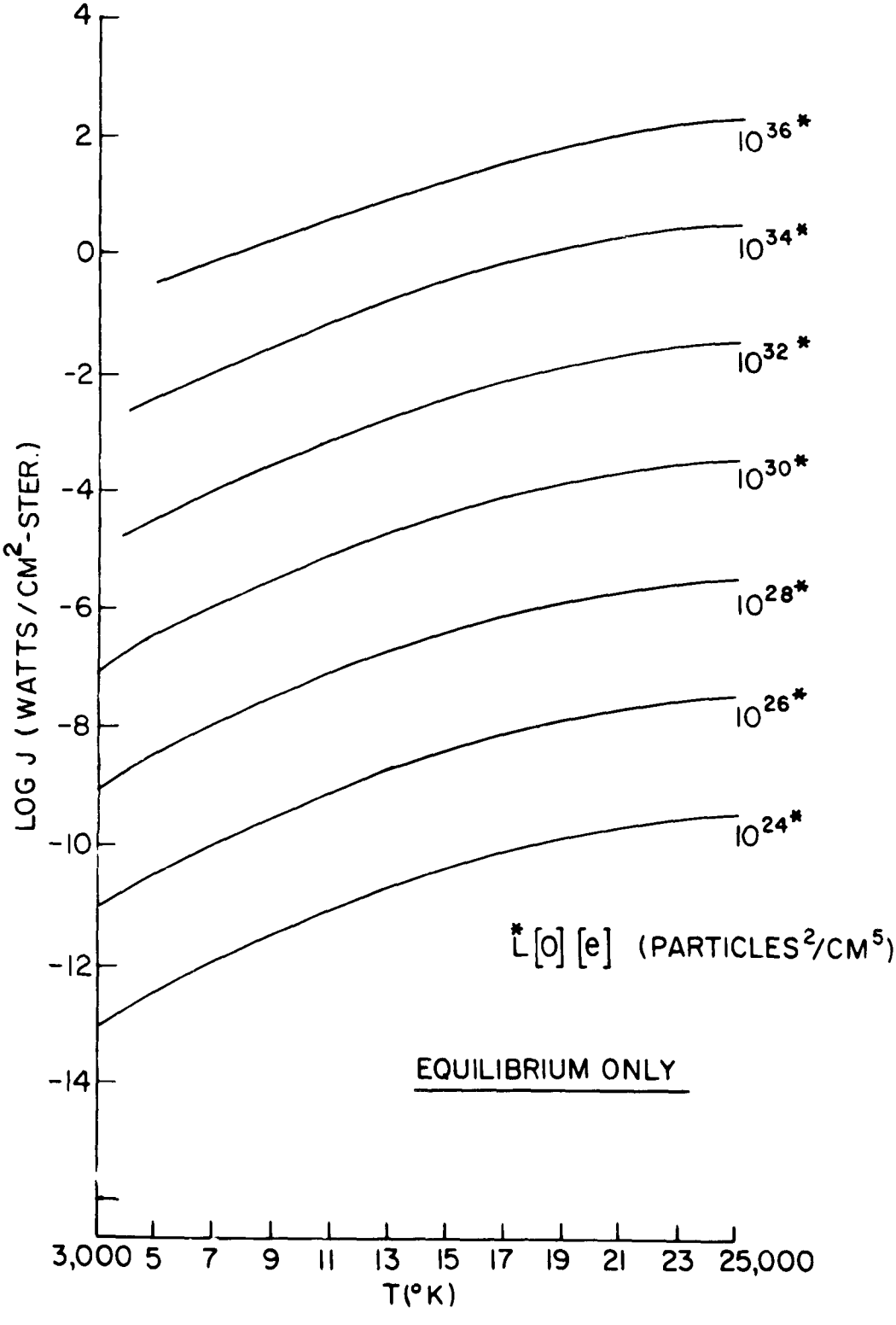

A202A552

Figure 58. Spectral Radiance of O Free - Free Continuum

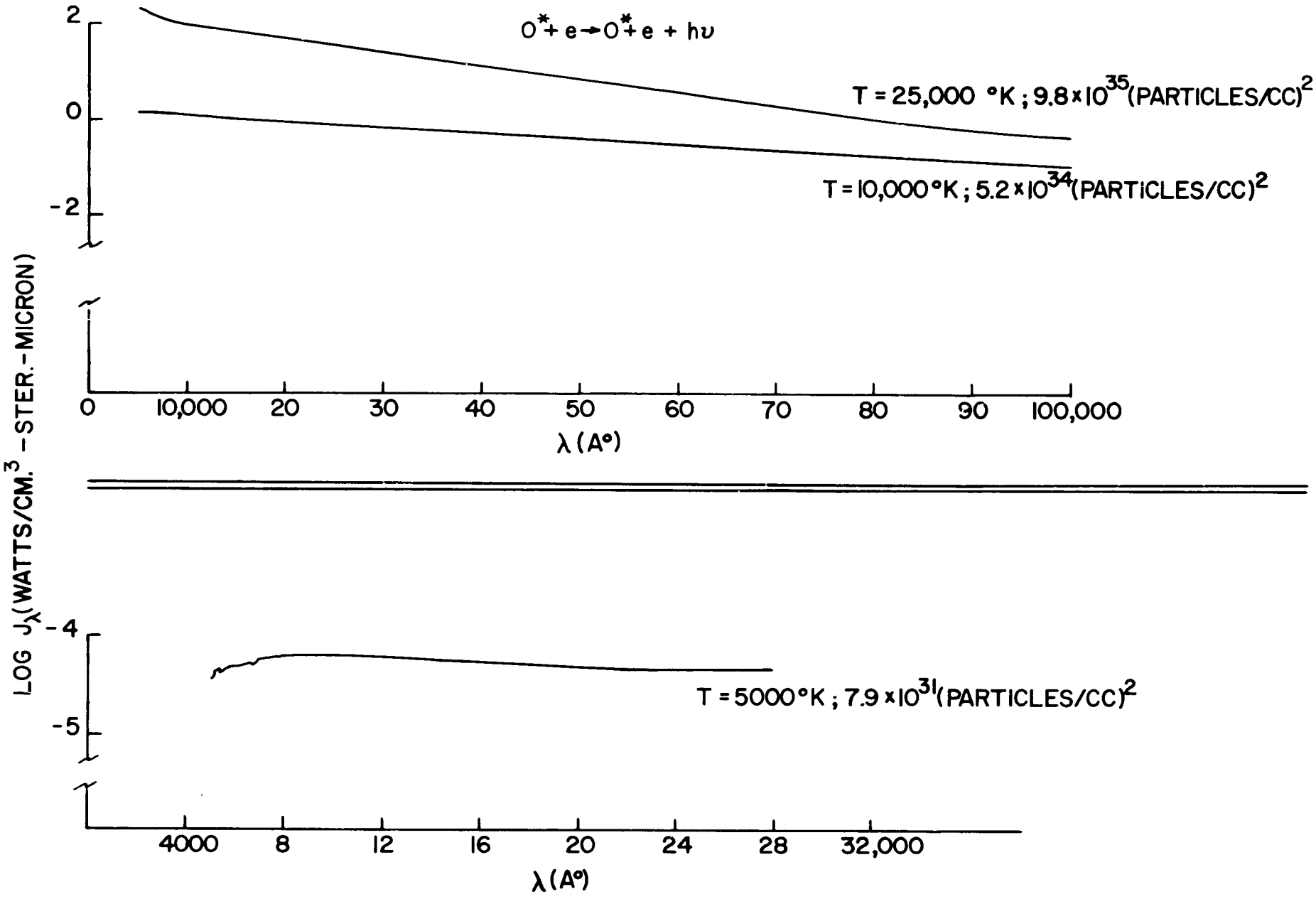

Figure 59. Comparison of Predictions: Spectral Radiance of O and N Free - Free Continuum in Infrared (8000°K)

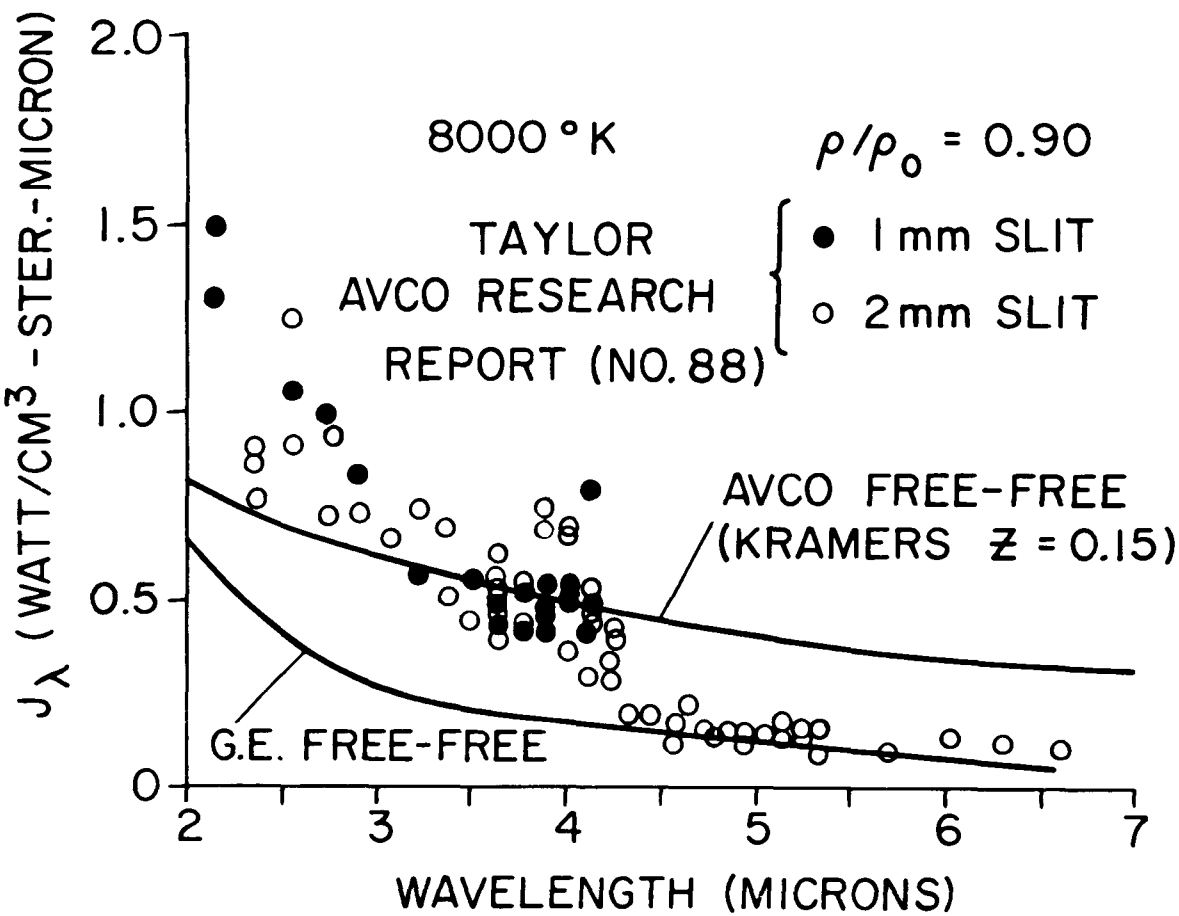

Figure 60. Radiance of N^+ Deionization (8000°K - 25,000°K)

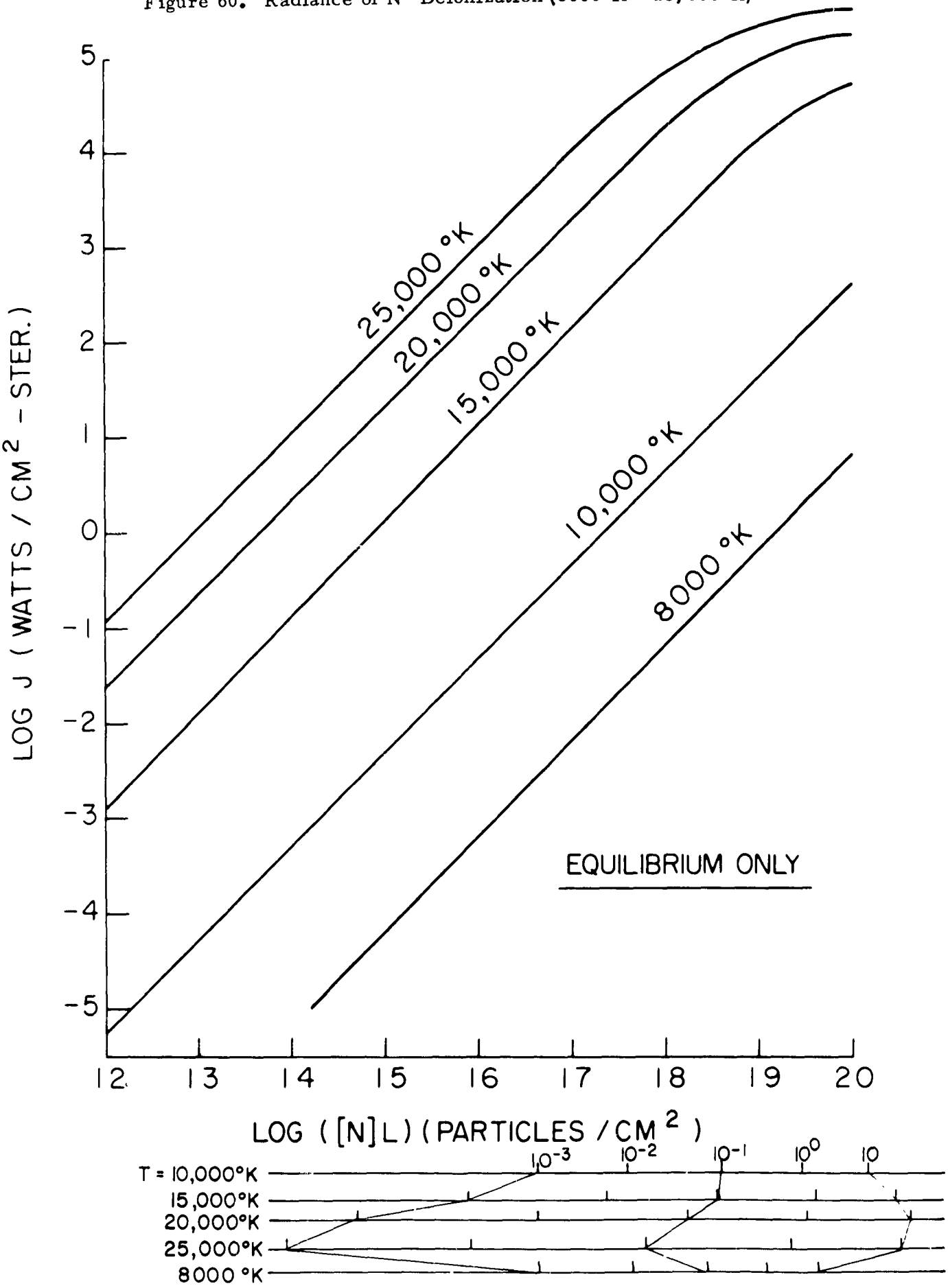

Figure 61. Radiance of N^+ Deionization (N Density 10^{12} - 10^{19})

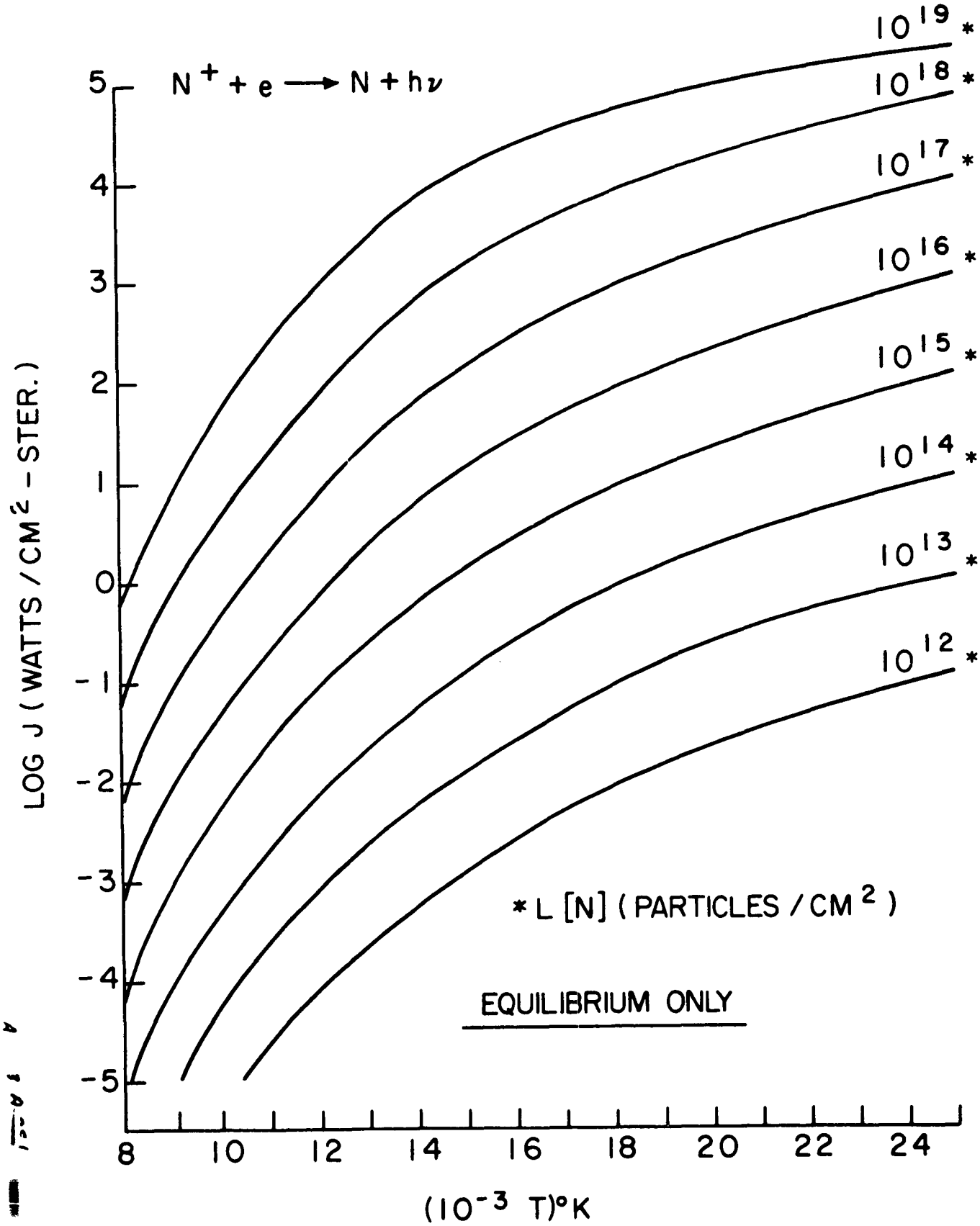

Figure 62. Spectral Radiance of N^+ Deionization Continuum

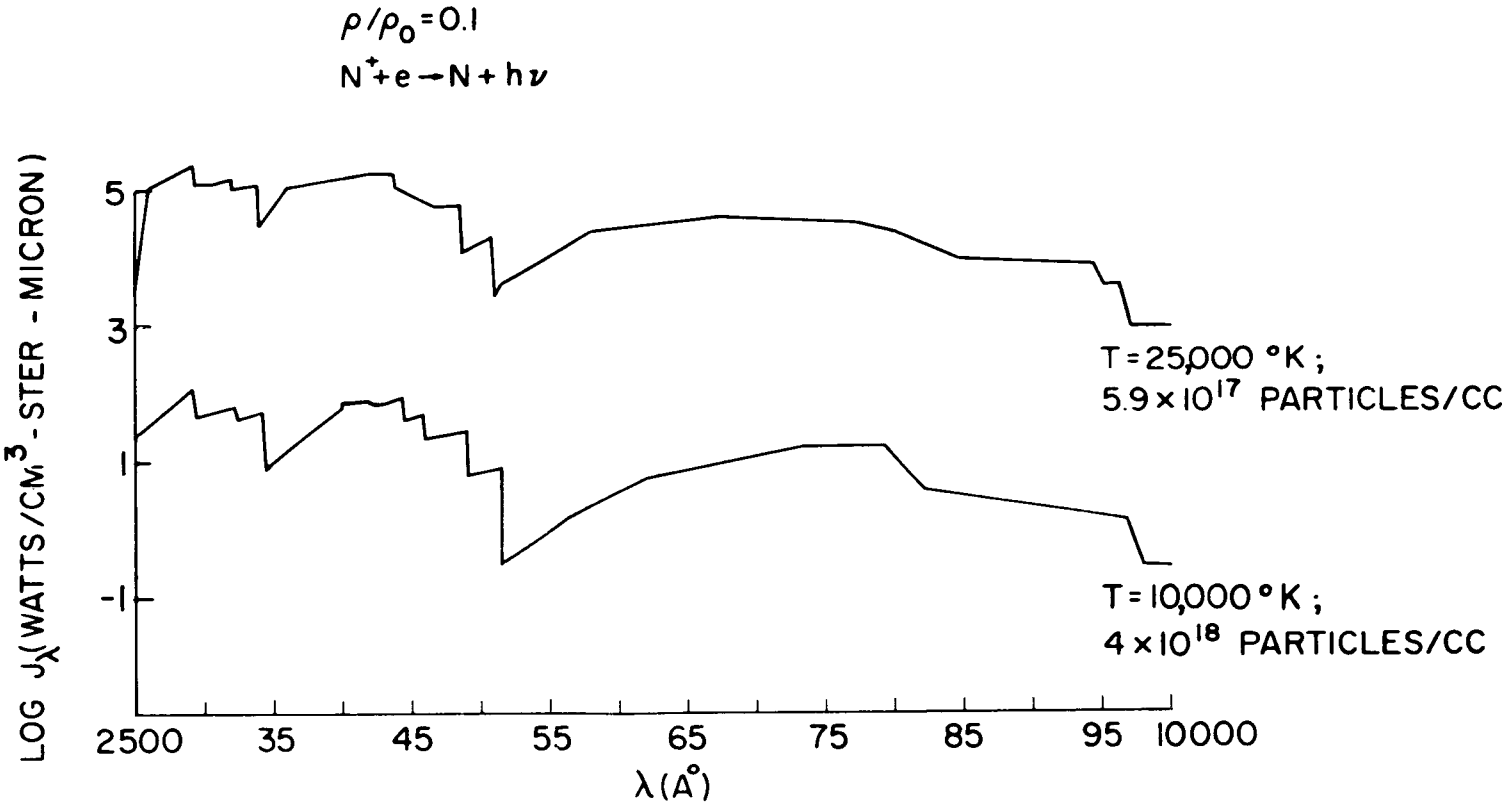

Figure 63. Radiance of O^+ Deionization (8000°K - 25,000°K)

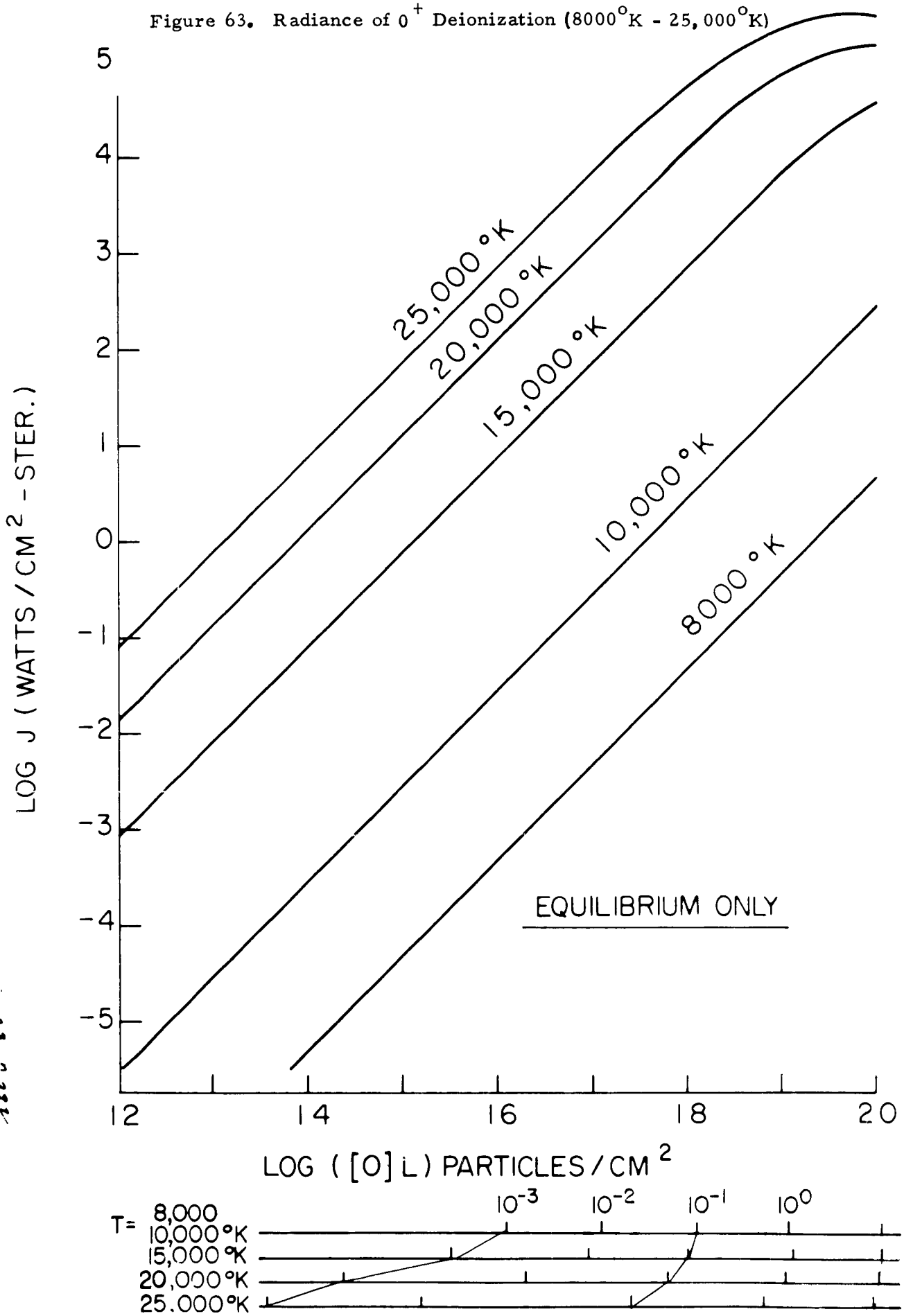

Figure 64. Radiance of 0^+ Deionization (0 Density 10^{11} - 10^{19})

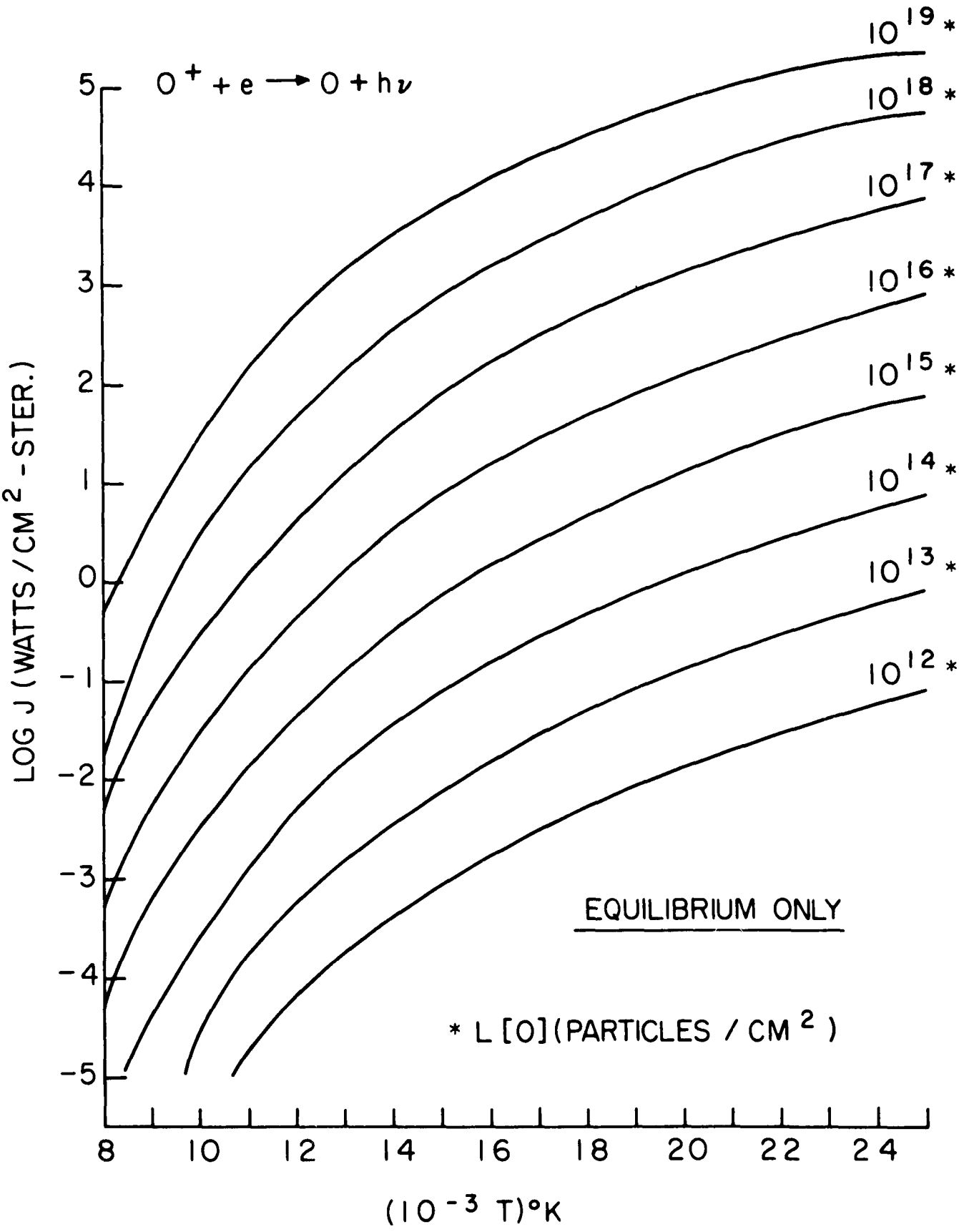

Figure 65. Spectral Radiance of 0^+ Deionization Continuum

$\rho/\rho_0 = 0.1$

$O^+ + e \rightarrow O + h\nu$

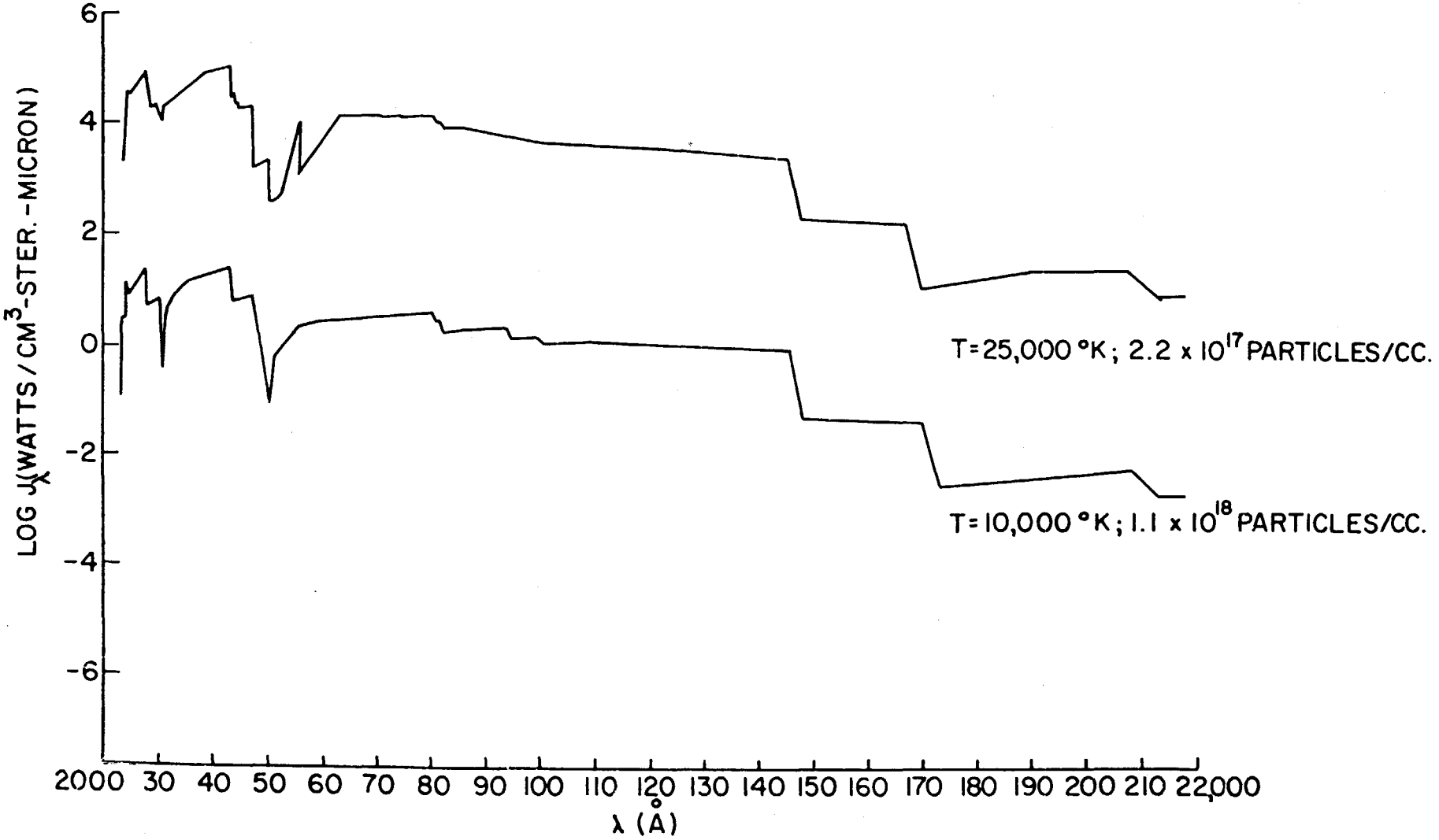

Figure 66. Radiance of ($N^+ + O^+$) Free - Free

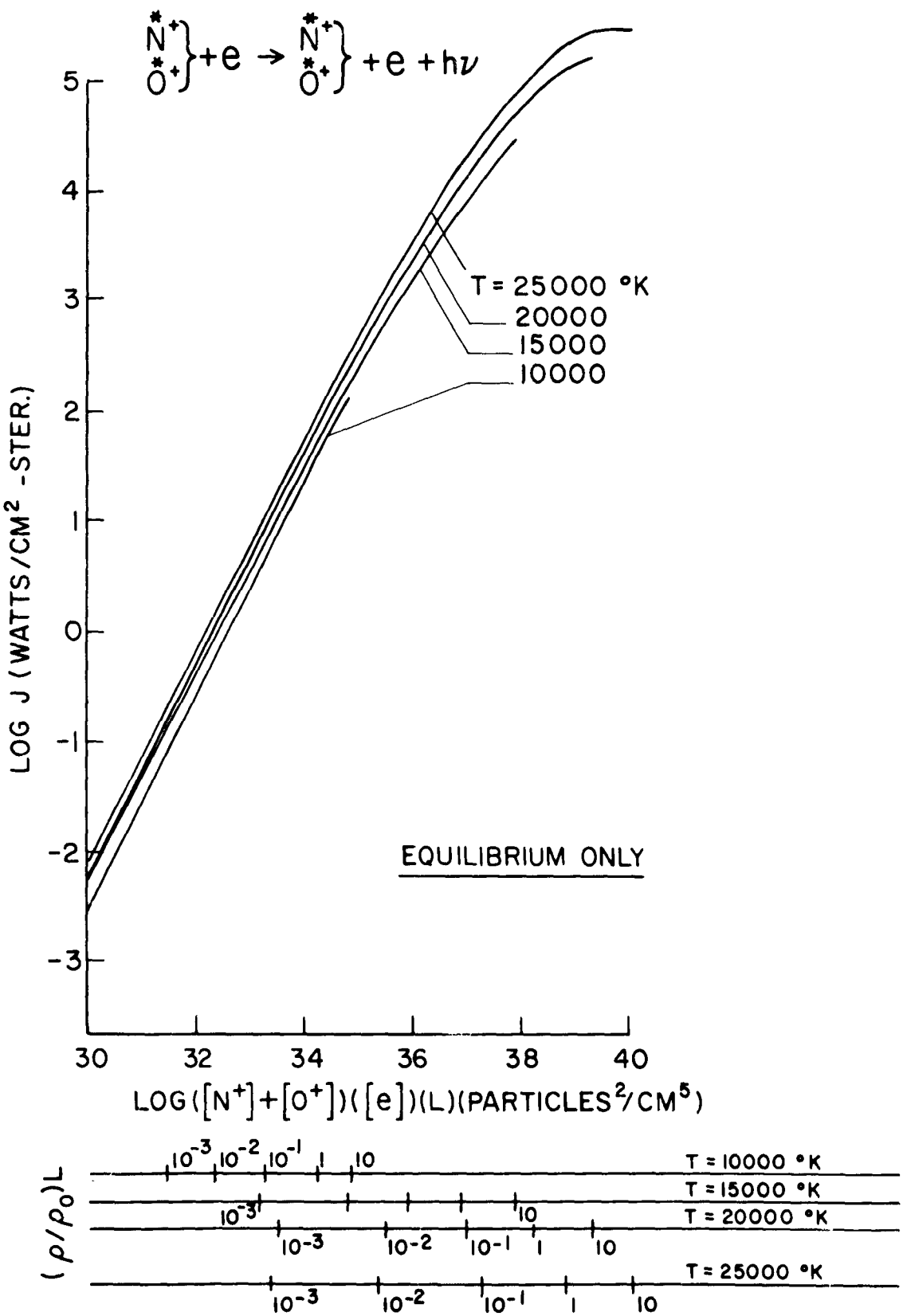

Figure 67. Radiance of $(N^+ + O^+)$ Free - Free ([ion][electron]Density Product $10^{30} - 10^{39}$)

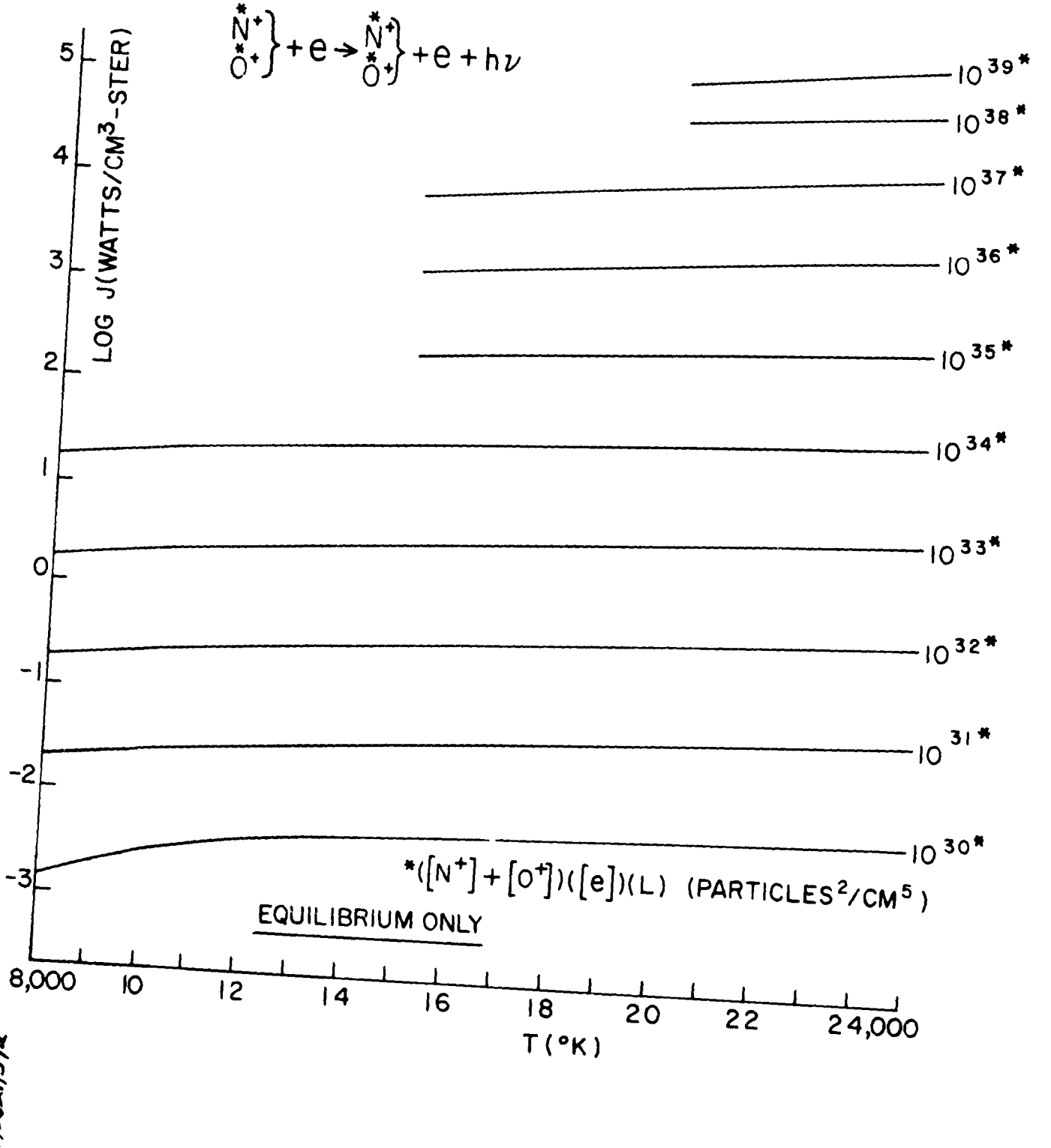

Figure 68. Spectral Radiance of ($N^+ + O^+$) Free - Free Continuum

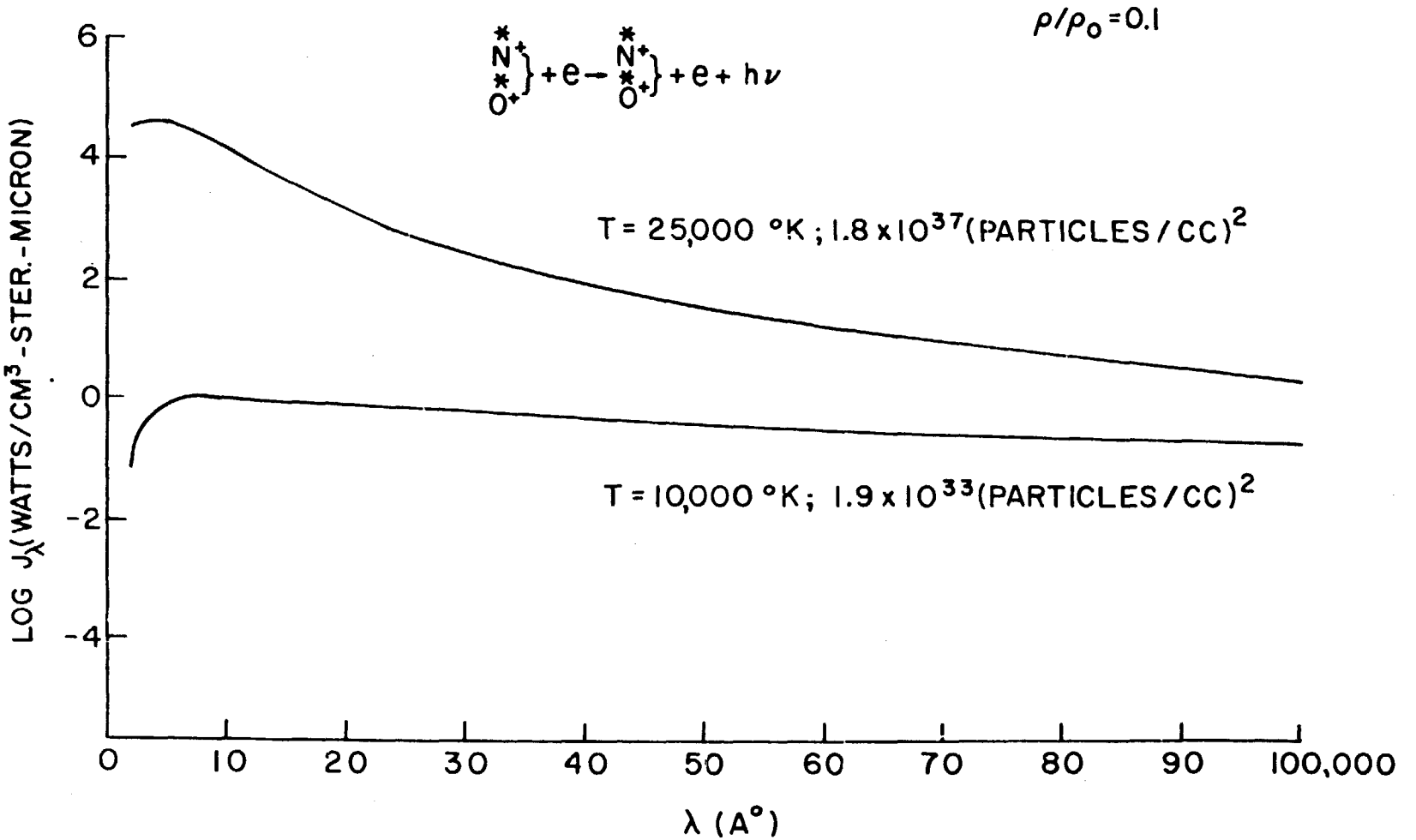

Figure 69. Radiance of O^+ Deionization (.05-.2μ) - (8000°K - 25000°K)

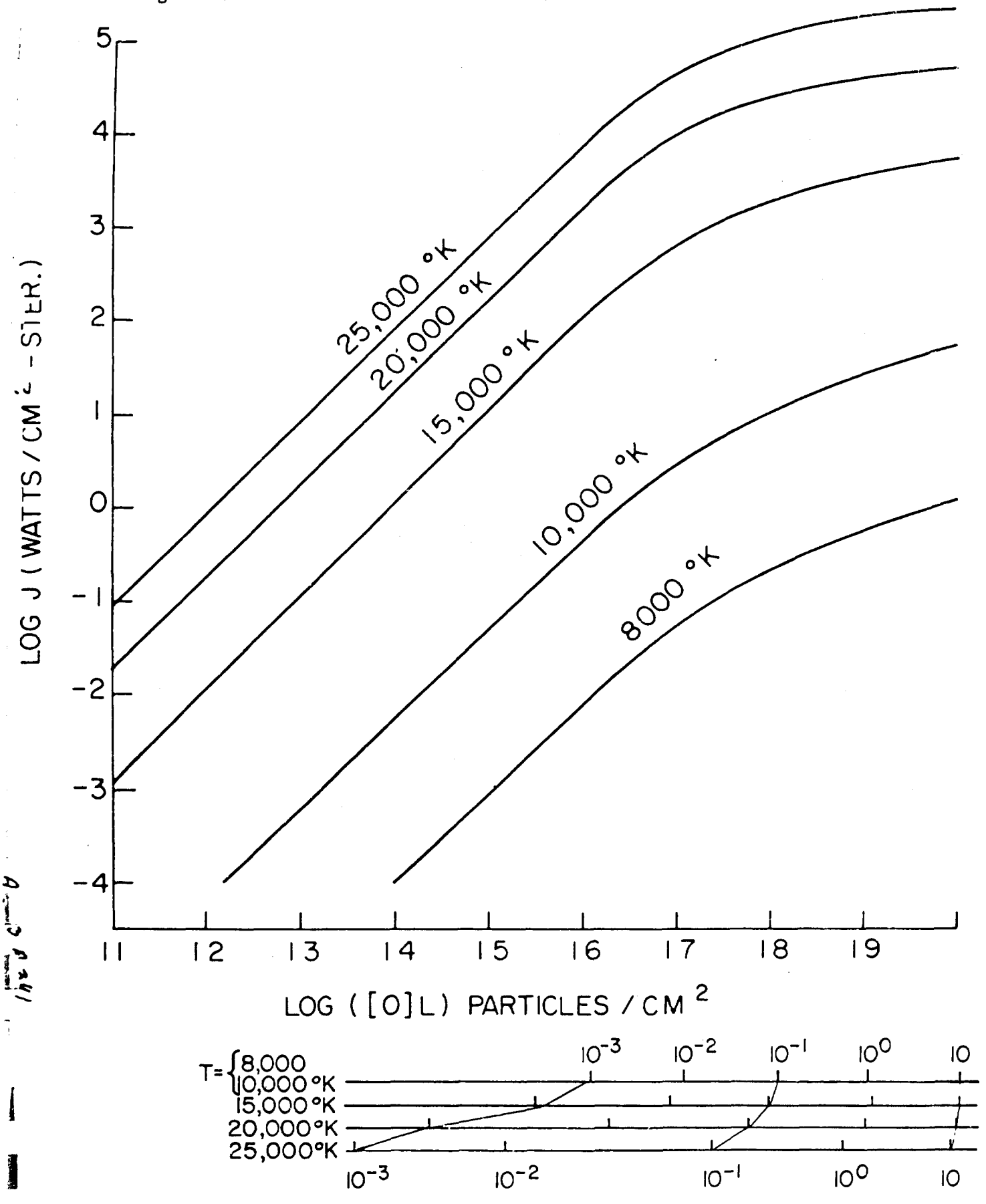

Figure 70. Radiance of O^+ Deionization (.05-.2μ) - (O Density 10^{11} - 10^{19})

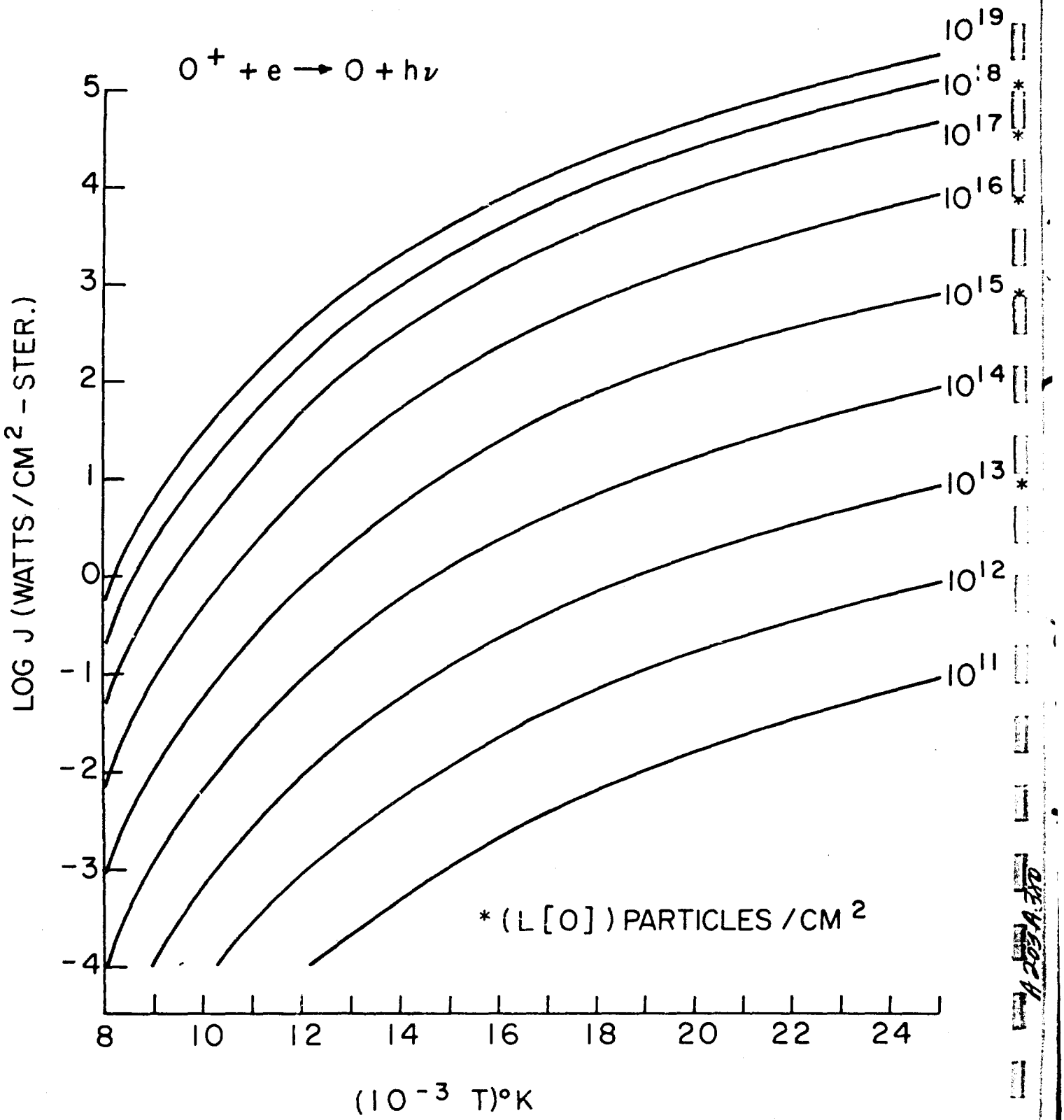

Figure 71. Spectral Radiance of O^+ Deionization Continuum (.05-.2μ)

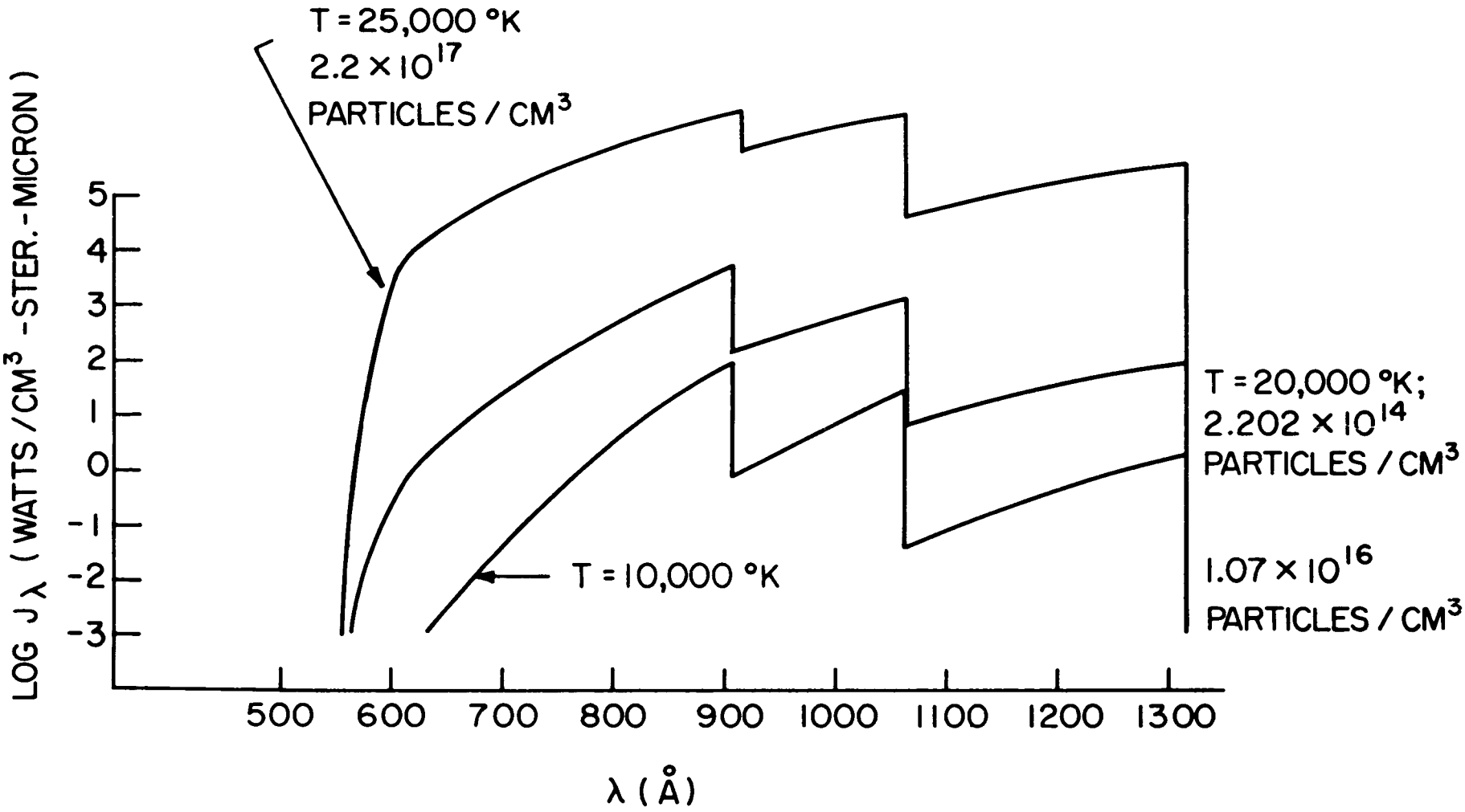

Figure 72. Radiance of N^+ Deionization (.05-.2μ) - (8000°K - 25000°K)

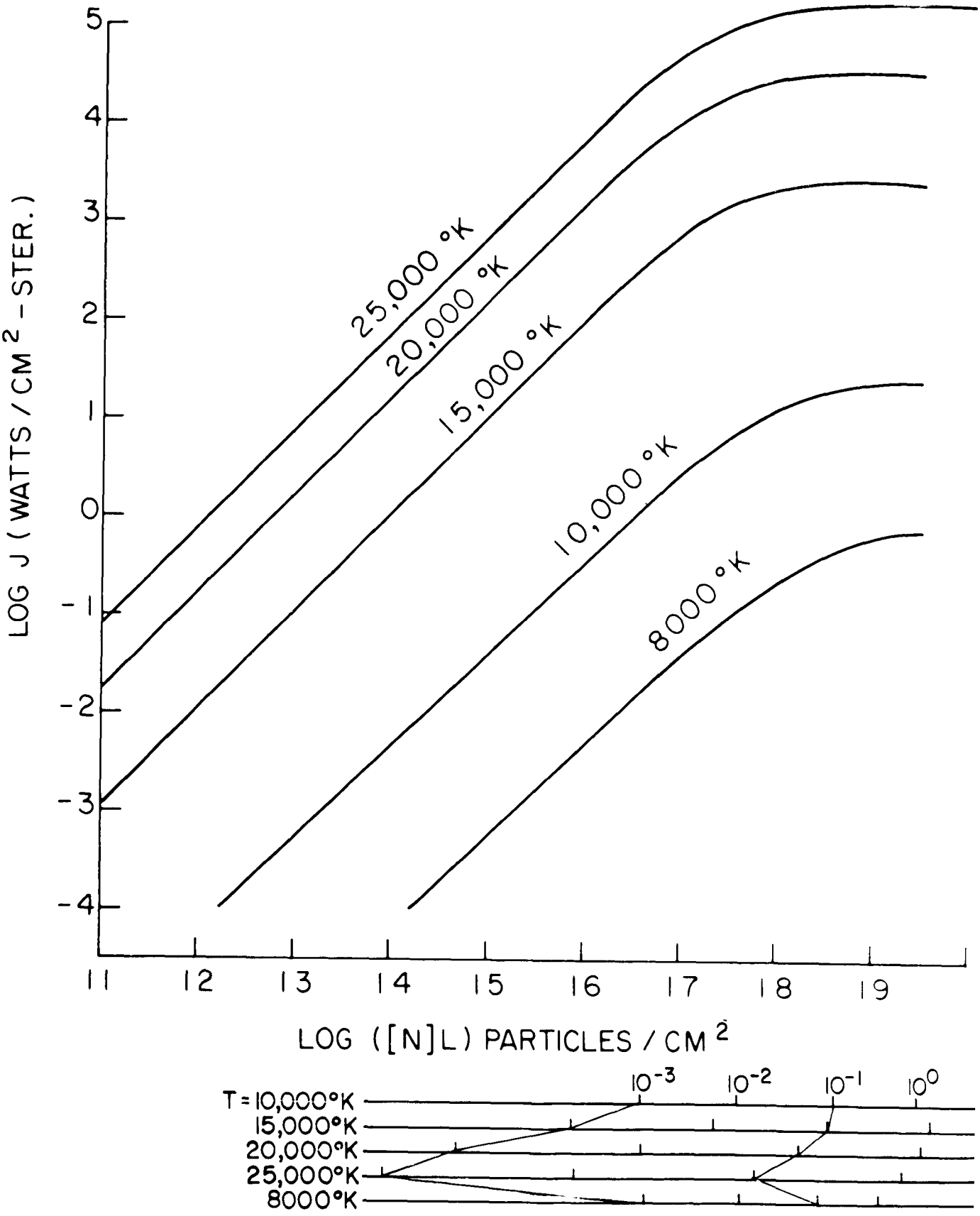

Figure 73. Radiance of N^+ Deionization (.05-.2μ) - (N Density 10^{11} - 10^{18})

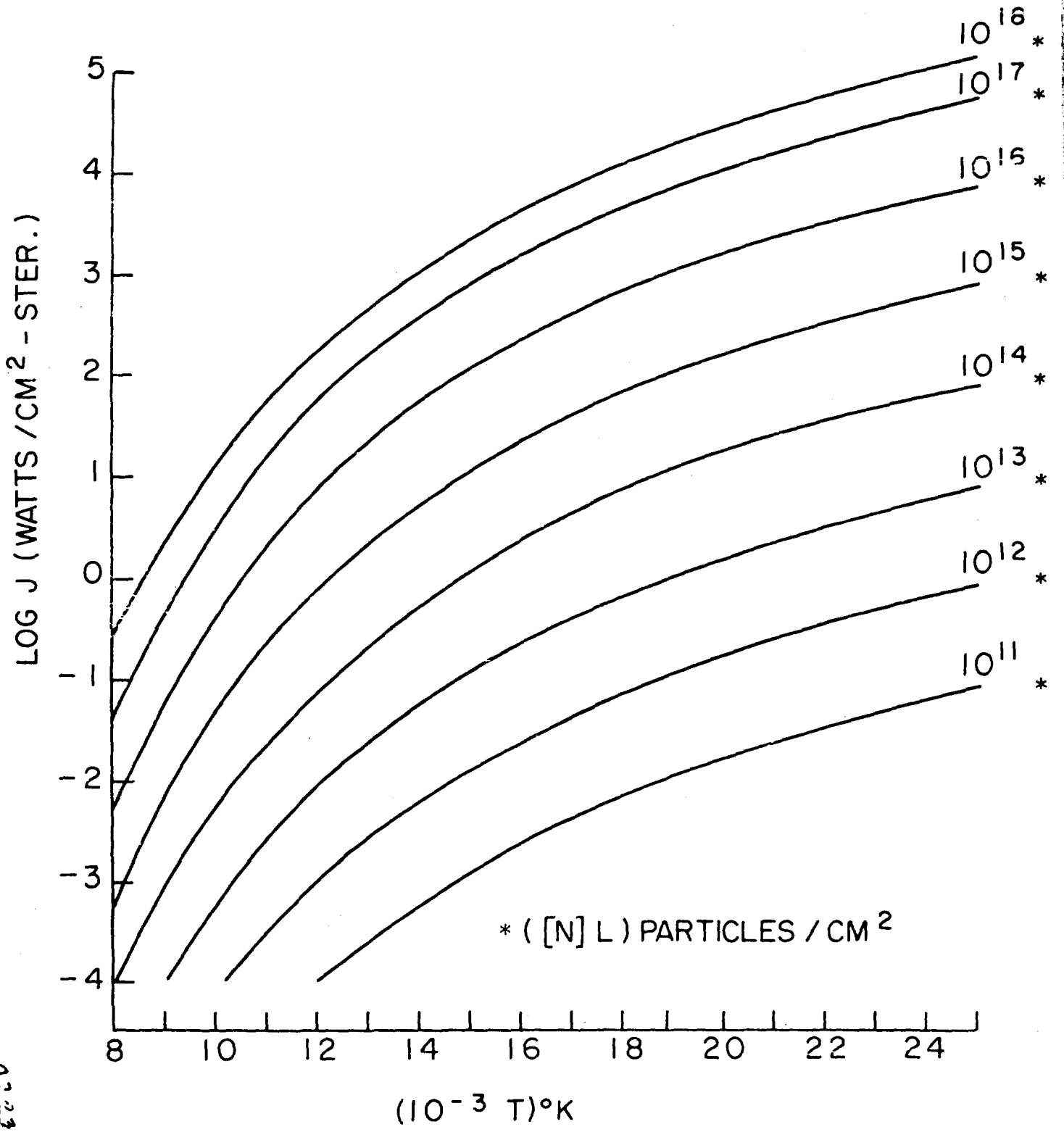

Figure 74. Spectral Radiance of N^+ Deionization Continuum (.05-.2μ)

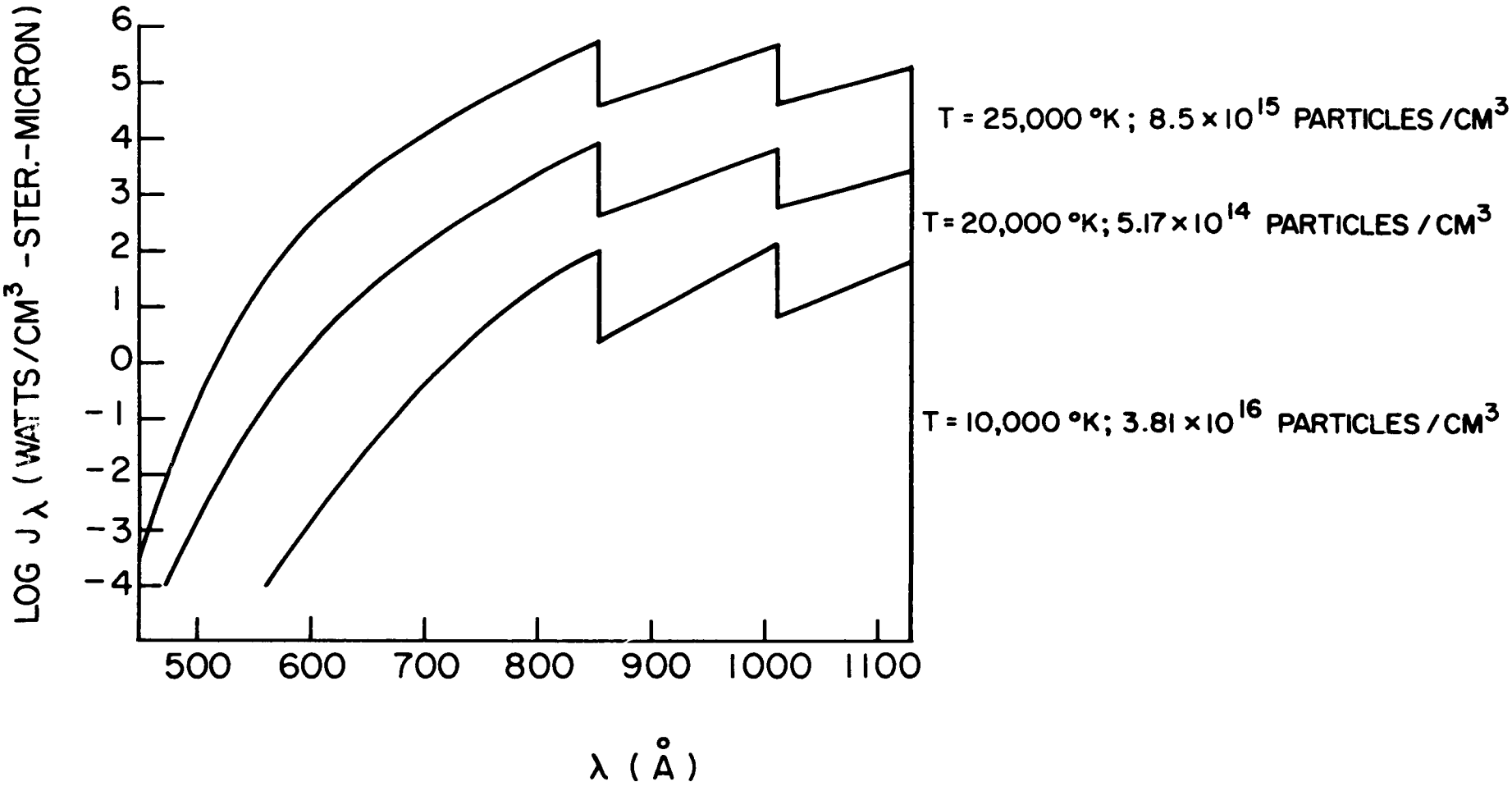

Figure 75. Radiant Intensity Behind the Normal Shock as a Function of Velocity and Altitude

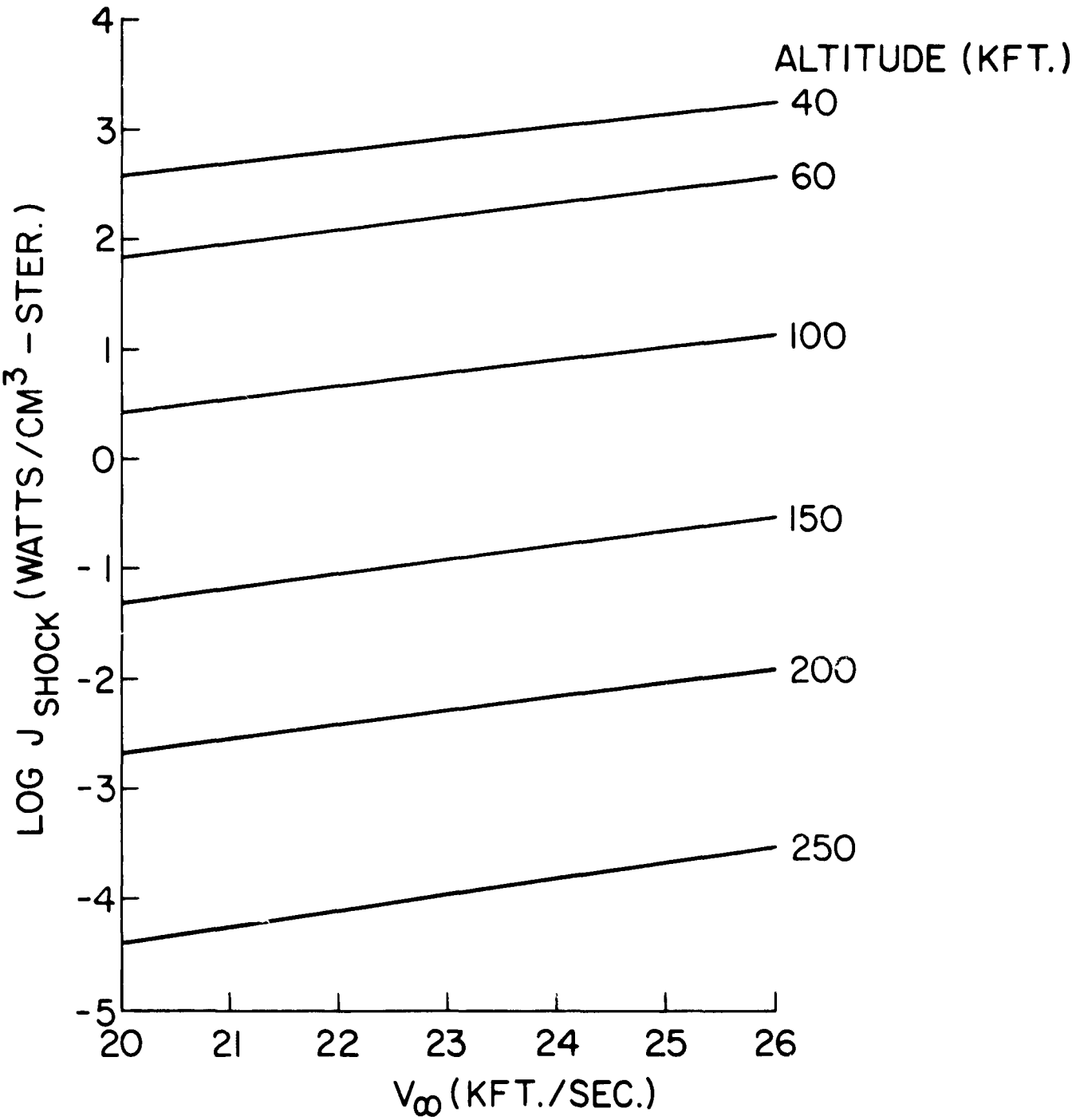

TIS R63SD3 INTERNAL DISTRIBUTION LIST

Valley Forge

H. Lew	Rm.	9167L
T. Riethof (5)		9531L
W. C. King		1314
M. Long		9549L
K. Wan		9545L
K. Coulson		9503L
A. Guttman		9507L
M. Nardone (5)		1315
S. Zeldin (5)		1315
W. Warren		1338
J. Gruszczynski		1334
S. Scala		7023A
C. Harris		1334
H. Sadjian		1326
R. Harner		1326
R. Hughes		9171L
L. Gilbert		7023A
D. Sampson		7023C
G. Sutton		9161L
W. Kaskan		9169L
M. Bortner		9543L
M. Linevsky		9539L
J. Golden		9533L
G. Gethke		9521L
F. Mezger		9503L
P. Gloersen		9523L
W. Browne		7216U
P. Friel		7216U
W. Perry		7223
J. Gilstein		3125
L. R. Trotta		3141U
C. Anderson		7216U

Chestnut St.

J. D. Stewart	Rm.	5501A
T. Shaw		5120A
M. Brunner		5206A
D. Nestler		5206C

HMED Syracuse, N.Y.

F. Rose, Court St. Bldg. 9 - Rm. 46

GENERAL ELECTRIC

SPACE SCIENCES LABORATORY
MISSILE AND SPACE DIVISION

TECHNICAL INFORMATION SERIES

AUTHOR	SUBJECT CLASSIFICATION	NO.
M.C.Nardone R. G.Breene S. S. Zeldin T.R. Riethof	High Temperature Radiation	R63SD3
		DATE June, 1963
TITLE: RADIANCE OF SPECIES IN HIGH TEMPERATURE AIR		G. E. CLASS I
		GOV. CLASS None
REPRODUCIBLE COPY FILED AT MSD LIBRARY, DOCUMENTS LIBRARY UNIT, VALLEY FORGE SPACE TECHNOLOGY CENTER, KING OF PRUSSIA, PA.		NO. PAGES 108

SUMMARY

The spectral and total radiance of the radiating systems in high temperature air have been computed for temperatures between 3000°K and 25000°K, and for relative densities (ρ/ρ_0) between 10^{-3} and 10. The total and spectral radiance of equilibrium air over the same temperature and density range has been computed from the composition of equilibrium air and the absorption coefficients of the individual systems. The results are compared with those obtained by previous investigators.

The results are presented in graphical form and equations approximating the results in regions of low emissivity are derived.

By cutting out this rectangle and folding on the center line, the above information can be fitted into a standard card file.

AUTHOR M.C. Nardone R.G. Breene S.S. Zeldin T.R. Riethof

M. C. Nardone R.G. Breene S.S. Zeldin T.R. Riethof

COUNTERSIGNED Joseph Farber

Joseph Farber